Ramifications of Projectile Velocity on the Ballistic Dart Penetration of Sand

Peter Anthony Sable
Marquette University

RAMIFICATIONS OF PROJECTILE VELOCITY ON THE BALLISTIC DART PENETRATION OF SAND

by

Peter Anthony Sable, B.S.

A Thesis submitted to the Faculty of the Graduate School,
Marquette University,
in Partial Fulfillment of the Requirements for
the Degree of Master of Science

Milwaukee, Wisconsin

May 2016

ABSTRACT
RAMIFICATIONS OF PROJECTILE VELOCITY ON THE BALLISTIC DART PENETRATION OF SAND

Peter Anthony Sable, B.S.

Marquette University, 2016

With the advent of novel in-situ experimental measurement techniques, highly resolved quantitative observations of dynamic events within granular media can now be made. In particular, high speed imagery and digital analysis now allow for the ballistic behaviors of sand to be examined not only across a range of event velocities but across multiple length scales. In an attempt to further understand the dynamic behavior of granular media, these new experimental developments were implemented utilizing high speed photography coupled with piezo-electric stress gauges to observe visually accessible ballistic events of a dart penetrating Ottawa sand. Projectile velocities ranged from 100 to over 300 meters per second with two distinct chosen fields of view to capture bulk and grain-scale behaviors. Each event was analyzed using the digital image correlation technique, particle image velocimetry from which two dimensional, temporally resolved, velocity fields were extracted, from which bulk granular flow and compaction wave propagation were observed and quantified.

By comparing bulk, in situ, velocity field behavior resultant from dart penetration, momentum transfer could be quantified measuring radius of influence or dilatant fluid approximations from which a positive correlation was found across the explored velocity regime, including self similar tendencies. This was, however, not absolute as persistent scatter was observed attributed to granular heterogeneous effects. These were tentatively measured in terms of an irreversible energy amount calculated via energy balance. Grain scale analysis reveals analogous behavior to the bulk response with more chaotic structure, though conclusions were limited by the image processing method to qualitative observations. Even so, critical granular behaviors could be seen, such as densification, pore collapse, and grain fracture from which basic heterogeneous phenomena could be examined. These particularly dominated near nose interactions at high projectile velocities. Resulting empirical models and observations from all approaches provide a baseline from which other studies across may be compared, a metric against which penetrator effectiveness may be evaluated, and an alternative way to validate computationally based analyses. Velocity analysis was further contrasted with piezo-resistive stress gauge data in an effort to pair heterogeneous mechanisms in the bulk stress response. Phenomena such as grain fracture and densification were successfully observed in conjunction with a unique stress signature. Comparing stress responses across the tested velocity spectrum confirm conditional similitude with deviations a low projectile velocities attributed to domination by heterogeneous mechanisms.

ACKNOWLEDGEMENTS

Peter Anthony Sable, B.S., E.I.T.

Obtaining a degree is not a solo pursuit, and to that regard I would like to express my deep appreciation and gratitude to:

To God, for the beautiful gift that is this life, along with the countless blessings of family, friends, and opportunities that I've been fortunate to have come with it.

My loving family, for their continued and persistent support of me both obtaining an education and pursuing my dreams.

My close friends and colleagues, both in and outside of Marquette, thank you for making every conversation, project, and day an adventure full of laughter.

My advisor Dr. John Borg, for the opportunity to work with him over these past few years, enabling me to grow as a student, engineer, and person. Thank you.

My colleague, mentor, and friend Dave Newman, for his guidance and comradery. Thank you for teaching me how to use a wrench the right way.

Annette Wolak for her patience and guidance with regard to all of us in Mechanical Engineering, thank you for all you do.

All the faculty and staff at Marquette University, the Milwaukee School of Engineering, and Northwest Missouri State University, for providing an incredible educational experience and for getting me this far.

Harold Sandusky and Joshua Felts at the Naval Surface Warfare Center (Indian Head) for their indispensable collaboration on this work, and for allowing us to use their facilities and equipment.

The Defense Threat Reduction Agency and Air Force Office of Scientific Research for their grant support without which this research would not have been possible.

TABLE OF CONTENTS

LIST OF TABLES

LIST OF FIGURES

LIST OF EQUATIONS

1. INTRODUCTION

1.1 MOTIVATION

The dynamics of projectile impact and penetration have long been an area of intense research given their potential implications across a range of fields. While a large portion of interest is military such as in ordinance science and ballistics, relevance extends to a range of disciplines from planetary science and geophysics, to fundamental studies in granular interactions [1, 2]. Recently, focus has been shifted to specifically study the dynamic behavior of heterogeneous terra-materials such as soils, sand, and concrete given their prevalence in the aforementioned applications [3-5]. These materials introduce a greater level of complexity due to the innate tendency of heterogeneous phenomena to drastically deviate from what is currently understood and explained by traditional continuum mechanics [6, 7]. With this in mind, the Defense Threat Reduction Agency is interested in characterizing behaviors unique to terra-materials, specifically those associated with extreme temperature and stresses, through the innovation of new investigative methods enabling a more complete understanding of the fundamental physics at play.

While interest has particularly increased in the last decade or two, due to higher relevance in modern applications, understanding penetration and impact is not a new idea. Explored thoroughly within the literature review (*Section 1.2*), the field's origins can be traced as far back as Euler and his student Robins modeling a target as a resistive force to trajectory functionally dependent on arrival velocity [8]. Key to Euler's formulation, and those of his predecessors, has been the reliance on empirical correlation for any predictive

success in the form of conditional constants embedded within governing equations. Because of this, understandably, much of the work that followed was focused on experimental measurements to define these constants for specific circumstances, which, given conventional techniques available, have all been *a priori* or *a posteriori* of the actual event [9, 10]. Given the relationships between the physical mechanisms at play are still not fully known, all of these approximations relied heavily on assumptions used in designing a feasible experiment and so empirical results were forced into parameter specific niches due to measurement limitations with very little generality. Similarly, when incorporating (or attempting to incorporate) a complete physical model of such a complex system, analytical models either yield unsolvable governing equations or feasible solutions dulled by necessary assumptions.

As with the many other disciplines, penetration mechanics took a leap forward with the rise of significant and efficient computational power enabled the implementation of complex numerical approximations to governing analytical models. Relevant implementations, in particular, included techniques such as the transient finite elements when maintaining the continuum assumptions, or to better capture heterogeneous behaviors solvers such as hydrocodes or peridynamics were used, all with their own implicit pros and cons [11, 12]. While these methods definitely aided progress, unfortunately, there was still a catch unavoidable in any computational framework. Inherent in numerical models are both current analytical models meant to model observed behavior, and the necessary numerical approximations deal with the rampant nonlinearities. This infers the accuracy of such techniques could only be as good as the

inherent behavioral model and the associated numerical algorithms. Both of these forcing one absolute necessity: validation.

Thus we come full circle, a reliance on experimental evidence to believe any analytical solution especially when arrived via numerical approximation. Due to instrumental limitations, results from many computational solutions to penetration events may only, best case scenario, be indirectly validated if at all [13, 14]. This leads to the current state of things, and a push to develop in-situ experimental techniques to not only improve our observed understanding, but from which to validate simulated/analytic solutions and thus refine our fundamental knowledge.

With the foundation now laid that new experimental techniques are not only useful but are a requirement to guaranty solid progress it is now prevalent to ask what information would be most useful to experimentally "know". Specifying the event of interest to be the penetration of heterogeneous terra-materials, specifically sand in our case, current techniques commonly at our disposal measure projectile velocity (make or break circuits), stress (piezoelectric gauges), final penetration depth into the target, and the final target/projectile deformation [10]. Of these, only the stress may be measured with any temporal resolution given normally used methods, and none yield any information with regard to material behavior during the event beyond general bulk results. An adequate characterization of such targets would go to describing the kinetics at play during such a dynamic event.

To this end, and the main discussion of this work, a method has been developed at Marquette University in which the projectile penetration of a dart into sand is visually accessible and is recorded. Through this, in conjunction digital image processing

techniques, it is now achievable to measure the propagation of momentum (in the form of a temporally and spatial resolved velocity field) through a two dimensional slice of a target [15-18]. This in-situ data, coupled with more traditional stress gauge measurements, allow for a unique opportunity to more fully describe sand behavior during penetration.

With this new dependent value now experimentally feasible to measure, important now is over what functionality would this metric best characterize a target. To answer this a logical place to start seems simple: projectile velocity and length scale. Why these specifically? Let me first pose a favored allegory Marc Meyers' mentions in his *Dynamic Behavior of Materials [19]*:

"Soft, free-flowing sand is effective against impacts of a velocity on the order of 1mile/s (30.06 caliber bullet speed). On the other hand, a simple knife can defeat [any] sand bag."

In other words, the rate at which you load a material (in this very relevant case, sand) has huge implications on the way it reacts, thus understanding behavior change as a function of loading, experimentally controlled in this case by projectile velocity, is imperative. Likewise, the phenomena associated with reaction to dynamic loading is implicit in material constitutive descriptions. While in homogeneous material this means bulk behavior derives directly from microstructure, behaviors local to the grain scale are equally influential and may cause significant deviation from the expected bulk response [20-22].

With all of this motivating further investigation, the presented work seeks to further characterize the ballistic penetration of a dart into sand, using novel in-situ techniques, such that the results may aid in current experimental endeavors, compliment current

empirical models, and serve as a metric for which potential numeric solutions may be validated. As referenced when briefly mentioning the experimental methods used, this is a direct predecessor of work done by Van Vooren, Morrissey, and Borg. Particular emphasis has been given to increasing the range of the investigated velocity spectra as well as developing empirical connections to various heterogeneous mechanisms on a bulk and grain scale.

1.2 LITERATURE REVIEW

The culmination of work that has contributed to the understanding of penetration into sand can not-so-neatly be separated into three fields of study trying to describe three distinct characteristics. First, and debatably the eldest, general penetration theory has done much to describe dynamic penetration and impact of a projectile into materials and describing bulk mechanisms at play. More so, recent studies have dove into heterogeneous phenomena and working to model complexities either through enhanced empirical correlations or computational simulations.

While this is where a majority of literature resides, many very useful concepts come from the metaphorical other end of the spectrum, specifically in non-Newtonian fluid dynamics. From this perspective, sand and other granular media could be modeled with pseudo-fluidic properties aligning with observed granular flow behaviors. Even including this body of work doesn't provide us with all the necessary background. While a middle ground in solid and fluid mechanics goes a long way to explaining penetration behavior of terra-materials, some phenomena is uniquely granular and thus the relatively new discipline of granular mechanics begins to close the gap. Keeping with this trend, when

reviewing past work, an effort will be made to summarize literature corresponding with the key relevant fields including penetration mechanics, non-Newtonian fluid dynamics, and granular mechanics. The most recent studies, which are some culmination of the three, are presented last.

The dynamics of penetration and impact has long been an area of investigation, tracing its roots to Euler, Poncelet, and Robins in the 18th century, being modeled as a negative acceleration into a medium solely as function of velocity and empirical constants as demonstrated in equation 1.1 [8, 24, 25].

$$-\frac{dv}{dt} = \alpha v^2 + \beta v + \gamma \qquad (1.1)$$

These modeling techniques were satisfactory, especially at low velocities given simplifying assumptions, up until the 20th century where the new age of warfare ushered in the necessity for a more intricate understanding of ballistics and penetration mechanics especially with regard to applicable terra-materials.

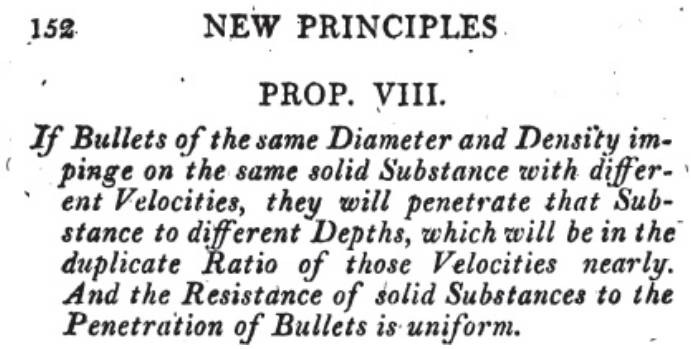

152 NEW PRINCIPLES

PROP. VIII.

If Bullets of the same Diameter and Density impinge on the same solid Substance with different Velocities, they will penetrate that Substance to different Depths, which will be in the duplicate Ratio of those Velocities nearly. And the Resistance of solid Substances to the Penetration of Bullets is uniform.

Figure 1.1 A quote from the *New Principles of Gunnery* (1742) by Benjamin Robins, a comprehensive work in ballistic theory, still relevant to this day [25].

A large, unmentioned, amount of work has been done in the realms of interior and exterior ballistics focusing on methods of projectile acceleration and the resulting trajectory. With regard to terminal ballistics (penetration mechanics), however, as huge

leap forward from basic force balance models was Allen and Mayfield's seminal article, published in 1956, on an ogive projectile penetrating sand served as an excellent review of work up unto that point on current models and was among the first to apply such techniques explicitly to a heterogeneous media and compare experimentally [3]. This article, in conjunction with the politics of the era, greatly increased interest in the topic and much experimental work was done concerning projectile geometry, effects of attack angle, failure modes, and penetration depth greatly expanding the "library" of scenarios per which empirical correlations applied [26-30]. Several of these excellent studies were conducted at Eglin Air Force Base were radiography was used to experimentally inform analytical equations designed to model both dry and wet sand behavior and compare with predictive codes at the time [14].

Another, considered to be seminal, work is that of Backman and Goldsmith published in 1978. Entitled *Mechanics of Penetration of Projectiles into Targets,* the authors thoroughly discuss the dominating elastic, plastic, or shock/hydrodynamic behaviors prevalent in respective bands of impact velocity including nominal, sub, and ultra ordinance regimes including how to calculating the limit velocities depending on material properties [31]. This served as *the* baseline study for the next few decades in which much experimental work was based in or compared to, and was (as far as this author can tell) the first complete implementation of yield criterion into penetration models.

Forrestal and Luk's *Penetration into Soil Targets* in 1991 also integrated specifically the Tresca and Mohr-Coulomb strength criterion into analytical penetration models via conservation equations and provided an approximation of elastic to plastic deformation including wave propagation [32]. Their work is particularly relevant as they

specifically applied their analytical developments to concrete and soil incorporating aspects such as locking density of grains.

More recently, while most experimental pursuits focused on homogenous materials such as metals (relevant to armor), there has been an uptick in focus on heterogeneous materials. For example, studies done at the University of Texas (Austin) picked up where Eglin left off in the 1970's and further experimentally investigated sand penetration behaviors at ultra ordinance and hypervelocity regimes specifically exploring a greater range of projectile geometries [33, 34].

While not specifically within the realm of penetration mechanics per say, a great deal of work done to describe the dynamic behavior of terra-materials in general has been by geophysicists, mostly regarding asteroid impact investigations. Of particular interest are studies done by groups such as Holsapple [35-37]. These focus primarily on using non-dimensional analysis to develop behavioral models given the scale of the event of interest. Prevailing are non-dimensionalization using energy or momentum methods yielding varying results. Given the similarity in phenomena at play, these provide another method of comparison for varying types of experimental approaches.

Continuing on, granular media, such as our sand target of interest, has a certain affinity to flow. It is this characteristic in fact, along with other factors such as grain size distribution, porosity, and other heterogeneous phenomena, that make targets such as sand the exception to many penetration models instead of following the "rules". These ideas of course were considered a long time ago and as a result many have set out to model sand and the penetration of it as a shear-thickening fluid, or at least use the same concepts to base alternative material models [38-42].

Relevant studies include discussion by authors such as Bi, Ciamarra, or Waitukaitis whom all investigate the idea of dynamic jamming which appear in shear-thickening fluids due to the propagation of stress throughout the medium builds up as particle resistance to disturbance from its neighbors increase as propagation radiates [42-45]. This is similar to the compaction wave propagating in sand during penetration, which lends well to connecting concepts of shear in a granular setting. Ciamarra even goes as far as to propose a jamming phase diagram using factors of friction and shear. Uniquely, Albert takes a look at drag induced by jamming and through doing so develops a boundary layer like description for the force propagation which was surprisingly minimally dependent on velocity [46].

Specifically giving more attention to shear in these fluid systems, studies done by Wagner, Brown, Murdoch and others do excellent work in investigating shear-thickening in general and the inherent effects on characteristics such as viscosity [47-50]. Brown pays particular attention to how particle size alters shear behaviors in non-Newtonian fluids. These provide additional insight into the additional mechanisms at play due to granular and more so the fluidic aspect of the target.

As discussed above, even when considering both a background in solid and fluid mechanics certain gaps exist in fundamental understanding with regard to the sand target, especially under dynamic conditions such as penetration. An exemplary mechanism is that of force chains. Not present in either fluid or continuum solid, the idea of force propagating through of granular media by spreading through chains of grains like Newton's Cradle is a special to granular mechanics. That is just the tip of the iceberg though, especially in the

course of a penetration event, granular concepts such as void collapse, grain failure, size distribution, modes of contact, and more all become very relevant [51].

To that regard some excellent works include those by Nesterenko and Cambou [51, 52]. The first discusses many analytical and experimental techniques used to analyze the dynamic behavior of heterogeneous materials in general, but specifically address nonlinearities which occur throughout wave propagation in granular systems. He includes several analytical and experimental comparison. In contrast, Cambou focuses specifically on exploring the mechanics of granular media, going in depth on the use of probability functions in calculations and developing a combined stress tensor to the model bulk system. Mostly taking an analytical approach, Cambou also goes into depth on numerical simulation and the use of discrete element methods in current research.

Complimenting the aforementioned overarching texts, studies such as the ones done by Stone or Jaeger extensively discuss the compaction of granular systems connecting directly to the jamming phenomena also seen in shear-thickening fluids [53, 54]. Additionally, Lade and several other groups add a layer to this, investigating the effects of grain failure and crushing with granular media under load and the resultant erratic behaviors observed in stress-strain space [55, 56]. Finally, Stephen Hostler and Rafael Goulding both wrote very informative theses on wave propagation in granular materials and mechanical properties of sand respectively, with Oelze doing additional experiments on sound speed measurements in soils [57-60].

A lot of work in the realm of granular mechanics is focused on numerical simulation such as the discrete element method, material point method, or peridynamics [12, 61]. Loosening the continuum assumption, these go a long way to capture granular interactions

and more so to accurately predict failure mechanisms such as yielding and spalling. While not utilized in this thesis, it is these types of predictive codes that require validation through which these results endeavor to help.

With a reasonable foundation in many of the relevant studies up to this point, it is time now to focus on the most recent and current works. Directly regarding sand investigations are either computational or experimental which can further be broken down into three distinct groups.

Computationally, most recent studies of relevance have been conducted by Borg, Vogler, Chhabidas, and others focusing on utilizing software such as CTH and peridynamics to model penetration and other behavior [62-64]. A lot of work has gone towards simulating non-uniform distribution of grains, resolving mesoscale interactions, as well as testing different contact models building on the basic Hertzian philosophy and exploring different descriptions of tribology.

Back in the experimental realm, investigators such as Chen at Purdue are exploring mostly single grain interactions. Chen in particular utilizes radiography to view grain fracture in-situ using a Split-Hopkinson bar configuration [65].

In a higher regime of loading are actually penetration experiments beginning at low (below sub ordinate, less than 30 m/s) velocities. Examples of this include Iskander's group at NYU-Polytechnic and this authors predecessor [15-18,66-68]. While the two groups' work has the same motivation, the methods used are quite complimentary in that one uses a visually transparent pseudo-sand media as the target allowing optical accessibility while at Marquette University the penetration event into sand is aligned near a Plexiglas window (to be explained fully in Experimental Setup) assumed to be of identical impedance and is

visually observed through said window. Both are novel in-situ experimental techniques and allow for new derivations of field quantities such as velocity and strain respectively.

In summary, it is the focus of this work to expand the velocity regime that has currently been investigated to better grasp of the phenomena at play and how that changes with increased dynamic loading, especially as plastic behavior becomes more prevalent. While the a much more robust spectrum of penetration experiments with regard to projectile velocity using traditional methods, here it is the author's endeavor to do so using new found experimental capabilities and in doing so allow for more informed experimental observation and for the validation of available computational models. Separate of change with regard to impact velocity, it is also apparent through the discussed studies across a range of disciplines that sand penetration is very much a multiscale phenomena and as such this work also seeks to explore behaviors as they manifest on both a bulk and grain scale level.

1.3 OBJECTIVES AND METHODOLOGY

As was briefly discussed in *Section 1.1*, the purpose of this work is to utilize novel experimental methods to better characterize a sand target during a dynamic penetration event. Characterization, in this case, is defined as attaining in-situ velocity field and stress information and determining the response functionality with respect to projectile velocity. Particular attention is devoted to extending the velocity range of previous works and evaluating experimental results to develop empirical behavioral relations which may be easily compared to computational simulations for validation. Length scale will also be

considered to evaluate whether this approach may resolve bulk and grain scale behaviors in the hopes of observing dynamic heterogeneous phenomena manifest on multiple levels.

All experiments will be conducted using the at Marquette University, where a gas gun will be used to accelerate the right cylindrical dart projectile into visually accessible sand target. Penetration events will be recorded via high speed photography and processed using digital imaging processing techniques to extrapolate a two dimensional, temporally resolved, velocity field. This, in conjunction with stress gauge data, will allow for a more complete characterization of the sand's dynamic behavior including a unique ability to link velocity and stress response to observed heterogeneous mechanisms.

2. INTRODUCTION TO PENETRATION MECHANICS

2.1 OVERVIEW OF PENETRATION THEORY

Prior to any experimentation in sand penetration, it is imperative to have a firm ground in the basic theory of penetration mechanics so the right questions can be asked to both properly understand empirical results and so that said results may better improve our current understanding. As the entire discipline of terminal ballistics is devoted to these concepts only a brief review may be presented here. For a more comprehensive and thorough discussion, and great foundation may be found in *Ballistics: Theory and Design of Guns and Ammunition* by Carlucci and Jacobson [69].

Simply put, penetration theory is an attempt to describe the interaction of a projectile (or penetrator) of varying geometry impacting a target of defined material properties and kinematic makeup. Several practical questions naturally arise, the most pertinent of which are: Does the projectile successfully "defeat" the target, and if so by what failure metric is defeat determined [69]? To answer these three key issues should be considered: the governing behavior of the projectile-target interaction, failure criterion unique to the given materials, and lastly the ways in which failure itself occurs.

Governing behavior of the interaction may be attained, as would be expected, via either conservation of energy methods or Newton's 2nd Law. For the exemplary case here, the latter will be used via force balance. Traditionally, theoretical analysis works to attain a final trajectory equation from a force description. That being said, beginning at time of initial impact of the projectile onto the target, lets assume the only force opposing the

motion of the penetrator is that of the target's strength resisting deformation. To calculate this force, stress at the penetrator nose must be integrated over the applicable area incorporating yield criterion. Taken from Forrestal and Luk [32], the basic force balance assumes the form

$$-F_z(\sigma_y, d) = m\frac{dV}{dt} = mV\frac{dV}{dz} \qquad (2.1)$$

where the force F_z is a function of yield stress and projectile geometry and the velocity V is the projectile speed in direction of impact. After integration of stress, we may further define F_z as

$$F_z = \frac{\pi d^2}{4}\sigma_y(\alpha + \frac{\beta\rho_{target}V^2}{\sigma_y}) \qquad (2.2)$$

with α and β being nose geometry factors and d begin the projectile diameter. Substituting into the force balance and integrating in z from zero to final penetration depth and in velocity from impact velocity to zero, final penetration can then be represented as

$$P = \frac{1}{2\beta}\left(\frac{\rho_{proj.}}{\rho_{target}}\right)\left(L + \frac{kd}{2}\right)\ln\left[1 + \frac{\beta}{\alpha}\left(\frac{\rho_{target}V_o^2}{\sigma_y}\right)\right] \qquad (2.3)$$

with an additional empirical constant of k required in derivation. While the focus of this study does not work towards validating or improving an analytical model such as this, seeing this initial theory does provide a few key insights. First, the dominating dependence of force (and later penetration depth) on projectile (impact) velocity and second, the only incorporation of mechanical material properties is with the implementation yield criteria, and lastly, the dependence on empirical information.

While the form shown is fairly generalized, after empirical tuning this is accurate to about 15% of experimental observations, limiting targets to homogenous materials such as metals [69]. Heterogeneous materials, soils (sand) in particular require additional

alterations which will be expanded on later. From an experimentalist perspective, maintaining the assumption that this model does accurately describe the interaction, confirms the importance of characterization as a function of projectile velocity.

Next on our list of considerations is yield criterion and how to evaluate failure. At this point still considering homogenous continuum materials, this part is actually fairly simple in that the user may choose his or her method choice and substitute. Traditionally a Mohr-Coulomb or Tresca model is used with an elastic-perfectly plastic assumption used to avoid a transition zone. In this way, the analytical model may be as complex or simplistic as one wishes [32].

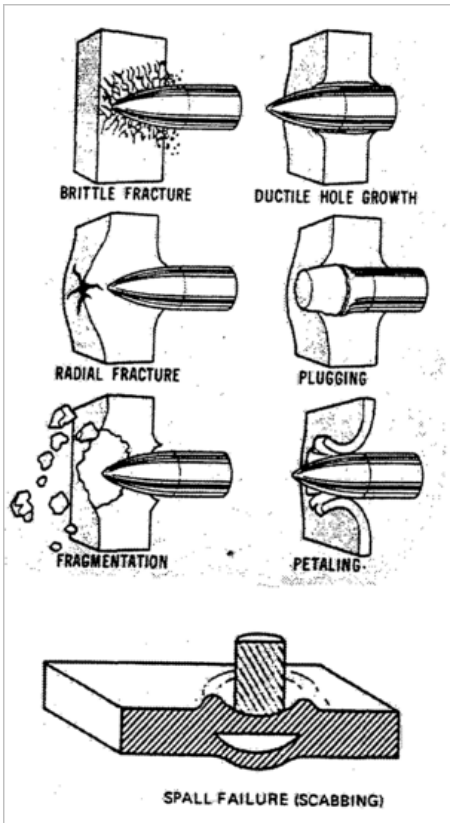

Figure 2.1 Cartoon description of various methods of failure due to ballistic penetration taken from the Army Research Lab, ARL-TR-1741 [82].

Lastly in describing a penetration event is the modes of failure themselves. Not inclusive and depending on boundary conditions, the penetrator may cause the target to fail via plugging, piercing, petaling, scabbing, or spalling (shown in Figure 2.1). All of which depend on characteristics such as target thickness, nose geometry and material properties (ductile or brittle). More generally, failure is very much a function of the wave propagation through the target after penetration. These behaviors are not theoretically incorporated in depth calculations shown and require alternative formulations [32].

2.2 SAND AND SOILS: GRANULAR CONSIDERATIONS IN THEORY

The aforementioned theory does not take into account mechanisms unique to heterogeneous and, in particular, granular materials. As the solution is both somewhat based on empirical tuning and material specific properties, the ability to alter the equation for granular (or any heterogeneous) considerations is fairly limited.

A relatively easy adjustment is in terms density. Prior to failure, it is assumed a granular system may compress to a certain limiting extent. This locking density can then be incorporated in a volumetric strain term

$$\eta^* = 1 - \frac{\rho_o}{\rho^*} \quad (2.4)$$

where η^* is the volumetric strain, ρ_o is the initial (bulk) target density, and ρ^* is the locked density or maximum elastic density. This is embedded into the governing physics via the integration of stress resisting projectile motion. Going a step further, though not written explicitly, Tresca and Mohr-Coulomb criterions may be combined to better model the improved resistance due to densification followed by the final plastic flow [69]. Tresca

and the associated Mohr criterion are specifically mentioned as per their common use in the literature, Mohr-Coulomb is especially useful as different tensile and compressive yield strengths may be implemented as is common in heterogeneous materials.

More comprehensive analytical solutions exist for granular systems undergoing more simplistic loading such as soliton wave propagations [51]. While these have not yet been expanded to include penetration events, they use Hertzian contact models in conjunction with probability to describe the propagation of load throughout the system. In general, theoretical modeling of sand penetration is still a hot area of research with many heterogeneous phenomena yet to be incorporated.

2.3 WAVE PROPAGATION

Deviating from strictly looking at penetration trajectory as is the case with many theoretical models, an alternative is to consider wave propagation present throughout the target induced by penetration. Starting simple, first consider a projectile “slowly” hitting a homogenous target with no resultant failure, in other words not actually penetrating at all. The projectile still transfers its kinetic energy into the medium which radiates from the point of impact in the form of a stress wave. No permanent deformation occurs and this wave is more acoustic in nature much like sound through air and, at most, results in some temporary, non-destructive, compression.

Adding some complexity to the scenario, lets now assume the projectile does indeed penetrate the target and travels some finite distance unimportant for this walkthrough. The elastic wave is still present, though now the projectile has enough energy to permanently deform the material i.e. penetrate it. This means the elastic wave is quickly followed by a

destructive plastic wave driving the system past some (material dependent) elastic limit into either an elastic-plastic, or (in higher energy cases) solely plastic stress regimes leaving destruction in its wake [32]. While this is a complete (though somewhat general) description of what occurs in a penetration event, this is not adequate to describe behavior for our sand target of interest –a heterogeneous material. Because of this, we must now conceptually depart from a homogeneous material to a land in which mesoscale phenomena make a world of difference. The easiest way to understand the difference is through a thought experiment.

Image yourself in a long narrow hallway. At the end, is an all expense paid trip to some tropical beach of your choice, while right behind you is a horde of very persuasive zombies whose intentions are far from benign. Keeping with this idea, these "boundary conditions" would serve as excellent motivation for you to run to the other end of the hallway as fast as physically possible. If the hallway is clear of obstacles, while exhausting, this task could be fairly straightforward and you are likely to reach your destination, free to enjoy some safe days in the Sun. Now imagine this hallway is filled with all sorts of obstacles: chairs, desks, other people, large craters leading to an abyss, you name it. Again making a run for it, you may find yourself now unable to outrun the zombie horde given the additional adversity, or even if you do it would be at an at least somewhat slower pace. This is exactly the difference between homogeneous materials such as aluminum steel and heterogeneous materials like sand studied here.

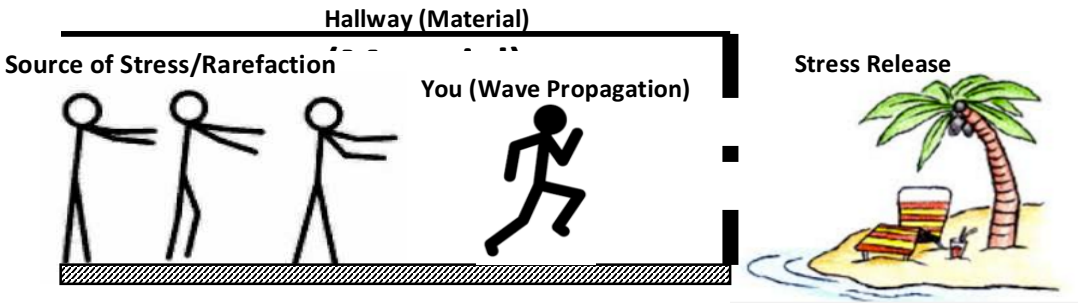

Figure 2.2 Wave propagation through a material is analogous to running through a hallway, where homogeneous materials are unobstructed and heterogeneous materials are full of obstacles.

Given some imparted energy (the zombie motivation), a stress wave propagates through a material (you, the runner). However, how quickly the wave moves through the target is entirely dependent on how clear (homogeneous) the hallway (material) is. In the homogeneous case, the hallway is more or less clear and the wave propagates straight through given minimal variations in density and little to no void space. In contrast, in the case of sand, the hallway (material) is crowded with all sorts of obstacles, except instead of tables and chairs the wave most overcome various void spaces, friction, boundary melting, surface reactions, and even fractures. All of which, for better or for worse, greatly slow the motion of the wave, altering the observed bulk response.

Nesterenko has done extensive work exploring and defining different heterogeneous phenomena. Figure 2.3 schematically demonstrates those most commonly associated with granular materials. Most are a direct results of differences between individual grain geometries and the inherent voids and friction that is therefore initiated.

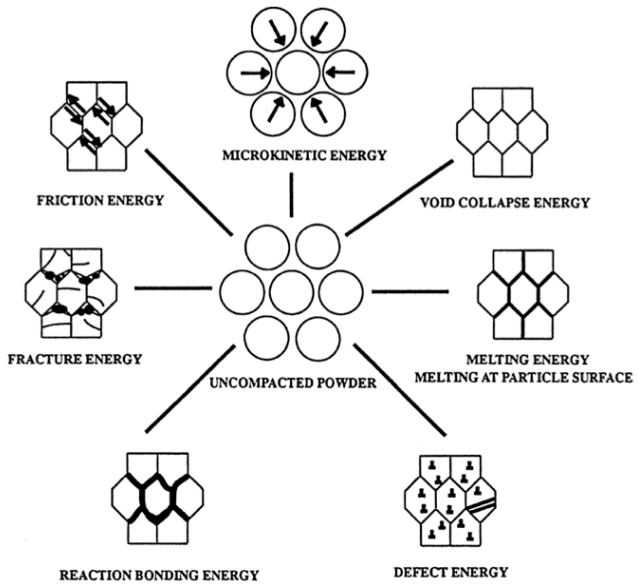

Figure 2.3 Heterogeneous mechanisms commonly present in powders, and expected in the loose dry Ottawa sand of interest. Caused by grain scale interactions these are indiscernible on a bulk level [51].

Given a more thorough understanding of what being a heterogeneous material implies, lets return to stepping through a penetration even and now consider our complete granular system. Initially after projectile penetration an elastic wave propagates radially through the medium. Given no potential for plastic destruction, this is similar to the previous case in that no permanent material failure may be caused, *however* loose sand is not optimally orientated, a packing factor of around 65% [83], and so the elastic wave may facilitate the compression of grains to a higher, locking, density. Additionally, wave propagation is no longer evenly radial, in other words the hallway is no longer clear. To move around the obstacles (void spaces), stress now propagates from grain to grain via a probabilistic network of force chains (stress bridges) like a very complicated Newton's Cradle, as mentioned in the summary of literature. Quickly following the elastic compression, a plastic wave propagates in the same manner. Unfortunately, this too has an

additional catch. Aside from material failure alone, the plastic wave now triggers the mechanisms presented in Figure 2.3, which in turn attenuate the original stress wave to a greater extent than in the homogeneous case. From an energy point of view this behavior is especially interesting. While plastic deformation occurs in all material, these various phenomena require, sometimes drastically, more energy being taken up by void collapse a grain fracture which the wave must facilitate before moving on.

While the presence of these phenomena can easily alter traditional dynamic behavior, the nail in the coffin is these processes are not a one-time occurrence within an event. During plastic wave propagation, stress bridges form via induced energy which triggers the discussed mechanisms, eventually though grains catastrophically fail. After this yielding, more voids form after which the plastic wave (before it may increase in stress and cause further damage) re-compresses the material. This results in a brand new (local) network of force chains and the process then repeats. That being the case, it is not only the presence of heterogeneity that causes such drastic bulk deviation, but the persistence of it throughout the system that has the dominating effect.

Regardless of hetero or homogeneity, the two key occurrences of elastic and plastic stress propagation happen regardless of the material (given the required amount of energy), but the way in which these manifest may be drastically different. Inevitably a certain amount of homogenous behavior is maintained regardless, but with heterogeneity breeds irreversibility and meaning mechanisms eat away at wave energy attenuating them as they radiate away from the penetrator nose. In contrast, more homogenous materials attenuate primarily through rarefaction and reflected wave interactions, in other words a plastic wave

traveling through sand would be expected to dissipate much more quickly then in a material without heterogeneity [51].

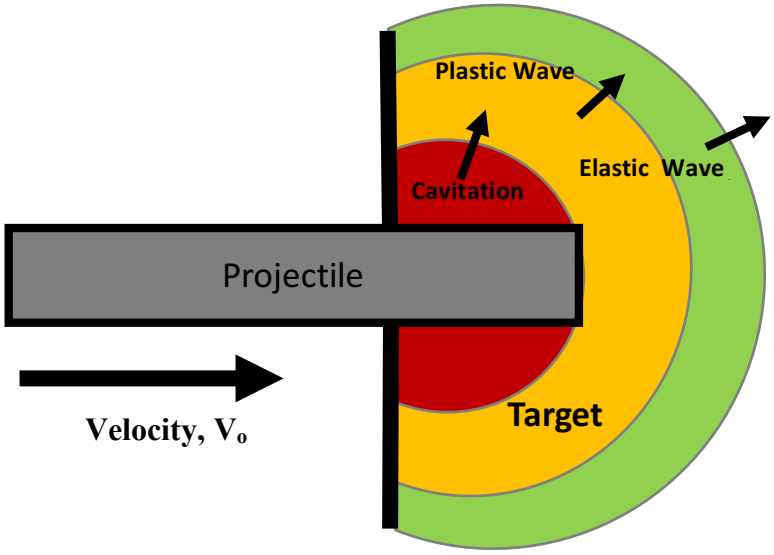

Figure 2.4 A 2D spatial schematic of elastic and plastic wave propagation away from a penetrator into a target along with associated cavitation.

Another relevant phenomenon present, though not a wave in the same sense as those previously discussed, is cavitation. Especially in systems with the ability to flow or compress, like our granular target, shear from the projectile wall during the penetration even pushes material forward and away causing cratering/cavitation. Given the propensity of granular materials to fill their containing volume (like a fluid as discussed in Chapter 1), this is fortunately almost nonexistent in sand penetration experiments *when blast air is isolated from the projectile penetration event.* All three types of waves that have been discussed so far are visualized in Figure 2.4 [32].

Up to this point, reference to destructive wave behavior has been referred to solely as elastic and plastic separately. In reality, plastic behavior and specifically its wave propagation can vary greatly depending on impact velocity. Referenced previously,

Backman and Goldsmith do a lot to define behavioral regimes defined in terms of projectile velocity as a function of material characteristics such as yield strength and Young's Modulus [31].

The major bound of interest is that of plastic deformation, or the impact velocity above which plastic behavior is expected. This is formulated as

$$V_E \leq \frac{\sigma_y(\rho_t C_{D,t}+\rho_p C_{o,p})}{(\rho_p C_{D,t})(\rho_p C_{o,p})} \qquad (2.5)$$

where σ_y is the target yield stress, ρ are the target and projectile densities, and C are sound speed formulations for solids, specifically

$$C_D = \sqrt{\frac{\lambda+2G}{\rho}},\ C_o = \sqrt{\frac{E}{\rho}} \qquad (2.6.1, 2.6.2)$$

with λ, G, and E being material elastic constants. Of course, as with any analytically determined behavioral boundary, this is more a transition zone than a defined (discontinuous) line.

Once into the plastic regime things get a little more interesting. Current analytical models treat yielding as a surface in principle stress space, meaning once at or beyond that point, the material begins to fail. However, reality is more complicated and as loading increases though, fundamental behavior begins to (sometimes very slow) shift over time. Increasing load, deviatoric stresses become negligible when compared to the thermodynamic pressure and hydrostatic stress terms, the the once solid material begins to flow as a fluid. This change can be seen in all materials at stresses high enough from aluminum and steel to heterogeneous systems including sand. Its because of this flow, that the regime is called hydrodynamics [69]. It is here we begin to see shock or hypervelocity

behavior dominate, where the elastic plastic transition begins to be neglected for solely "perfectly" plastic phenomena.

In an effort to separate these behaviors, traditional plastic behavior is separated from hydrodynamic and hypervelocity (strong shock) regions. This boundary is quite concisely represented as

$$V_P \leq \sqrt{\frac{\sigma_y}{\rho}} \qquad (2.7)$$

As with the elastic boundary, this is of course a theoretical guideline where in reality a transition occurs as principle stress dwarf deviatoric contributions.

Understanding wave propagation throughout a dynamic event is fundamental to understanding the discussed dart penetration of sand. Fortunately, wave speed and stress can be experimentally measured and used to help characterize both a target or projectile of interested. In this way, the well characterized properties of a projectile material can be used to extract those of the target or vice versa.

2.4 OVERVIEW OF EXPERIMENTAL TECHNIQUES

With a base foundation in theoretical knowledge provided, I well rounded understanding of penetration mechanics requires a brief introduction to experimental techniques, as it has been discussed at length how a majority of the discipline is devoted to empirical observations. Grounded within the realm of ballistics, penetration experiments are vastly the business of exterior and terminal ballisticians. In other words, the trajectory of the projectile to the target and the interaction thereafter [32].

Limiting ourselves to measuring only characteristics relevant to the terminal regime, a familiar set of variables is seen: velocity and stress, with the additional interest

of attack angle, penetration trajectory, and fragmentation as has been previously referenced as defining parametric values.

It the vast majority of experimental setups, the most feasible velocity metric is limited to that of the projectile itself as the target is (usually) not easily accessible. The projectile's flight itself then must be evaluated previous to entry. Currently, this can be done in one of three ways: make/break circuitry, laser optics, or electromagnetic flux. In order, make and break circuitry is a simple as it sounds. Prior to the projectile of interest penetrating the target, it is funneled through a sort of switch which either breaks a currently connected circuit, or (as is most easily done with conducting projectiles) the projectile itself or the fly by causes connection to be made thus spiking a circuit. Laser optics are quite similar, with the system being triggered when the projectile blocks laser radiation, dropping the voltage of a detector. Definitely the most intensive to setup and get "right", projectile velocity may also be conducted by passing through coils and inducing a voltage. This process, however, requires certainly electromagnetic properties be met, or in vague terms that a voltage will indeed be induced by the projectile –inferring the need for some sort of magnetic potential or even the presence of plasma, which is the case at high speeds. No matter the choice, at least two of such setups are required, and the inverse of the resulting difference in make/break time multiplied by known separation provides a velocity estimate.

Fortunately, stress is a much simpler measurement and can be acquired directly. Well countless types of gauges exist to facilitate this most rely on one of two basic principles in physics. The first examples commonly implemented are resistance gauges. While perhaps not so simple to have developed, now that they exist (and the scientific community is certainly grateful that they do), the idea is fairly basic; as a resistor is

subjected to strain (and therefore stress), the change in voltage over the resistor is proportional to stress loading, and so with a simple calibration curve the gauge may directly measure stress. Distinct from these, are piezo electric gauges. Again fortunate for the scientific community, as a piezo electric crystal (such as types of quartz) are loaded they induce voltage corresponding to load, and "eureka" another direct method of measuring stress.

Continuing onto to angle of attack, the most effective way to measure this is visually. In other words, a camera is placed near the target, facing perpendicular but ideally precisely parallel to the shot direction. Triggered correctly, the camera footage may then be uses to establish angle of attack prior to penetration. Last for consideration, are methods to acquire penetration trajectory and any fragmentation. These are truly terminal ballistic qualities are both are generally measured only after the dynamic event has concluded. Notably, this work is an exception with regard to projectile trajectory, as it is uniquely tracked during penetration due to visual accessibility.

In most setups, after the experiment the maximum penetration depth is measured and this is the metric compared to most models and used for characterization. However, in the cases where the goal is to penetrate *through* a target instead of *into* it, fragmentation (and failure in general) should be measured. This is generally accomplished two was. In-situ, a camera is placed parallel to the shot line facing the target (similar to the angle of attack setup). During penetration, any fragments may then be tracked with high speed imagery. In contrast, a simpler (and less precise) method is to place a record plate is a calculated distance behind the target. During penetration, fragments are embedded within and their scatter and size distribution may be analyzed.

3. EXPERIMENTAL SETUP

3.1 METHODOLOGY AND DESIGN

An experiment was designed in which a 12.7mm (1/2”) bore single stage gas gun was used to launch a flat faced, cylindrical dart projectile into a target tank filled with loose, dry Ottawa sand. The target tank was designed such that the two dimensional plane of the penetration event was visually accessible. This novel implementation, created by Borg et. al. [15-18], allows for a velocity and stress within the target to be uniquely characterized in-situ providing the opportunity for experimental observations previously unattainable.

The sand target consisted of 720-micron average grain diameter with a standard deviation of 170 microns and an average bulk density of 1.56g/cc. While sand is known to vary greatly in composition, this was ensured to be approximately 99% pure quartz (SiO_2) with rounded grains, and was not pretreated prior to testing. Target material was chosen as a middle ground between “real” sand seen in applications but with more consistent features in grain shape and material composition.

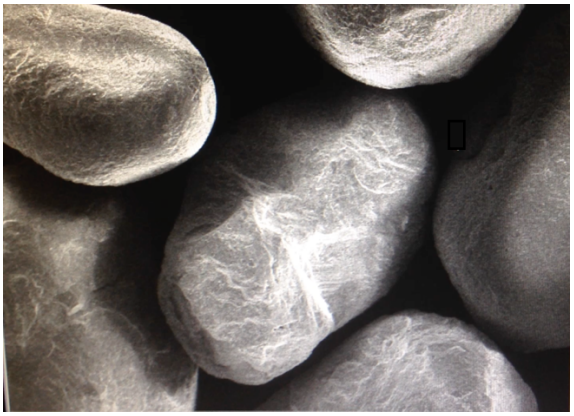

Figure 3.1 Scanning electron microscopy (SEM) of Ottawa sand (x95 magnification, 15kV). Note the consistent rounded geometry of the quartz grains.

The gas gun is capable of achieving velocities ranging from 90 to approximately 320 meters per second. Systematically, the building provided “shop” air (~100psi) is compressed and pumped, using a Haskel Gas Booster, into a reservoir which is isolated from the barrel via either a fast-acting solenoid valve (for lower end speeds), or otherwise Mylar burst disks. Using the valve, varying pressure allows for shot velocities of up to 90 m/s, after which the speed of the solenoid limits the rate at which compressed air reaches the projectile to the point at which the resultant velocity is also limited. Mylar disks remedy this, rupturing at approximately 3.45MPa (500psi) per sheet and so to increasing the velocity regime. Though this process is easily repeatable, slight variations in burst pressure do cause minimal variations in projectile velocity as not all Mylar sheets are created equally.

In our setup, the gun and tank are orientated such that the projectile is shot horizontally into the tank. Gravity is neglected as the projectile is guided by a nylon sabot, despite experiencing free flight for approximately 4 cm between the barrel and target. This is justified when considering the specific aluminum dart.

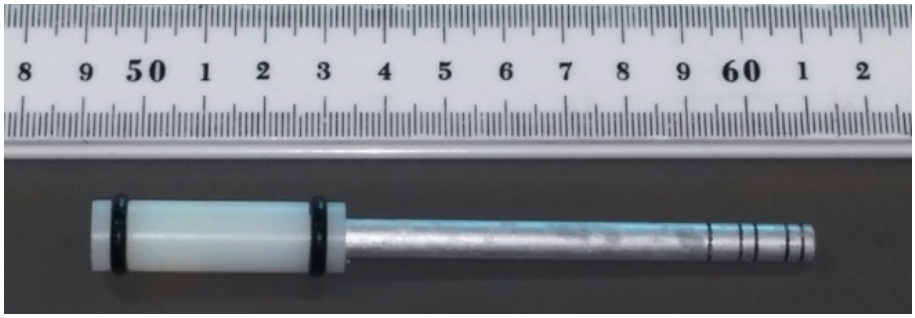

Figure 3.2 Final Aluminum dart design embedded in a Nylon sabot fixed with O-rings. Metric shown has units of centimeters.

Dimensions are such that it is a flat-faced rod .635 cm in diameter and 9 cm long, with the nylon sabot being 1.143 cm in diameter and 5cm in length. The projectile can be

seen picture in Figure 2. The dart nose can be seen to have fiducial markings used in digital image analysis discussed at length later.

The projectile is guided into a tank of sand with dimensions given as 22.9cm (shot direction) × 22.9cm x 17.8cm. Unique to these experiments, a 1cm thick (transparent) polycarbonate window served as one wall of the tank. Aligning the barrel such that the shot line was parallel to the window, on the centerline of the tank, and in near proximity (almost tangential) allowed the penetration event to be visible [15-18]. Due to this, two-dimensional high speed imagery could be taken of the experiment in-situ, enabling the qualitative observation of heterogeneous phenomena and quantitative analysis of the kinetics at play within the target.

As polycarbonate has a comparable impedance to that of the quartz grains, boundary effects of the window are assumed to be minimal, with other (tank) boundaries assumed to be far enough away from the penetration event to be considered semi-infinite. This is sufficient as the main objective is focused on granular interactions closer to the dynamic event and not far field interactions. Figure 3.3 shows the visually accessible sand tank completely assembled prior to an experiment.

Figure 3.3 Target tank aligned with the stripper box and gun barrel. Not visible, a stress gauge is embedded in the sand below the shot line.

A stripper box, which may also be seen in Figure 3.3 and 3.4, was designed and placed between the barrel and target tank. In conjunction with housing break pins for projectile velocity measurement, this serves to strip the sabot from the dart as it hits the target. The sabot isn't stripped until it hits the back wall (labeled the stripper plate). The stripper plate has a tapered hole with diameter greater than that of the dart, but less than that of the sabot catches while the dart passes through.

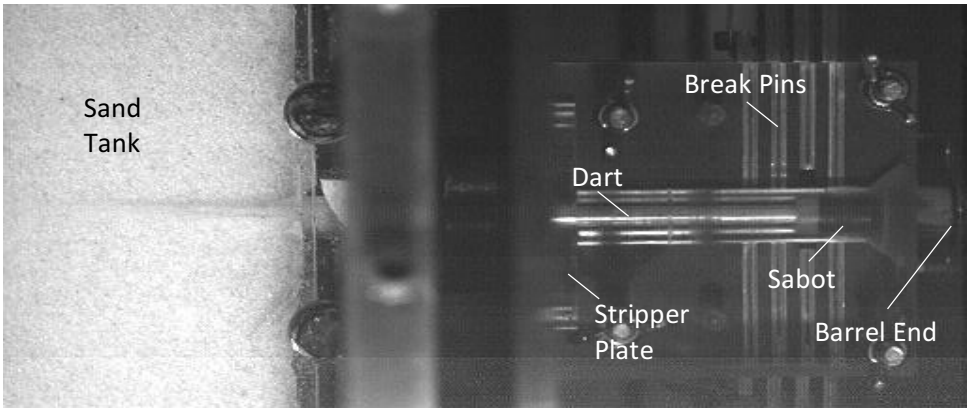

Figure 3.4 An alternative orientation showing the gun, velocity block, and sand tank aligned. The dart and sabot can be seen passing through the break pin circuit.

This also serves to "guide" the dart/sabot into the velocity block to make sure the dart is consistently aligned as it enters the sand tank. The sabot then plugs the hole in the stripper plate, blocking air from entering the sand pit. This blast air was seen in initial experimentation, and greatly altered results as the pre-cavitation caused by the air allowed greater penetration but not due to projectile interaction. Additionally, dart dimensions were such that the sabot actually breaks the velocity pins and *not* the dart itself, which meant (given spacing) projectile velocity was measured *at* penetration.

To complete the experimental setup, the various measurement diagnostics are implemented including a quartz piezo-electric stress gauge within the sand target and a

high speed camera placed normal to the visually accessible tank wall. These described in great detail in the next section, but a view of the complete experiment ready to go may be seen in Figure 3.5.

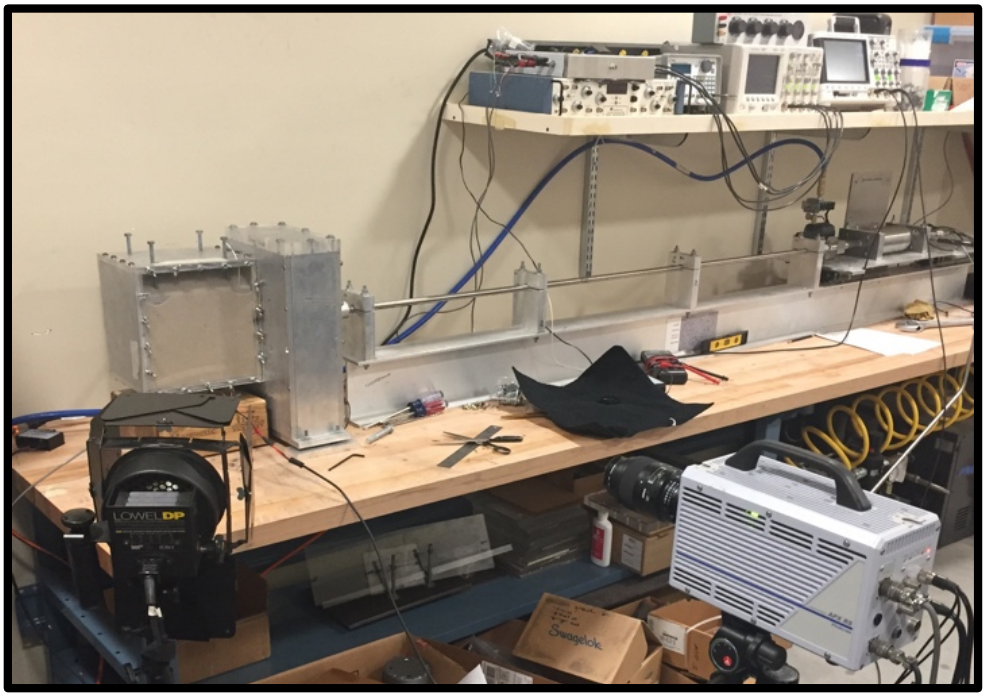

Figure 3.5 Final experimental setup showing the ½" bore gas gun, stripper box, visually accessible sand tank, and the high speed digital camera setup.

3.2 INSTRUMENTATION AND DATA ACQUISITION

3.2.1 Piezoelectric Stress Measurement

Many different types of gauges were tested to accurately measure the stress wave transmitted through sand by burying them directly in the target, free floating. These included Vishay Manganin strain gauges, Tekscan's FlexiForce piezoresistive gauges, and PCB Piezotronics 208C01 load cells. Hydrostatic and atmospheric pressures were calibrated out leaving only the transmitted wave to be detected. Initial testing was done

using this free floating method and compared to other gauges which were fixed in place. When the gauges were free, they would "flow" with the sand throughout the event. While this may be more representative of what the sand experienced, this does not tell us the true strength of the transmitted stress from penetration.

With this in mind, a fixed gauge set up was decided on, using a Kistler 211B2 transducer. Assuming radial wave propagation from the shot line, the gauge is set 4.445cm (1.75") directly below the target line and 3.81cm (1.5") from the target entrance wall, with a transducer sensitivity of 1.133mV/psi.

3.2.2 High Speed Camera Setup and Description

Implicit in the experimental method used here, a large portion of this work is dependent on high speed photography and the resulting image processing. Logically then, things like camera setup, image resolution, field of view, and even lighting become critical to good data acquisition. Before detailing the specifics required in camera usage, it is necessary to narrate two distinct setups corresponding with exploring two length scales.

The first and primary setup is relevant to the more bulk or continuum view field of view. These experiments were done with the Photron APS-RX digital camera at the Marquette University Shock Physics Lab. Capable of up to 250,000 frames per second (fps) and a maximum resolution of 1024x1024 pixels. Increasing the fps of course requiring a decrease in the available resolution. In general, 10 to 12 thousand fps was used as a compromise to achieve a 512x1024 pixel resolution resulting in an approximately 30cm by 61cm field of view (FOV), with the camera being physically placed approximately 68.6cm from the target wall. This allowed for approximately 8-12 frames of the dart nose within

the frame of view (depending on shot velocity), and resolution in accordance with about 4 pixels per sand grain. Increasing fps would of course increase temporal resolution, but with the decrement in spatial view and so this arrangement was deemed acceptable.

In the interest of investigating a lower length scale (grain level), spatial frame of view was willingly sacrificed but introduced a new problem: the available Photron camera could not only resolve that space, but could get at most only a single image or two of the penetration event. It was to remedy this issue, that the Naval Surface Warfare Center at Indian Head, Maryland was kind enough to allow us access to their facilities, particularly their Cordin 550 Camera. A rotating mirror camera, the Cordin had the necessary capabilities to capture very small fields of view. This camera can a (number of mirrors) maximum of 64 images with a high resolution of 1000x1000 pixels and fps ranging from 120,000 to over 1,000,000. For our setup, we used 400,00 fps with a field of view at approximately 5cm x 5cm, resolving to about 40 pixels per grain.

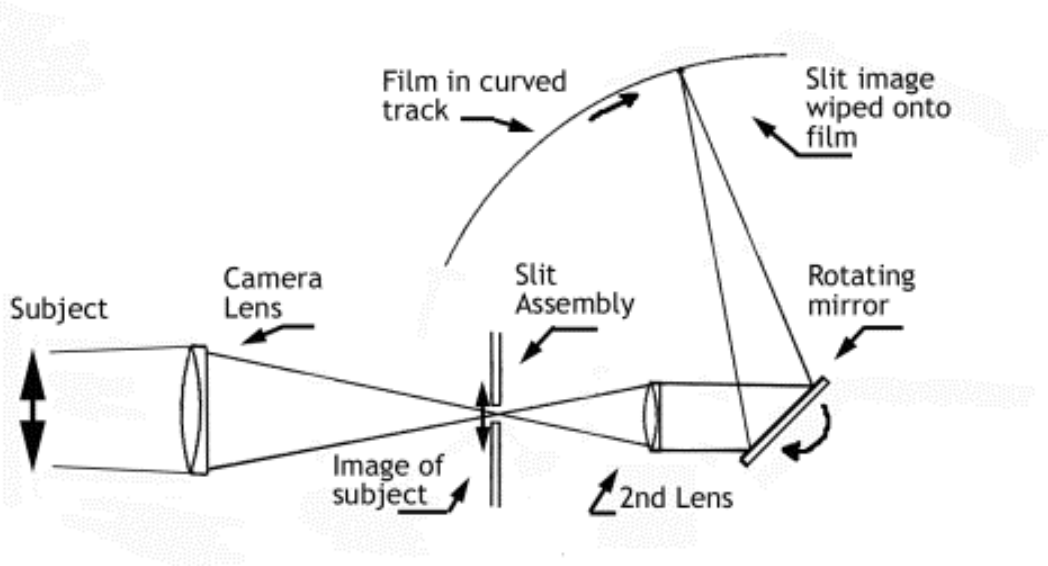

Figure 3.6 Schematic description of a rotating mirror camera [70]. A mirror is physically spun at high rotational velocity to embedding image light onto a finite number of chips to obtain very high frames per second. For the Cordin 550, these settings ranged from 120,000 up to 1,000,000 fps, with 64 available frames.

With such a high acquisition rates in both cases, light exposure time is very small (on the order of microseconds) and thus additional lighting to supplement room light is essential. use of a time triggered flash halogen light. When using the Photron camera a 1kW LowelDP light is adequate, whereas with the Cordin a halogen flash lamp was required which was had to be triggered mid-experiment due to its 120 microsecond long flash duration.

3.2.3 Triggering and Synchronization

The synchronization of data and more so the ability to capture these events which occur on the order of microseconds created the need for a coordinated triggering system. This is best presented by example, so a brief walkthrough of a typical experimental run is provided.

The projectile is first launched, leaves the barrel first encountering the graphite break pins within the stripper box used to measure projectile velocity. These pins are embedded into a break circuit measured on a near by oscilloscope. Next, the projectile begins to penetrate at which point it punctures a make switch set between the threshold of the stripper box and target tank. This, in turn, triggers both an oscilloscope to begin acquiring stress data from the transducer while simultaneously initiating the camera to begin recording. This ensures the stress and high speed imagery maintain temporal synchronization.

While implementing the acquisition systems was fairly straightforward, efficiently capturing each penetration did require preliminary estimation of projectile velocity for both frames per second calculations and for triggering the halogen lamp with the Cordin setup.

This was facilitated via basic Newtonian physics calculations based on the known burst pressures for Mylar disks, with later predictions based on shared experience. The process can be seen from beginning to end schematically pictured in Figure 3.7.

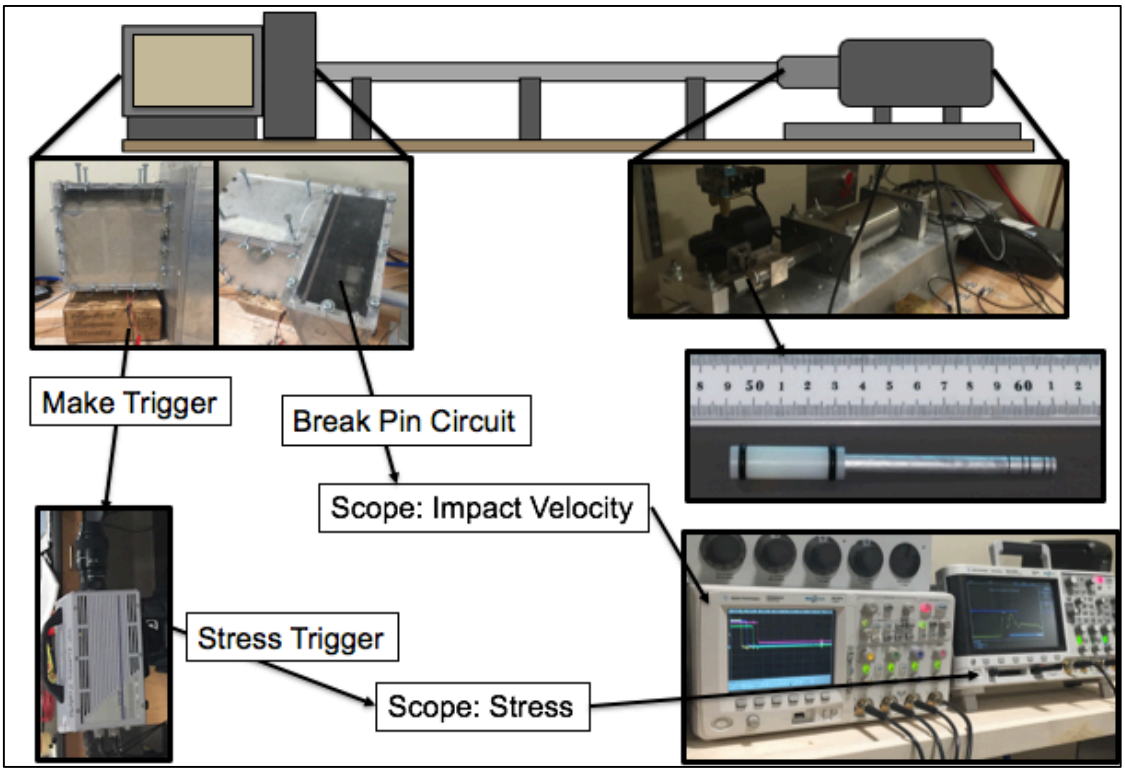

Figure 3.7. Schematic view of a typical experimental setup including triggering and data acquisition methods.

4. DATA ANALYSIS AND PROCESSING

The described experimental procedure yields two distinct sources of data useful to analyze the ballistic dart penetration into sand: stress via a transducer, and the high speed (digital) photographic record. While the first may be used analyze the system directly, the later requires additional processing which, luckily, has a whole field of clever individuals devoted to it: digital image processing. Used in this work specifically, is an algorithmic technique called Digital Image Correlation (DIC), which systematically compares sequential images to quantify any changes. The process itself may be used to extrapolate a great deal of physical information, including deformation, displacement, optical flow, and even instance strain (as is done in much of Iskander's work [66-68]). Keeping our motivation in mind, this study will use DIC to derive spatially and temporally resolved velocity fields in a process termed Particle Image Velocity (PIV). This section endeavors to describe this method to the extent necessary to understand how results were derived and their inherent limitations. To drive the point home, a single experiment will be processed from beginning to end, with all other results presented thereafter assumed to have undergone the same process with any and all deviations specified.

4.1 INTRODUCTION TO PARTICLE IMAGE VELOCIMETRY

The application of DIC specifically known as Particle Image Velocimetry (PIV), compares temporally sequential images and, based on changes in pixel values, extrapolates a velocity field. This post processing technique comes in several different flavors using software such as *LaVision*, *OpenPIV, mPIV,* or several other brands, all of which have their own unique strengths and weakness. All data here was analyzed via *mPIV*, chosen due to

its MATLAB script-based format enabling easy alteration of the program for our customized purposes. There are many excellent sources for full, in-depth, discussions on PIV and DIC techniques in general [71-74], which are highly recommended, but in the interest of brevity only a short explanation will be provided here.

Best termed through example, the PIV method begins with the isolation of two images in sequence lets call them *image 1* and *image 2*, where *image 2* was collected directly after *image 1* after some interval of time (frame rate). Each image can be considered a simple matrix, lets call them *A* and *B,* of numbers each element ranging from $0 - 2^n$, where *n* is the bits of your camera, or in the case of this work $n=8$, therefore each matrix entry ranges from 0-256 based on grayscale color. These matrices are $g \times h$ in size where *g* and *h* describe the resolution (in pixels) in the x and y directions respectively.

The PIV method places a mesh (coined interrogation windows) over these images dividing every overall image matrix into subset matrices. Each interrogation window will, at the conclusion of the algorithm, be assigned a single velocity vector which is representative of that area. The primary customizable aspect of PIV, therefore, becomes changing the interrogation window size to match the desired velocity field resolution which can be done at the expense of both computational power and at some point convergence.

A visual example (seen in Figure 4.1) taken from Borg [17], shows a visually accessible region of the sand target taken 2.5 microseconds apart. This particular sample was captured with the Cordin camera at the NSWC Indian Head facility, thus the high resolution (~70 pixels per grain diameter). The grid imposed serves as an example interrogation window mesh two of which, corresponding to one another, are emphasized in red and blown up to view side by side.

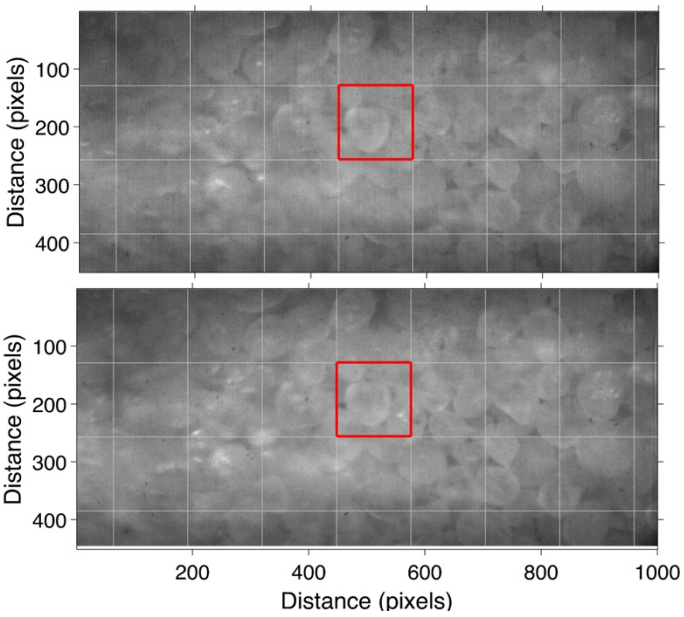

Figure 4.1a Two succesive example images of a grain scale field of view obtained 2.5 µs (1/fps) apart. The superimposed grid represents a interogation window grid of a user specified 130 by 130 pixel resolution.

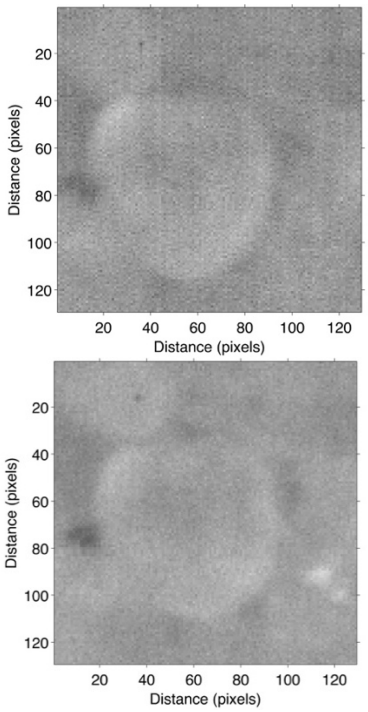

Figure 4.1b The individual interrogation windows shown in the Figure 6a, blown up for comparison.

These individual interrogation windows are consequently overlaid on top of each other and compared (via a correlation algorithm) shifting pixel by pixel in an effort to find a maximum likeness, in other words, how much does *image 2* need to be shifted in the x and y directions to best match *image 1*, as seen in Figure 4.2.

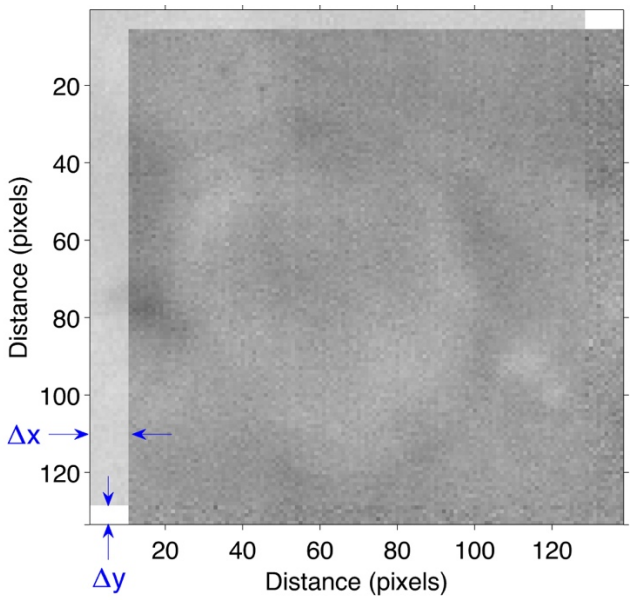

Figure 4.2 Interrogation windows indicated previously in red, superimposed with translation of Δx and Δy corresponding to a maximum correlation value.

Mathematically, there are many of potential ways to calculate correlation, only one of which will be presented here being the relevant method used throughout experimentation. Called the *Minimum Quadric Difference* (MQD) method, correlation is found implementing the following algorithm,

$$C_{MQD}\left(\Delta x,\Delta y\right)=\left[\sum_{i=1}^{N}\sum_{j=1}^{N}\left[\left[f_1\left(x_i,y_j\right)-\bar{f}\right]-\left[f_2\left(x_i+\Delta x,y_j+\Delta y\right)-\bar{f}\right]\right]\right]^{-1} \tag{4.1}$$

Necessary to employ this method, f_i and f_j are an interrogation window from an image pair. The $\bar{f}$ value is the pixel-to-pixel ensemble average calculated by taking the image pixel averages of a set of unchanging calibration images of the sand target. Embedded in the mathematical relation, this is subtracted from the image of interest to reduce noise which will be discussed at length later. The size of the interrogation window (with regard to both directions) in pixels, *N,* depends on the camera setup and is something selected and may

be tuned by the user. As is apparent, this correlation coefficient is a function of displacement in both Δx and Δy offset. When applied to the example set, the resulting 3D visualization can by seen in Figure 4.3.

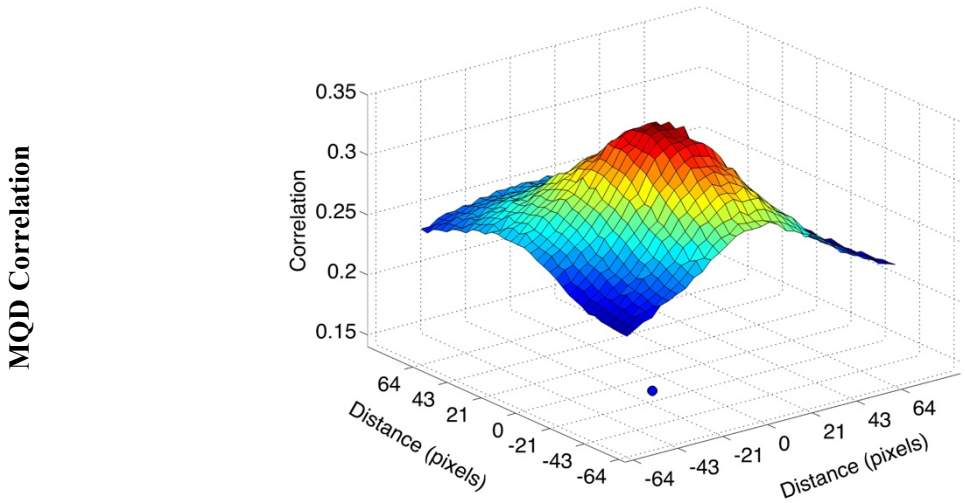

Figure 4.3 The MQD Correlation method applied to interrogation windows presented in Figure 4.2. The x-y displacement showing maximum correlation is displayed on the bottom x-y surface as a blue dot.

As mentioned, there are endless ways to go about this correlation process, so the obvious question is why choose this? The answer is simply the robustness embedded in the mathematical approach. Whereas a great deal of correlation techniques rely on, primarily, multiplicative operations, MQD is entirely addition and subtraction (other than the entire equation being inverted). This implicitly allows for convergence even in the presence of noise, whereas other methods would "blow up" in error due to magnification done by multiplication. Of course this is not full proof as divergence to infinity is still possible, but it does help considerable.

MQD is unfortunately not without cost. The same mathematic mechanism which ensure robust applicability also reduce its effectiveness. The entire point of the correlation process is to quantify differences an identify where this is minimized. That being the case,

multiplication also magnifies valid differences to a greater degree making correlation sharper. As exemplified in Figure 8, MQD has a rounded (mountain-like) appearance making the maximized correlation less apparent. Adding to this issue, the analog process that is the true penetration event may result in an optimum display that is a subpixel value. To facilitate this possibility, additional numerical approximation can be used in the form of Gaussian curve fitting, provided below, from which a more precise displacement, resolved to a sub-pixel level, may be found and thus yield a more accurate approximation of the true velocity field.

$$\Delta x_{\max} = \Delta x_{\max,i} - \frac{1}{2}\left(\frac{\ln \Delta x_{i+1} - \ln \Delta x_{i-1}}{\ln \Delta x_{i+1} - \ln \Delta x_i + \ln \Delta x_{i-1}}\right) \tag{4.2}$$

Regardless of method, the resulting maximum yields to a corresponding maximum x and y offset that corresponds to maximum correlation. These offsets, to be physically meaningful are converted from pixels to meters via a scale calibration image, often a snapshot of the FOV with a ruler within it. These displacements are then divided by the known time difference (1/fps) then yield an experimental velocity vector (m/s) for that area of the interrogation window. Repeating the process for all interrogation windows yields a vector for each one and thus a time varying velocity field for the entire image over the course of the penetration event.

It is here some unavoidable limitations may start to be seen, in that the velocity field is only as resolved as the interrogation window mesh and cannot be assumed to represent more localized characteristics such as individual grain movements or grain rotation for that matter. While reducing window size does indeed increase the spatial resolution of the overall domain, this is not limitless and become divergent algorithmically

long before computational demands dominate. The velocity field temporal resolution is unfortunately even worst off as time is discretized by the cameras frame rate. No part of the method can increase this resolution, but only by increasing the camera fps. Additionally, each PIV calculated vector field requires two images as input and so in a set of 10 frames only 9 time varying steps will be found.

In an effort to combat this, a parametric game can be played with various aspects of the algorithm in which results can be pseudo-optimized within the realm of discussed limitations. To that end, several notes regarding implementation are detailed hereafter explaining how to "play" this game.

4.2 IMPLEMENTAION AND USEFUL PARAMETERS

Fortunate for those of us without a large background in software engineering, implementing PIV is as simple applying a MATLAB black-box script and toolbox to a series of images. However, the resulting data could potentially be invalid without understanding the background above, and preferably to an even greater extent than that (as may be facilitated by listed sources). It is only through that understanding, and even more so through practice, that application may be done correctly and physically meaningful results may be found. Of the many subtleties that make PIV successful, three of the most imperative parameters and how to best use them are described in this section including interrogation window size, window overlap, and recursion.

Being the most critical, first consider the dimensions of the interrogation windows themselves. The entire method is reliant on comparing their sequential frames, and the spatial resolution of the entire velocity field depends only on this choice. With that

statement alone, the natural inclination would be to have windows as small as computationally feasible. Unfortunately, this is guaranteed to eliminate any hope of the method converging. The correlation algorithm itself is dependent on quantifying the differences in images and minimize that (maximizing likeness) at a found displacement. If an interrogation window were, say, smaller than grain, then two scenarios become plausible.

The first is if displacement is small between frames, in which both interrogation windows would visually see almost the exact same image; the face of the grain itself. The grain looking nearly identical in both positions mathematical results in no difference being detected and thus a meaningless velocity of zero being calculated. Generalizing to non-sand specimens, on a continuum scale it would always be possible to zoom in close enough to where no change would be apparent and thus the same problem persists.

Alternatively, at a given window size, displacement could be too great between sequential frames resulting in the first window viewing a grain and in the next none (of the grains previously viewed) are present. The algorithm then either searches endlessly never finding an adequate correlation, or yields a false positive assuming one grain corresponds to an entirely different one. Both are nonphysical and thus nullify any knowledge of the velocity field within the bounds of that window.

While this circumstance certainly limits the resolution that can be achieved, it also gives us a suggestion in which to avoid the problem. The rules are simple, choose the smallest interrogation window size possible in which at least one grain remains between two frames. Luckily, applying PIV is a post-processing measure and so the sequence of images associated with each experiment is readily available prior to analysis. All that is

necessary then is to view each shot record observe the distance traveled by a grain (in pixels) throughout the event. Keeping in mind also the size of a grain, the user may then make an estimate of appropriate window size. For example, lets say, in an experimental penetration event, a grain (4 pixels in diameter) moves approximately 12 pixels at most between frames. An educated estimate would then be to set interrogation window dimensions at about 16 by 16 pixels ensuring grains would be kept within the same window for at least two frames.

Given 2^n is the common basis for computational size and structure, window sizes are generally chosen by some factor 2^n, most prevalent being 16x16, 32x32, or occasionally even 64x64 or higher for resolution images.

Even with an appropriate window size chosen, a dense interrogation mesh can often times be computationally intensive, especially when criteria imposed to ensure accuracy are applied (discussed at length in the next section). This isn't too hard to imagine as each window must be compared pixel by pixel to its predecessor. To decrease computation time without sacrificing resolution an overlap method may be utilized.

Instead of having a uniformly spaced, grid-like mesh of interrogation windows, as was first presented, windows may be allowed to overlap each other. Say you have an overlap of 0.5 (50%) in both the x and y direction this effectively doubles resolution, but is much more computationally intensive and aids in convergence as contrast between frames is more likely to be detected in a large area window. If windows are set to overlap at all it is generally less than or equal to 0.5 otherwise the computational advantage is more or less lost and a decrease window size is recommended.

Similarly, a sort of opposite approach can be taken, starting high resolution and instead limiting pixel comparison. Ideal with larger fields of view (small grain pixel sizes), if it becomes apparent that even with lower resolution grains are translating minimally between frames then (to reduce computational requirements), the algorithm can be told to only compare sequential windows by a maximum displacement amount. Imagine two windows, to be compared, begin completely superimposed. This parameter would limit the algorithm to displace the second image a maximum number of pixels in any x or y direction instead of every pixel by pixel comparison, greatly reducing the necessary number of operations.

Lastly in this non-comprehensive list of useful parameters, is the process of recursion through which the accuracy of the correlation algorithm itself can be improved. In addition to the single correlation the original algorithm performs on each image a recursion iteration ('n' number of recursions may be performed) performs two additional operations iteratively reducing the interrogation window size by 2^n. Not only does this decrease the window size (increasing resolution), but each subsequent recursion is centered on the previous displacement point at which maximum correlation was found, steepening the peak. This can drastically increase the Signal-to-Noise Ratio (SNR), discussed at length in *Section 4.3*, a metric of overall image noise and achieving a much greater level of accuracy. It should be noted though, that the limitations of interrogation window size regarding convergence still apply and as such it is often necessary to start large and iterate down to a window size known to be acceptable otherwise convergence may not occur.

Most important when applying PIV to the experiment set, holding true for any scientific investigation, was validation. Looking back on various discussions in this

chapter, there are huge opportunities for error to be introduced into the analysis and blur the nonphysical trends with any potential physical results. As such, validation with experimental benchmarks becomes the only way to "know" such results are realistic.

In the case of PIV, the best way to do so was to have the algorithm calculate a velocity of something known to the experimentalist, in this case projectile velocity. Fiduciary marks, mentioned previously, were placed on the dart nose at known distances. In the first frames of the shot, the dart may be seen during initial penetration. PIV is applied to this and an average velocity is found which should correspond to the projectile velocity recorded by the break circuit. As an additional check, the time between frames was known along with a length scale and so a hand calculation could also be made. With these corresponding, the velocity field results could be considered with more confidence.

4.3 ERROR, NOISE, AND INTERPOLATION

As with all e50xperimentation there is a certain amount of error present, both systematic and random. In the case of the digital analysis used here, systematic error was vastly due to image noise commonly caused by issues with depth of field (camera focus), lighting, and in the worst cases physical jitter, with the latter being the most disruptive. Focus and lighting could generally be prevented with cautious setup prior to a shot, whereas jitter was a somewhat unavoidable result of the rotating mirror method utilized by the Cordin camera. Due to extended use, the physical chips in the rotating setup were slightly misaligned causing the collected images to be skewed either via translation or rotation, resulting in artificial velocity and vorticity when PIV was applied. Fortunately, this wasn't an issue for the Photron, but an unavoidable hurdle to cross when analysis on

shorter length scales was desired. Correcting for misalignment and other sources of noise therefore became a priority with several techniques used.

Leaving jitter for later, due diligence was taken to assure camera lighting was adequate and depth of field was appropriate to observe each shot. Despite this, every image has a certain amount of floor noise associated with pixel values which, lumped with any remnant light and focus error, are attributed to random deviance. This issues being well known, the *mPIV* toolbox comes with several useful features meant to ensure accurate data.

A prime example of these is the signal to noise or SNR criteria, which was mentioned briefly in the previous section. Here we now define the SNR as

$$SNR = \left(f_{i,\max} - f_{i,\min}\right) \Big/ \frac{1}{N}\sum_{i=1}^{N}\sqrt{\left(f_i - \bar{f}\right)^2} \tag{4.3}$$

with definitions from the MQD correlation algorithm holding. This metric compares floor noise, defined as the standard deviation of image pixels, to maximum and minimum pixel values. Implementing this, a minimum SNR is specified for a given correlation ensuring any corresponding displacement values are a threshold above floor noise.

An additional side-effect of a (high) noise floor, once a peak correlation is identified, it is not always trivial to determine which is the true maximum. Especially in methods such as the MQD, either the maximum is smeared over a large number of pixels or other peaks could exist nearly as dominate. To address this a Peak to Peak Ratio Criteria (PPR) was implemented. Easily applied, this requires a peak to be $\sqrt{3n_x}/2.5$ pixels from another maximum to be considered distinct while the largest peak must be 1.1 times higher than its highest competition to be considered maximum. If this does not occur, then no

vector is assigned meaning divergence and either algorithm settings must be changed, noise eliminated in an alternative way, or that window neglected is neglected altogether.

A last safeguard, similar to the PPR and SNR, the maximum to mean ratio (MMR) criteria is an additional measure to ensure the peak is significantly above the noise floor in this case by comparing the pixel-to-pixel average. For the purposes of this study, at least 10% or greater was considered satisfactory.

Despite the many techniques used to encourage the convergence of all interrogation windows to a final value, divergence was not an uncommon issue. With great care taken, *most* of each velocity field converged, but almost every frame included a few windows too ill conditioned to achieve convergence. Interestingly, these cases were often due the heterogeneous behaviors which make sand so interesting in the first place. Specifically, grain interactions, fracture and void collapse particularly, were too complex to be resolved by PIV and thus left that window "velocity-less". While not indicative of the real behavior observed, gaps could, and at times were, approximated using standard interpolation techniques from neighboring cells. This were provided directly in the tool box and included linear, cubic, and spline fits as default options.

With other error sources adequately addressed, it is necessary now to return attention to jitter. As previously mentioned, this problem was nonexistent when using the Photron, but unavoidable when using the Cordin camera to experiment on a lower length scale. Due to logistical constraints, the camera itself could not be recalibrated and instead a post-processing technique was developed. After initial experimentation, the frame-to-frame jitter associated with each camera run was observed to be consistent between separate runs. Under this assumption it was thought a sequence of transformation (rotation)

matrices could be developed for each of the 64 frames bringing each image back to the same (first image) reference frame. To facilitate this, a *MATLAB* script was written (utilizing the *imwarp* function) which compares two of the same images (one skewed from the other) and yields a transformation matrix which when utilized rotates the second image such that it matches the original. A series of calibration images were therefore taken on the Cordin on which this script was applied resulting in a transformation matrix for each image.

While not completely eliminated, this did greatly reduce the the visible jitter, allowing reasonable analysis to be conducted on the digital images. Validation, conducted as in previous cases already discussed, confirmed PIV was now in the right ball-park but the persistence of jitter error. Detailed to a greater extent in the *Chapter 5*, this imposed much greater limitations when observing the penetration event on a grain scale, though key insights could still be made.

4.4 REPRESENTATIVE PIV POST PROCESSING

Given the shear amount of information involved in each ballistic penetration of a dart into sand, analysis for only a single shot will be shown here from beginning to end, with the same process assumed for each trial conducted thereafter and any potential differences stated. Results and conclusions reached from each portion of analysis will be discussed at length separately in *Chapter 5*.

The presented representative shot was conducted utilizing no Mylar burst disks, but instead relied solely on actuating the solenoid valve releasing reservoir pressure to the projectile loaded into the barrel. The resulting projectile velocity achieved was 127 meters per second as per the break pin circuit. Photron camera settings were 10,000 frames per

second (one tenth of a millisecond between each frame) with a shutter speed of 1/500,000. Given the dart speed, about 10 frames were captured containing the dart nose before it passed beyond the field of view. It should be noted here that most experiments run at this field of view used either 10 or 12,000 fps (depending on shot velocity), with this particular shot done at the lesser setting. The camera's field of view was about 11x10 cm resulting in a grain to pixel ratio of about 4 pixels per grain, this too was consistent across trials. As planned, the dart fired, all triggers were activated and both high speed photographic and stress data were obtained. Only the processing of the former will be described here as results from stress may be interpreted directly.

Continuing on, particle image velocimetry was then performed with interrogation window dimensions of 32 by 32 pixels, 1 recursive iteration, and Kriging interpolation used to fill divergent windows. As mentioned, the smaller the interrogation window, the more highly resolved the flow field is, but too small a window can lead to possible convergence issues if at least one single grain doesn't persist through two sequential frames, thus the larger size and one recursion (increasing accuracy and likelihood of convergence). With each shot being slightly different the size of interrogation window and recursion techniques vary slightly with regard to the rest of the experimental set.

With the described settings, the PIV script algorithmically calculated a 2D velocity field temporally resolved every two images throughout the penetration event. Overlaying the PIV velocity field on the corresponding shot images the sequence in Figure 4.4 is created. Note, beginning at time zero for initial penetration the dart (nose) and associated wave of interested is in the field of view for about 1.2 milliseconds, four of the nine relevant PIV images are shown for convenience. Axes have been scaled such that the shot line is at

y equal to zero. In the final image the dart velocity is shown resolved estimated at 120 meters per second and considered acceptable for validation.

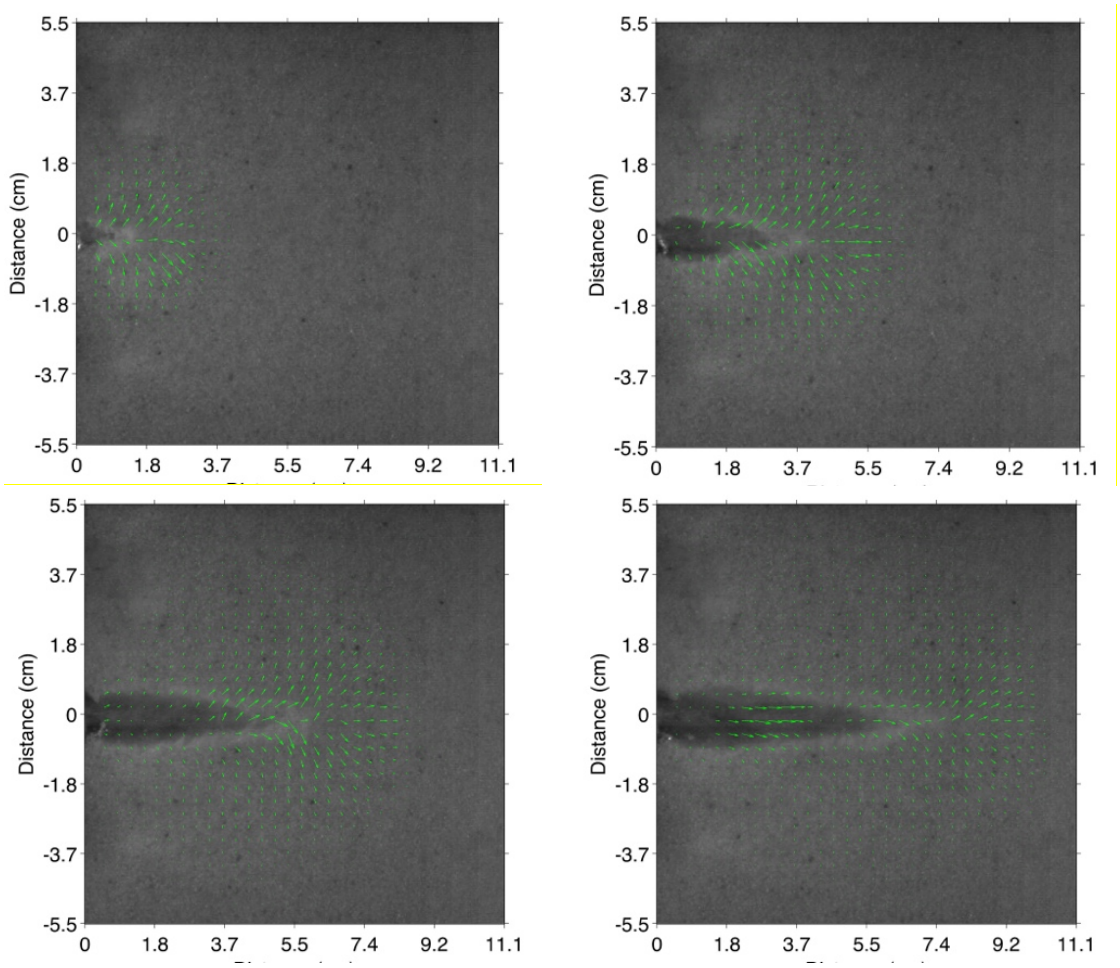

Figure 4.4 PIV derived velocity field sequentially shown. Settings: 127 m/s shot velocity, 10,000 fps, 32x32 pixel resolution. At time 0 (initial penetration), 0.4, 0.8, and 1.2 milliseconds respectively.

This initial visualization is most useful as a proof of concept as the velocity field is indeed resolved, it is worth noting that the vectors visualized are scaled to the dominate velocities present in each individual frame, the magnitude of which can not be visually interpreted in this form. This is particularly evident when the dart velocity is resolved, as the remaining vectors (and generally the ones of most interest) are visually scaled back and become barely visible.

With this in mind, the magnitude of the velocity is found and the vector field is replaced with a contour map. For increased comparative efficiency, the velocity magnitude is further normalized by the projectile velocity. This results in a more visual presentation of the velocities seen, the result of which (on the same sequence of frames) are shown in Figure 4.5. As can be seen when referencing Figure 4.4, the entire field of view is slightly larger than the axis shown. All the action happens within a smaller window (about 3 by 5cm of the dart nose) and so the view was cropped to get a better look. In a pseudo-Lagrangian, and to take advantage of the large FOV, the window follows the dart nose as can be seen by the shifted axes.

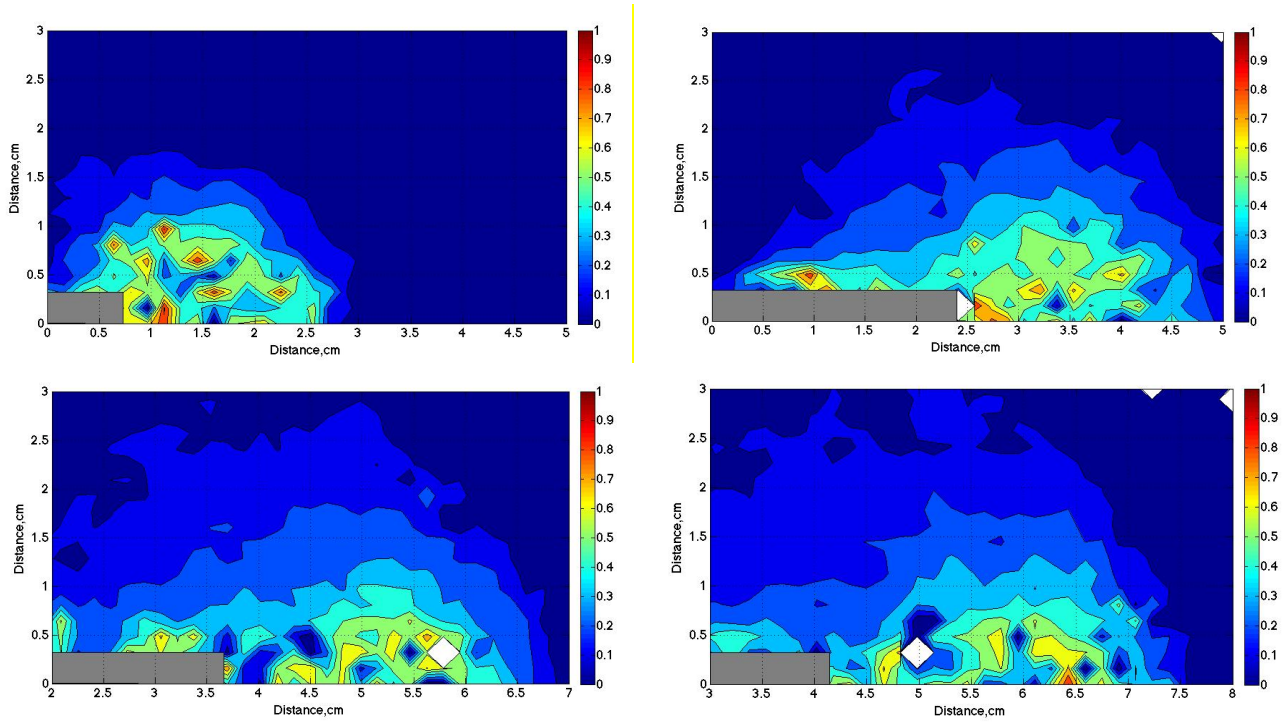

Figure 4.5 A contour plot of the same sequence of images normalized with projectile velocity. Consistent with Figure 4.4, these frames are at time 0.4, 0.8, and 1.2 milliseconds respectively from top left to bottom right.

Note the dart is superimposed to give the viewer a sense of orientation and, while the entire field is processed, only the top half of the field is shown to allow a more focused

view (acceptable as symmetry as maintained). Calculated velocity values have been normalized by taken the magnitude of x and y components and additionally dividing by projectile velocity. This allows for a fairer judgement when comparing across multiple shot velocities.

From these plots, the diffusion of momentum from a dart projectile into a sand target can be quantified, in-situ, and used to better understand system behavior. Alongside additional stress information from the embedded transducer, this provides a previously nonexistent opportunity to develop predictive relationships both by correlating observed behavior, and by providing an experimental metric by which computational simulations may be validated. The implications of this technique are explored thoroughly in the following results section in which several approaches are taken to ensure the various potential inherent in the method is understood.

5. EXPERIMENTAL RESULTS AND DISCUSSION

Now that the experimental methodologies have been explained in full including a discussion of post processing using DIC, a comprehensive report of results is presented. The experimental setup in Chapter 2 was used to launch the aluminum dart projectile into the Ottawa sand target at velocities ranging from approximately 120 to the equipment's currently tested limit of about 320 meters per second. Results initially presented were conducted with a FOV of approximately 11x11cm such that bulk, continuum behavior could be analyzed. Results from an additional set of tests (over the same range of penetration velocities) have a magnified FOV (5x5cm or less), to view grain scale interactions. As alluded to previously, the results with a lesser FOV could not be post processed because of the higher noise floor leading to a lack of adequate validation, however valuable qualitative observations were still possible. This will be discussed at length in *Investigating the Grain Scale*.

Given the large number of shots were done over the course of years [15-18], some associated with optimizing the experimental setup itself, in many cases the data presented will be compressed to aid in visual presentation and discussion. This chapter is structured such that, first, DIC analysis results from bulk scale experimentation are shown over the entire range of tested projectile velocities, with qualitative observations discussed. Taking the next step, the DIC results were utilized to quantify in-situ velocity behavior via numerical approximation of the derived vector fields.

Next, this velocity analysis is linked to stress gauge measurements, with particular attention devoted to identifying self similar behaviors across the tested velocity regime and connecting velocity field behavior with stress wave structure. Throughout the chapter,

discussions of heterogeneous mechanisms present in the data and how they may manifest will be included.

Lastly, *Section 5.3* will be devoted solely to observations seen on the grain scale. Of specific concern are whether observed, qualitative results correspond well with those seen on the bulk scale. The adequacy of the method itself, and how it resolves such behaviors is also considered. Limitations will be revisited, along with additional connections to irreversible processes observed.

5.1 CHARACTERIZATION OF IN SITU VELOCITY BEHAVIOR

5.1.1 Qualitative Observations

As planned, first we compare the results of the DIC post processing for all shot velocities. The most effective way to accomplish this is by choosing a representative set consisting of four individual experiments ranging from 127 to 310 meters per second as are presented in Figure 5.1. As was proved in the *Section 4.4,* these results are shown side by side as contour plots of velocity magnitude normalized by projectile velocity.

The particular plots shown are all taken at approximately the same penetration depth, though not quite exact due to temporal discretization. These all also correspond to the frame immediately after initial penetration (when the dart first enters the FOV), at which point momentum transfer appears in it's full "glory" both near the nose and propagating into the target.

Not fully detailed earlier, it is important to note that, in these results, kriging interpolation was used but only if the converged displacement values were within three standard deviations of the average set of that from. Doing this, ensures that any sort of

"glitch" fails will be ignored while significant behavioral deviations can still be detected such as grain fracture or void collapse. In other words, the few divergent outlier frames that could not adequately correlate motion because of issues detecting pixel differences (or grains not remaining within the same window) are interpolated, otherwise real behaviors due to physical effects like plasticity are still not resolved, more true to the method's actual limitations.

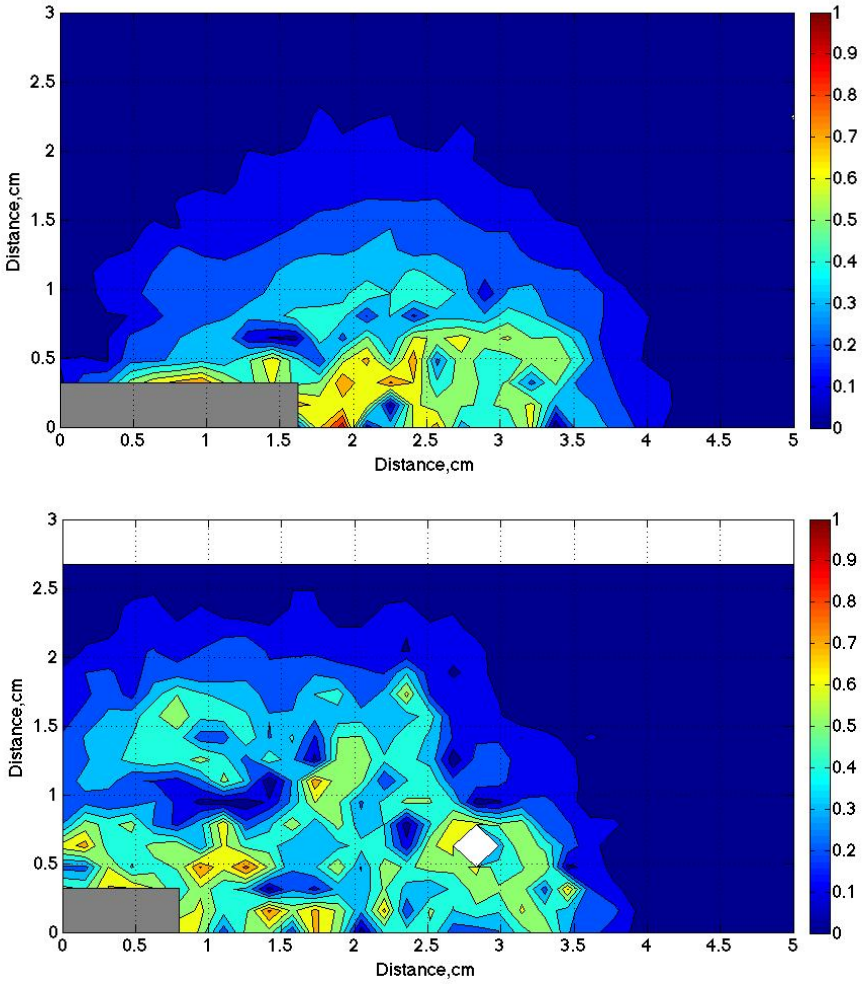

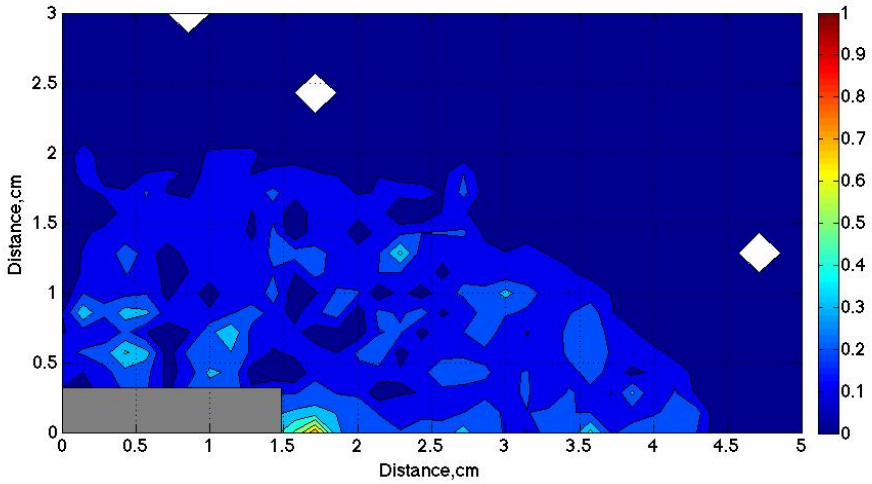

Figure 5.1 Contour plots of penetration events with projectile velocities of (from upper left to lower right) 127, 220, and 310 meters per second. Plots taken at approximately the same penetration distance for side by side comparison.

Qualitatively, many characteristics become apparent using just these basic visuals for comparison. First, consider overall structure. In all cases, initial impact of the flat dart nose into the target creates a sort of ball of transferred momentum in form propagating elastic and, depending on impact conditions, plastic waves radiating away from the nose source. Naturally, as these waves propagate further into the target where more and more energy is dissipated (via simple Coulomb friction, compressibility, or other irreversible process) as momentum spreads through the sand via mechanisms like force chains. In the resultant plots, this "ball" can be seen forming at initial penetration and then propagating outward.

This structure changes temporally of course, as is illustrated in Figures 5.1 and 5.2 (below). The dart nose interacting with sand grains being the major source of momentum diffusion, as the projectile moves onward through the target, kinetic energy imparted by the dart decays as does the effective "radius of influence" associated with the penetration event. In time, wave attenuation is somewhat delayed by shear imparted to the sand by the

dart side, though this is minimal with little propensity to effect the target more than half a centimeter away from the penetration cavity.

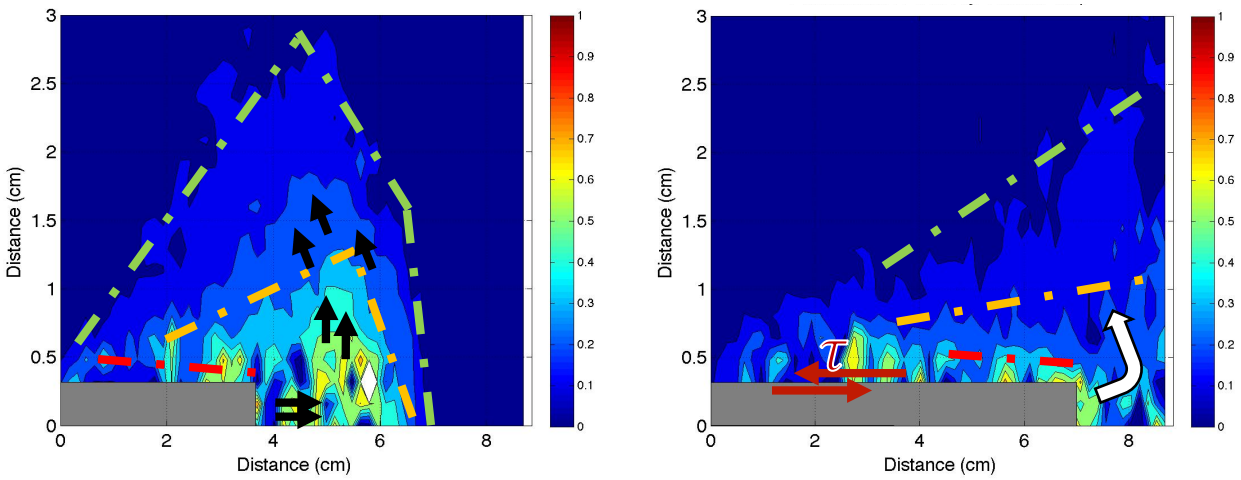

(a) (b)

Figure 5.2 The calculated contour velocity field, with an impact velocity of 127 m/s, taken at times 1.0 (a) and 2.2 milliseconds (b) after initial penetration. Several characteristics of interested are emphasized, including general granular flow behavior, regions of distinct velocity, and wall shearing. The aspect ratio has been altered to visually emphasize behavior propagating away from the shot line.

Taking a more localized look at the velocity field, Figure 5.2 details an experiment with views taken at times just after penetration and then again right before the dart leaves. Chronologically, Figure 5.2a shows the consistent overall structure described previously with momentum diffusing away from the dart nose. There are details within this structure that require attention. Most interesting, highlighted in the Figure, are regions of distinct velocity magnitude which would seem to correspond with different stress regimes. This is more apparent temporally as the regions seem to propagate separately of one another, prior to any attenuation. Referring back to the discussion regarding penetration theory, this observation corresponds well with the idea of elastic and plastic waves propagating from the projectile source [69]. It can be theorized then, that what is seen in the contour time line is an elastic wave radiating (outlined by the green dashed line), quickly followed by a

plastic wave (and associated grain failure) closer to the nose, outlined in orange. Keeping with the theoretical explanation, cavitation could also be possible, but in the case of these experiments the cavity is right along the dart wall (emphasized in red) given the granular systems fluidic tendency to fill its containing volume.

While observation fits well with these conjectures, it is always preferred to have a bit more validation instead of taking the velocity field *prima facie*. Some encouragement is present though. PIV is, fortunately, able to resolve the motion of the dart itself (through fiducial marks), which do show velocities near to that of the measured projectile velocity. While this is reassuring, it does not guaranty the presence of specific stress behaviors.

First, reconsider the wave propagation discussion in particular the equations (2.5) and (2.6) giving a means to determine a tentative minimum velocity at which some plasticity would be expected. Using quartz material properties provided in the appendices [64], this analytical solution suggests a threshold of about 34 meters per second, which is well below the current tested regime of velocity. Not leaving analytical modeling to validate pseudo-numeric results consider now Figure 5.3.

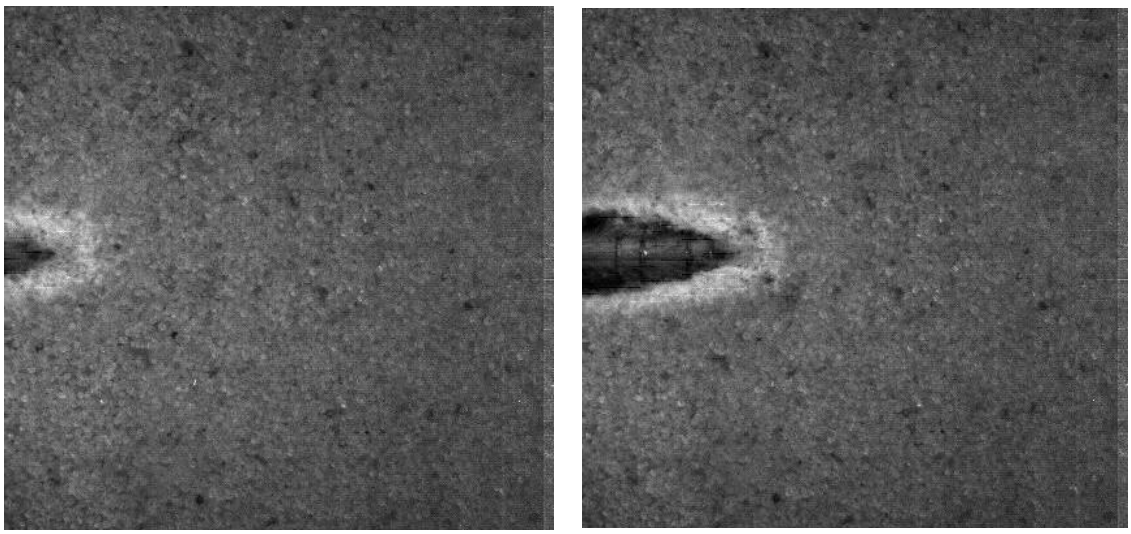

Figure 5.3. Raw high speed camera (Photron) footage taken of an experiment conducted with a projectile velocity of 150 meters per second. Not the "brighter" more reflective grains next the dart nose signaling grain fracture. Frames at 0.0833 and 0.1667 milliseconds after initial penetration.

Work done by Van Vooren and Borg [17, 18], discusses how the reflectivity of a sand grain increases when undergoing fracture, demonstrated within the context of both projectile penetration and in single grain loading. This can be readily observed throughout this study, and as shown in Figure 5.3 with grains fracturing around the dart nose and visually lighter. This area corresponds directly with conjectured plasticity region seen in contour plots, and thus we may more validly assume the PIV analysis, within the limitations of the field of view, is indeed resolving the bulk propagation of momentum through both elastic and plastic processes.

A next concern then sprouts regarding shots done at higher velocities, even the ones shown in Figure 5.1. One would logically assume that as higher projectile velocities penetrate the system with a greater amount of momentum, that more plastic processes would occur in the form of more grains breaking and the like. This should manifest itself as greater velocities being experienced near the dart nose, or (at least) a consistent amount

as the plots are normalized by impact speed. Instead, a lower percentage of projectile velocity is seemingly achieved emphasized by apparent spots of “zero” velocity. Physically, grains experiencing catastrophic failure would fragment and no longer support any load, and thus no momentum would be seen. However, zero spots could also be due to issues with the PIV method itself.

As previously discussed, the requirements of the PIV algorithm to find a velocity vector associated with a convergence correlation value depends entirely on the ability to capture grain motion within one interrogation window. Plastic phenomena such as grain deformation and fracture are, as such, fundamentally undetectable as the method is searching for maximum likeness and the grain in question is no longer the same at all. This results then in one of two vector assignments, either divergence (which is in turn not interpolated over due to not-a-number values), or false zero values.

Returning our attention to Figure 5.1, a few of these false zero (and the rare NaN) values are present in all experiments within the approximated plastic deformation regime. These are especially apparent in higher velocity shots, which keeping the method limitations in mind, compliments the idea of more irreversible mechanisms taking place at higher dynamic conditions.

A final qualitative look, the depth to which momentum has diffused can be compared by way of the length between the dart (shot line) and point into the target by which all velocity (momentum) transfer has attenuated away. Logically, a safe assumption would be that momentum transfer is greatest at initial penetration and would then decay as the projectile loses energy. For this reason, Figure 11 is again reference as any easy way to see multiple experiments and their associated “depth of influence” side by side.

What jumps out the most is that diffusion actually reaches approximately the same distance around 2-3 centimeters at the highest point, regardless of projectile velocity at the point of penetration. This is quite interesting, and while cannot be conclusive, it does allude to potential self similar behavior as the plots are normalized. Not necessarily contradictory to that idea, with more dynamic load, more irreversible processes are present and so to momentum decays more while undergoing transport. That could mean that despite higher energies, greater impact velocity produce a near similar effect as a result of some granular system limit enforced by heterogeneous mechanisms. This concept, however, may not be validated by simply breaking down the raw results, but instead a direct quantitative comparison is necessary.

To that end, having presented the various observations that can be made of in-situ behavior just by inspection, the task now becomes to quantify this new data source to better characterize the target. As this approach to ballistic dart penetration into sand is a path not yet treaded, several derivable measures meant to quantify behavior will be presented with their associated implications included.

5.1.2 A Radius of Momentum Diffusion

As discussed in qualitative observations, the velocity fields presented via contour plot signify the diffusion of momentum from the dart into the system of sand. The spread of this hinted at some potentially interesting, and self similar, characteristics conceptually. Given, we have the numerical velocity vectors (and magnitudes) associated with FOV, it is feasible to take the visual observation and quantifiable compare momentum diffusion across the entire velocity spectra. Doing this, it may be possible to address several

fundamental considerations for characterization such as the overall effects of increased dynamic loading, the degree of self-similarity or similitude, and/or decay of momentum diffusion strength over time.

To this end, a few terms are defined which will be referred to hereafter. First, a radius ***r*** is defined as the distance in the vertical (y) direction between the shot line and the edge of momentum diffusion defined by some threshold, which in this context of these experiments was arbitrarily defined to be two percent of the penetration velocity. Length ***L*** is the dart location (i.e. penetration depth) taken from the wall of the sand tank. The graphical representation of these terms may be seen in Figure 5.4.

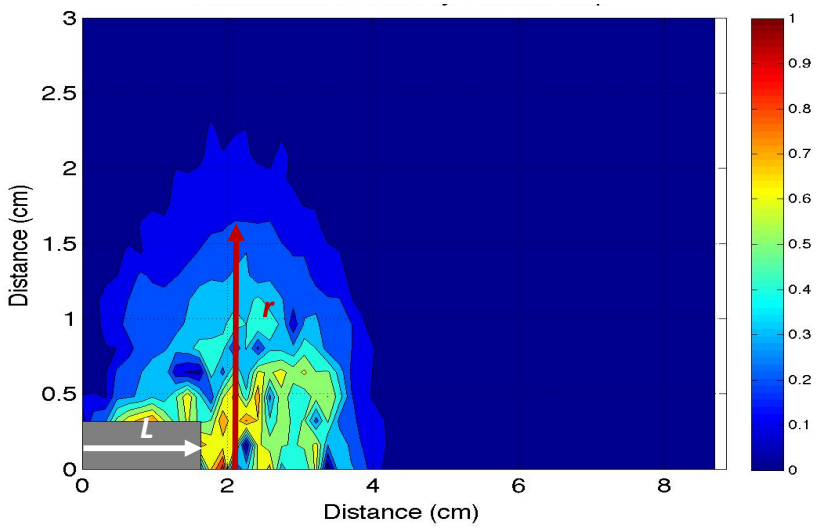

Figure 5.4 A visualization of what the momentum diffusion radius **r** and penetration depth **L** quantify on a standard contour velocity field.

It is fair to suggest the radius **r** as a general, but adequate, quantification of momentum diffusion into the target, but this metric alone fails to incorporate variations in experimental parameters, including in situ deviations, and thus would not allow for a fair comparison of trials side by side. In an effort to leverage any potential similitude, this is rectified by normalizing the defined momentum diffusion radius by the defined penetration

depth **L**. This incorporates an indirect measure of how much momentum has been lost up until a point in time, or in other words how much penetration has already taken place and thus decay occurred. Though both are measurements of length, the ratio of these can conceptually then be considered a non-dimensional metric of the momentum exerted on the sand currently over the momentum already lost at any given point in time.

Taking things one step further, it is interest to not just get a static view of diffusion, but rather see it decay over time. Still utilizing similitude methods for better comparison, time is non-dimensionalized with projectile velocity and dart diameter, further incorporating additional experimental parameters most importantly impact velocity. The final implementation of this can be seen in Figure 5.5.

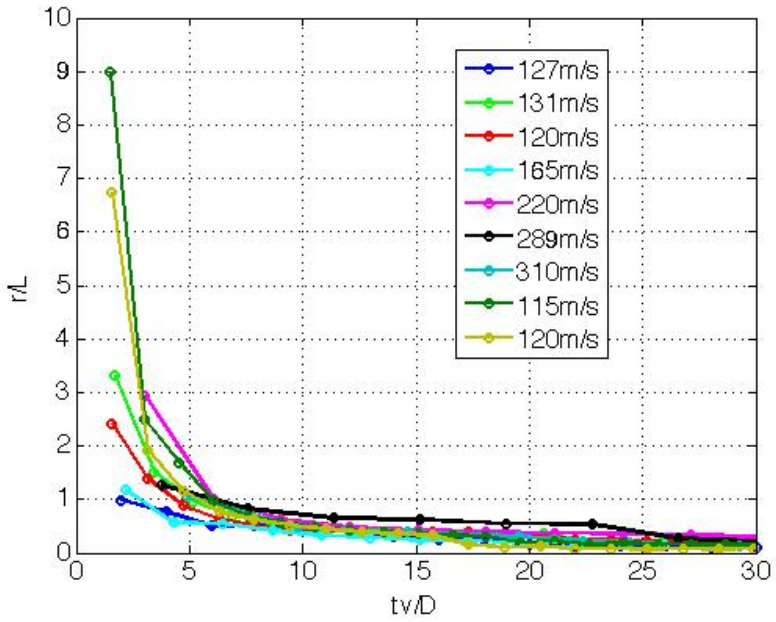

Figure 5.5 The ratio of r/L plotted throughout each trials respective penetration event, time shown non-dimensionalized. Note at zero, just at or prior to impact, the ratio is undefined and is therefore not plotted.

The result, when plotting each experimental set against one another, is a decaying exponential-like trend. While these do not fall completely on top of each other, which

would represent absolute similitude they do form a tight band suggesting a high degree of self similarity.

Starting from the beginning, while overall behavior is undeniably consistent across the board, the spread seen at initial penetration cannot be ignored. This could be due to explained by two occurrences, one non-physical and the other physical. First is to consider how the value **L** itself is calculated. The dart location is manually tracked through frames using the *getpts* function in *MATLAB* and thus is subject to natural user error. This was minimized by repeating the measurement multiple times, but at initial penetration this could still potentially lead to spread due to the low or undetermined value of L present in the denominator. However, with great care taken the observed spread did persist, and while this is not proof of physical meaning, it then became relevant to consider what phenomena may be playing a role.

As previously mentioned, while these results look quite self similar, there is still scatter, so when considering what physical mechanisms could cause discrepancy the scatter was the first place to look. Interestingly, as can be reference in Figure 5.5, no apparent pattern stands out. No correlation of of initial **r/L** values with projectile velocity (the only variable being changed) whatsoever. While this is sort of perplexing, this actually greatly reduces the list of usual suspects. Other than the projectile velocity, the only change of consequence between experiments is the sand target itself. Of course, the material itself was not change, but between each shot the tank was emptied to retrieve the projectile and then refilled. This step almost guarantees the arrangement of grains are different with regard to each experiment. Given different initial arrangement, each penetration event is subject to different reaction to loading as different force chains could form throughout the

target during penetration, or not-necessarily-slight variations in local bulk densities could shift system response.

Continuing to look at additional structure, aside from the exponential trend visually evident, there seems to be a slight kink in each trace towards the end of the event. To explain this, recall the images presented in Figures 4.5 and 5.2. As previously discussed, the primary source of momentum diffusion is through interaction of the nose with the target, with the dart walls on being responsible for minimal shearing. The "kink", best seen in Figure 5.5 ($V_{penetration}$=289m/s), corresponds with the time at which the diffusion caused by the nose leaves the field of view and thus the maximum diffusion radius drops to that caused by the wall --a significantly lower value around half a centimeter.

This calls to mind the limitations of this method of quantification, and all methods hereafter that rely on PIV analysis. Any conclusions, results, discussions, thoughts, concerns, quagmires, or any other form of advanced thought or analysis may only be applicable to phenomena at play within the high speed camera field of view. While assumptions could be potentially made about goings on after, such as the dart slowing to a final penetration depth corresponding with decaying momentum, is, no matter how logical, only conjecture.

That being said, this measure of momentum diffusion radius finds the further threshold velocity value in the vertical direction within the field of view, so when the dart nose leaves that FOV, and coming back full circle, the radius drops to that produced by wall shearing and is not a measure of the true decay of momentum transfer. However, safely assuming that shift is due to the dart nose no longer being visible, decay up to that

point is valid and of great interest as it provides insight into the nature of bulk kinetics at play and the range of their effects.

To further investigate the idea, given the persistence of exponential behavior, a log-log plot was created to illuminate further discrepancies as well as to take initial steps towards developing some empirical relation by which this behavior may be described.

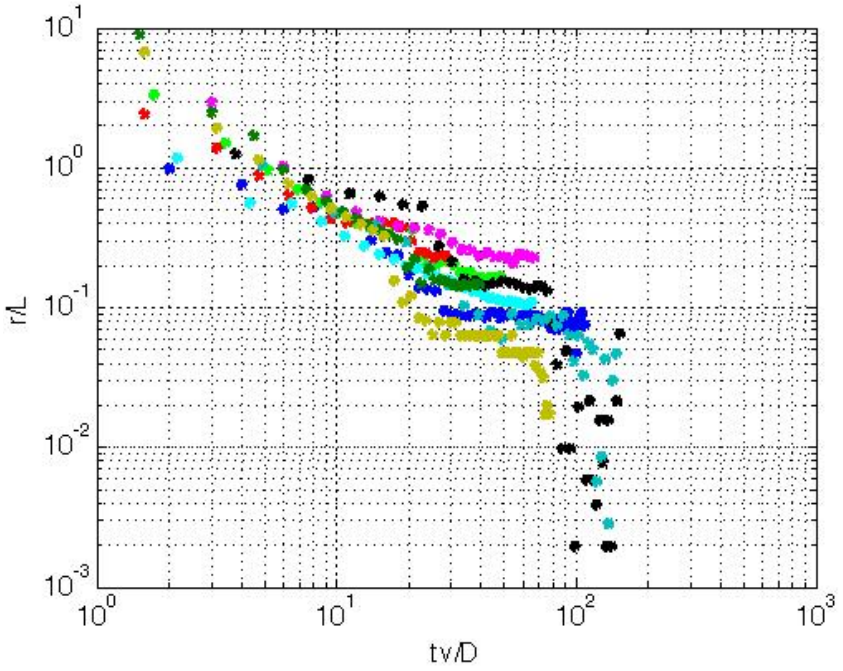

Figure 5.6 A log-log plot of each the momentum diffusion radii with respect to time (both non-dimensionalized). An approximate linear relationship may be seen with a steep drop at the conclusion of the penetration event.

Shown in Figure 5.6, linear logarithmic behavior can be seen with all penetration events following approximately the same path, regardless of projectile velocity. Just as in Figure 5.5, there is still a detectable amount of scatter, proposed here to be attributed to heterogeneous phenomena or, in the case of the far end, due to (Figure 5.6, left) the nose leaving the field of view. Very noticeable here, some trials can be see to not have a drop off, this is due to analysis ceasing once the dart has left the FOV, a direct result of realizing the discussed limitations after analysis of some initial shots.

The result is a band of data all following the same quasi- log linear trend. While deviations with the initial and final temporal areas have been discussed, plotting the data this way reveals an interesting occurrence between 20 and 70 **tv/D**. Here the band of data seems to expand and flatten. Mathematically this makes sense as the trend in Figure 15 is not perfectly exponentially and comes to a sort of plateau. This actually not surprising, as while momentum diffusion from the nose does lessen after initial penetration, it is somewhat sustained by wall shear deviating from what would otherwise, seemingly, be exponential decay.

As with the overall trend, there is no apparent correlation in the scatter of this middle, plateau-like, band. This is temporally when the dart is in the center of the FOV, and the dart nose is easily tracked, and so previously discussed errors are not present (or at least minimized) which lend to the idea of heterogeneity causing discrepancies, while the effects of increasing projectile velocity seem to show similitude in a bulk sense.

Most intriguing about this perspective is its potential, not only as a foothold to develop in-situ empirical relationships, but the chance to use those relationships to validate computational works as was motivated in the first chapter. It is computationally feasible, within the domain of a simulation, to quantify and even visual this same diffusion of momentum through means as simple as plotting local velocity values. Do so, instead of having to rely only on prior and post experimental characteristic, in-situ phenomena could be confirmed.

While this could be done simply by plotting against the results presented here, it is more concise to develop an empirical model from which to benchmark. Numerically approximating the overall behavior with a trend line in log-log space results was done as a

first-pass to model momentum diffusion radius throughout the penetration event. Using the power law, the trend line becomes

$$\frac{r}{L} = 4.827\left(\frac{tv}{D}\right)^{-0.9998} \approx 4.827\frac{D}{tv},\ 0 \leq \frac{tv}{D} \leq 70 \qquad (5.1)$$

in real space. Where the numerical constants are taken from the slope and intercept points of the above trend measured to be -0.9998 and 1.5743 respectively. At the user's discretion, given the trend line was calculated in MATLAB and subject to some error, the relation may be additionally simplified as shown.

Taking a more detailed approach we can expand this equation to include the two distinct regimes observed, the initial penetration following a more precise exponential decay, followed by a quasi-steady dwell due to momentum transfer from the dart side continuing to pass by. Applying the same process in the separate temporal regions, this results in

$$\frac{r}{L} = \begin{cases} 5.508\left(\frac{tv}{D}\right)^{-1.0665}, & 0 \leq \frac{tv}{D} \leq 30 \\ 0.237\left(\frac{tv}{D}\right)^{-0.1367}, & 30 < \frac{tv}{D} \leq 70 \end{cases} \qquad (5.2)$$

where the constants are again taken from trend line measurements and the non dimensional time boundaries approximated based on observed behavior. Note both equations are only valid for a threshold velocity of 2% of the shot velocity and only up until the dart leaves the field of view, after which no true observations have been made.

Plotting these relations against the entire data set, as shown in Figure 5.7, visually the empirical fit falls onto the scatter, especially when the dwell is incorporated. As was done in the developing the fit, data points taken after the dart nose (and associated momentum "bubble") were neglected as they did not accurately reflect the diffusion behavior.

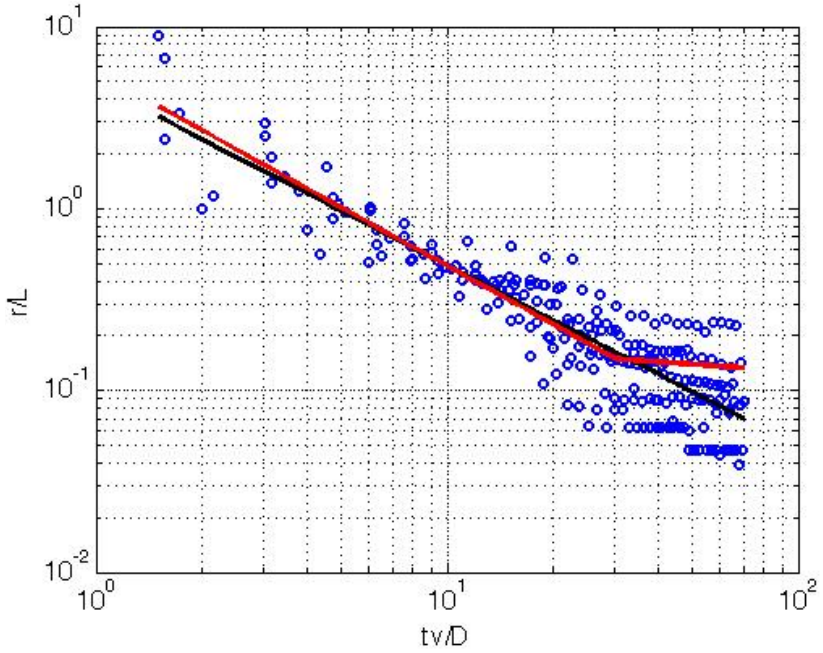

Figure 5.7 Neglecting the irrelevant end of the event, behavior can be approximated via trend line with regard to either the overall trend (black) or two part initial penetration followed by a quasi-steady dwell (red).

Overall, what can be interpreted from this is that the diffusion of momentum from the dart into the sand during a ballistic penetration event, has a nonlinear positive relationship with projectile velocity, shown through self-similarity, with respect to experimental parameters such as penetration depth and dart diameter. However, this behavior is not absolute, and is potentially greatly effected by the presence of heterogeneous factors, such as grain orientation, causing variations to bulk system response.

While this analysis was done in such a way that variables were indeed non dimensionalized, this study was conducted changing only penetration velocity, and as such the observed trends may not hold when other characteristics are altered. Dart diameter, or nose geometry in general, is known to have a substantial impact on penetration behaviors and is not explored in this work [33]. Additionally, the target Ottawa sand is known for its

fairly homogeneous distribution and round grain geometries (quasi-monodispersed), which could have additional implications as the ratio of grain to nose diameter has been a recent topic of intrigue [13]. If heterogeneous mechanisms are really responsible for the observed scatter, then altering the target to less forgiving materials such as concretes, soils, or more homogeneous sands could greatly impact penetration behaviors. Most importantly, as this is a relatively new way of characterizing the velocity behavior in sand, this is only one attempt to quantify behavior, the rest of which are discussed in the following sections.

5.1.3 Dilatant Flow in Granular Media

An alternative to quantifying the diffusion of momentum into the target, as was attempted in the previous section, a differing perspective may be taken view the system as a dilatant fluid. This, however, is not a novel idea, as was mentioned in Chapter 1, and many have adequately used associated assumptions to model a granular system as a continuum [47-50]. An excellent plot defining dilatant behavior can be see in Figure 5.8.

For a quick background, regarding a traditional (Newtonian) fluid, Newton's law describes the shear stress to be proportional to the gradient of velocity in the perpendicular direction [75]. In other words, the familiar

$$\tau_{rx} = \mu \frac{dv_x}{dr} \tag{5.3}$$

where τ is the r-x shear stress, v_x is the velocity in the direction of flow, and μ is the material dependent viscosity. However, any phenomena that alters this equation, such as compressibility, can not be represented as such because shear is no longer directly proportional.

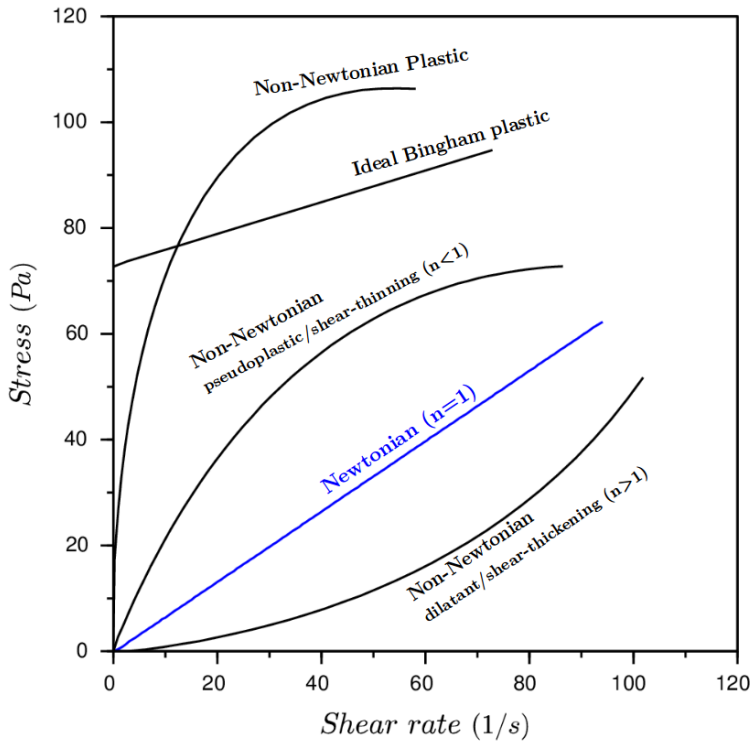

Figure 5.8 Classification and comparison of non-Newtonian fluids when plotting stress over various shear rates (equivalent to velocity gradient). Note dilatant fluids are shear thickening with a shear rate exponent greater than one [76].

Therefore, when examining fluids with non-Newtonian characteristics, a slight alteration must be made. The chemists Ostwald and de Waele [77, 78] developed a power law which simply, but effectively, models non-Newtonian behavior through the introduction of a *flow behavior index n*

$$\tau = K\left(\frac{dv_x}{dr}\right)^n = \mu_{eff.}\left(\frac{dv_x}{dr}\right), \qquad \mu_{eff.} = K\left(\frac{dv_x}{dr}\right)^{n-1} \tag{5.4}$$

where K is a term analogous to viscosity coined the *flow consistency index* with units of Pa-s^n in SI units. Additional representations are included alternatively lumping the nonlinearity into an effective viscosity.

This efficiently models differing dependence on the velocity gradient, but unfortunately, no matter how it is represented, demands knowledge of the added *flow*

behavior index (n). This is most commonly (and feasibly) determined through experiment, and given past work is known that fluids with an n value of greater than one are considered shearing thinning or pseudo-plastics, while those with an n value of less than one are termed shear thickening or dilatants.

With the quick rheological introduction out of the way, knowing sand does indeed "thicken" or compress with an increase in loading (shear), we are now interested in seeing if a dilatant model is applicable to the acquired, in-situ, velocity data set. If successfully applied (and validated), the implementation of this approach would allow for the approximation of shear stress as a function of distance from the shot line. A value easily extracted in computational contexts as or comparison, and could also be measured experimentally to confirm the adequacy of the PIV analysis itself. To accomplish this, most importantly is acquiring the velocity gradient from PIV results. As is common, first consider only maximum shear, which occurs at initial penetration. Before diving in head first, lets initially take our favorite example shot, done at 127 m/s.

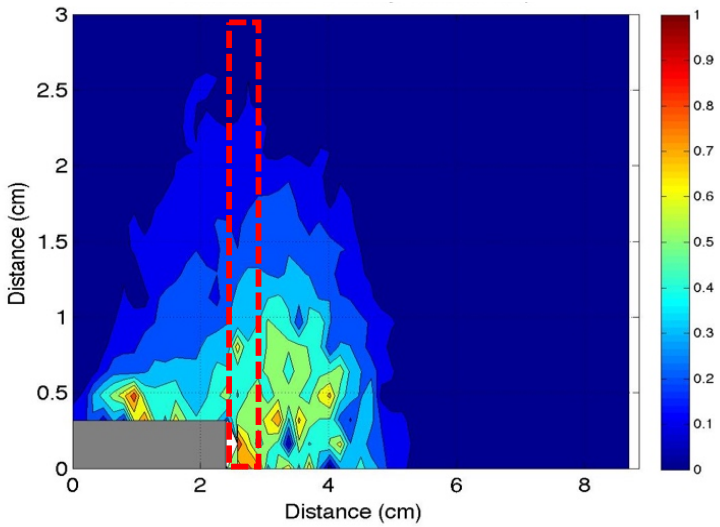

Figure 5.9 Vertical slice of horizontal windows isolated during a frame of initial penetration. To be used to extrapolate an empirical equation for x-velocity as a function of y.

Figure 5.9 shows a snapshot of the velocity field 0.3 milliseconds after penetration. Taking this information, velocity with respect to distance may be directly plotted, as seen in Figure 5.10. As the domain is spatial discretized, there are a finite number of data points equivalent to have of the number of interrogation windows in the vertical direction, or in this case, twenty-eight. It should be noted that PIV calculates both an x and a y velocity component, and while the contour plots have all shown magnitude, only the x direction velocity is presented as it is relevant to equation (5.4).

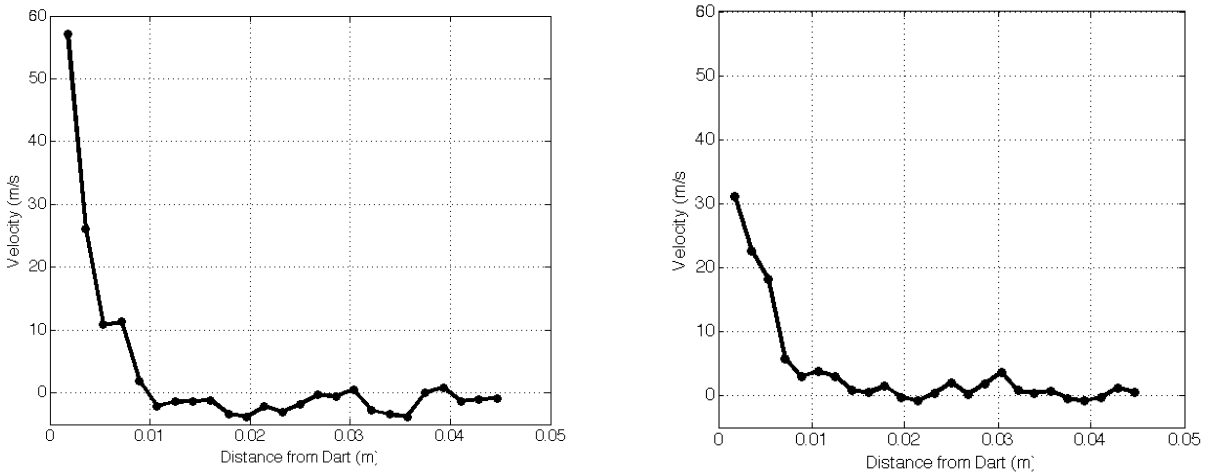

(a) (b)

Figure 5.10 The x-component velocity profiles with respect to distance from the shot line, zero being at the dart wall. Taken just after initial penetration, the dart nose at this point is 2.39 centimeters into the target. These represent two different vertical slices, with (a) being 10 interrogation windows from the left boundary, and (b) being 14.

To avoid any confusion, Figure 5.10 lists the final distance from the dart to the end of the FOV as around 4.5 centimeters whereas in previous plots the limit has appeared to be more around 3. This is because plots were cropped to the extenuate high interest points (though consistently so across experiments. Avoiding digression, two distinct velocity profiles have now been obtained ripe for use in the Ostwald-de Waele Power Law. Naturally, Figure 5.10a has a higher peak than its counterpart as it is taken right adjacent

to the dart nose where more momentum (and thus velocity) are seen. More interested in near nose interaction continuing only (a) will be considered.

Knowing a derivative is required later within due to the gradient, this profile can be approximated using a five term polynomial fit described by

$$v(r) = (-1.072E10)r^5 + (0.1453E10)r^4 - (7.486E7)r^3 + (1.816E6)r^2 - (2.058E4)r + 8.453E9 \quad (5.5)$$

where the constants have been simplified to compact the equation, with a more complete version provided in the appendices. Plotting this against the experimental velocity profile, in Figure 5.11, an excellent fit can be seen.

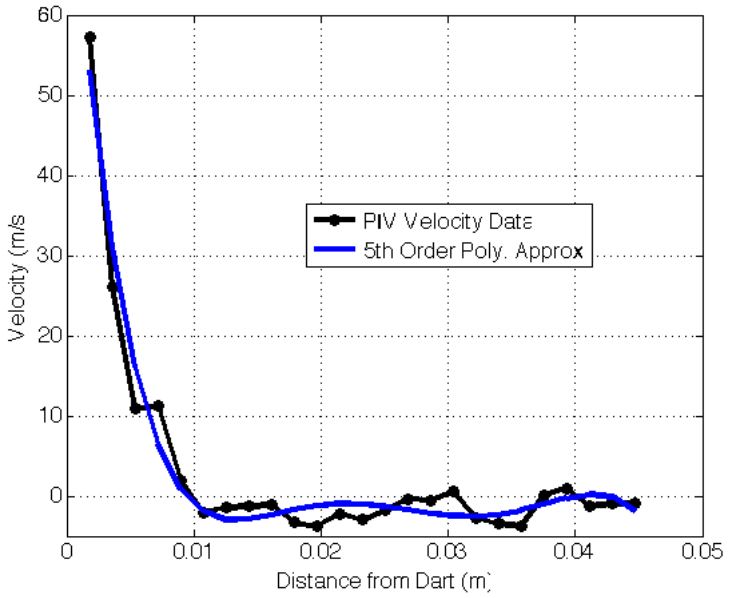

Figure 5.11 The five term polynomial approximation of the experimental velocity profile, for use in determining the velocity gradient relevant to shear stress.

Direct from experimental results, with the implicit post processing, a velocity gradient can now be readily calculated by taking the derivative with respect to y. Doing so, and incorporating the result into equation (5.4), provides a method of calculate in situ shear stress within the granular media at any point within the field of view.

$$\tau(r) = K\{(-5.36E10)r^4 + (0.5812E10)r^3 - (2.2458E6)r^2 + (3.632E6)r - 2.058E4\}^n \quad (5.6)$$

Unfortunately, equation (5.6) is still not fully defined, and therefore may not be properly implemented. Starting from the beginning of derivation, the first necessity is the not bad (but not trivial, nor spot on) assumption that the Ottawa sand acts similar to that of a dilatant fluid. Next, the penetration event is quite a dynamic process, so to find shear using the method presented would require taking a single instance in time, choosing one vertical slice of experimental velocities, and deriving an equation for that time and place only. These initial concerns could be overcome. The first is "just" an assumption, which while not perfect, given the right experimental tuning it is fairly justifiable. Time and space constraints could be also, foreseeably, be worked through especially with computational aid, using just the experimental setup described here. Unfortunately, there are two other not-so-minor hiccups; the flow behavior and consistency indices **n** and **K**. Before this equation can yield an actual number, regardless of its functionality, these values would have to be defined.

While not feasible within this study, given the limitations of the described experimental set (Chapter 3), the properties **n** and **K** could be defined for the system. Stress gauges could be embedded in the target and set at multiple points *within the field of view*. As this measurement temporal, and location is known, equations like (5.6) relevant to that trial could be set equal to the measured stress and simultaneously solved, thus yielded a complete spatial (and potential time varying) stress field for the target describing in-situ behavior. Completing this will be recommended fully in Chapter 7 when discussing future work, and though the flow behavior and consistency indices weren't defined here, this

method still provides a path, given these new experimental method, through which a complete characterization of a granular target under going penetration may be defined.

5.1.4 Quantification of Irreversibility

While previous sections have focused on specifically characterizing in situ velocity behaviors through the concepts of momentum transfer and dilatant fluid behavior, PIV results also provide a unique opportunity to quantify other derivable characteristics equally important to understanding fundamental behavior. With the effects of heterogeneity popping up throughout the analysis of the in-situ velocity field, it becomes of interest to quantify these effects particularly.

To begin this process, consider the problem from and energy perspective. As always the first thing done, to this end, is to perform an energy balance; considering the sand tank to be a control volume with all heat transfer, work, and mass flow neglected save for the dart entering the volume. Further neglecting potential energy, the problem reduces to a balance of dart kinetic energy, granular kinetic energy, and any irreversibilities present. This is shown mathematically in equation (5.7)

$$KE_{Dart} = KE_{Sand} + Irreversibilities$$

$$\rightarrow \frac{1}{2} m_{Dart} v_{shot}^2 = \frac{1}{2} \int_{t_i}^{t_f} \frac{\sum_{i=1}^{N} m_{sand} v_i^2}{\Delta t} dt + \gamma \qquad (5.7)$$

$$\therefore \frac{\gamma}{KE_{Dart}} = 1 - \sum_{j=1}^{k} 0.65 \sum_{i=1}^{N} \frac{m_{sand}}{m_{Dart}} \left(\frac{v_i}{v_{shot}}\right)^2$$

where m_{sand} is the mass of the sand found, on average, in a single interrogation window of size 4 by 4 grains, N is the number of interrogation windows, and v_i is the velocity of the corresponding interrogation window, $\boldsymbol{k}$ is the number of time steps until the dart has

left the field of view, and Δt is the discretized time step. The constant *0.65* is the maximum packing factor, given mass was calculated as a set cube (with dimensions described) this accounts for some porosity. With irreversibilities known to be present, as in any system, it is assumed the remainder of energy goes to non-isentropic processes which lumped into the γ term. This assumes non-instantaneous transfer of kinetic energy from the dart to the sand, with each time step showing kinetic energy over the discrete time step. Therefore, total kinetic energy is acquired by integrating (summing) over time. Change in time further cancels and so all that is required is the ratio of window velocity to projectile velocity (squared) summed over space and time.

Now the issue becomes implementing this algorithmically on the all experimental PIV results. Conservation may only be applied if all granular flow may be accounted for. This infers that once momentum transfer reaches the edges of the FOV, after which grains flow outside our observed area and the summation would be inadequate. That being said, this method is still viable prior to that point, and could provide useful insight. Applying this to the derived velocity fields, Figure 5.12 shows kinetic energy measured within the sand system plotted as a percentage of initial dart kinetic energy over time. Understanding that the energy balance is invalid after any grains leave the field of view due to momentum transfer, the plot was refocused (b) which was confirmed by contour plots and raw high speed footage to be the point at which fringe grains left the FOV.

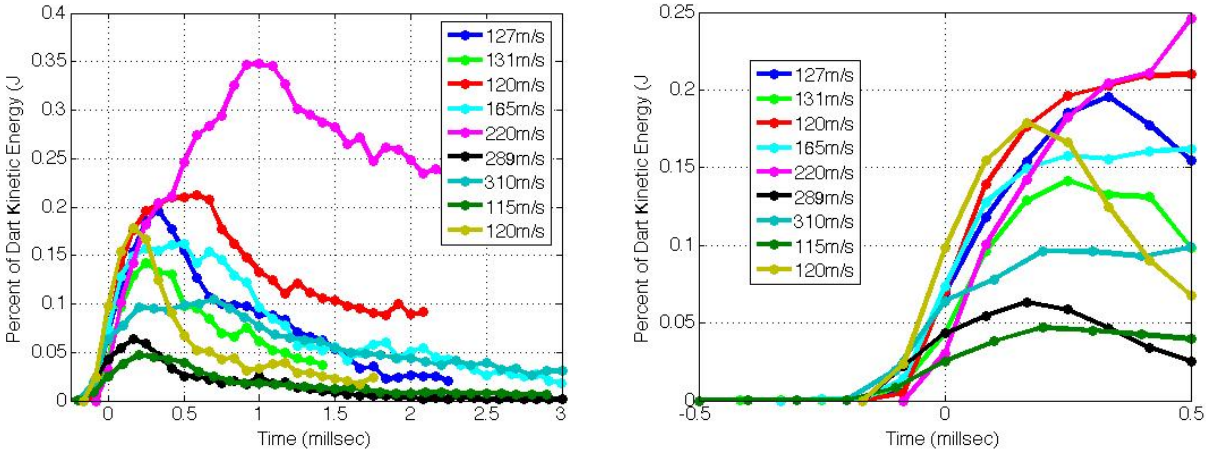

Figure 5.12 (a) An overall plot of the kinetic energy in the sand system including after the compaction wave and dart travel outside the FOV (~0.5 milliseconds) after which the results are inaccurate. (b) The same plot focused on the viable region of data. This represents $\sum_{i=1}^{N} \frac{m_{sand}}{m_{Dart}} \left(\frac{v_i}{v_{shot}}\right)^2$ plotted over time.

We then numerically integrate and incorporate the packing factor showing that, *at most*, approximately 64% of the dart's kinetic energy is being transferred to the sand as *kinetic* energy at initial nose penetration, with the worst case scenario being as little as 15%. The rest is depleted either after nose penetration or through irreversible processes such as grain fracture, densification, heat generation, and even sound.

As when analyzing the proposed momentum diffusion radius, while general behavior seems similar across the tested projectile velocity range, there is quite a bit of discrepancy. More so, these discrepancies do not, in any way, correlate with penetration velocity which again suggests the non-trivial effects heterogeneous mechanism have on the bulk response.

Though simple and not robust, this approach takes a step towards numerically quantifying the effects of heterogeneity in such a way it may be compared to future work including computational simulations. Additionally, this is the third such circumstance in which scatter in behavior, not identifying changes as function of projectile, suggests that

heterogeneity could very well be responsible for the disparities seen in various form throughout collected data.

5.1.5 Distribution of Velocity States

In implementing the calculation of kinetic energy discussed in section 5.1.4, we readily have the velocities of each interrogation window at each point in time available for study. This provides a foothold for a more statistical approach to analyzing available velocity data and allows a distribution to be found of what velocities are experienced during a ballistic penetration event.

To accomplish this in a comparable way, a conceptual box is placed in front of the dart nose. The box, with dimension of 4 centimeters in the direction of the shot line and height corresponding to the momentum diffusion radius in both directions, follows the dart for the duration of the shot, while in the field of view of course. This ensures a consistent frame of reference when comparing penetration events regardless of resolution.

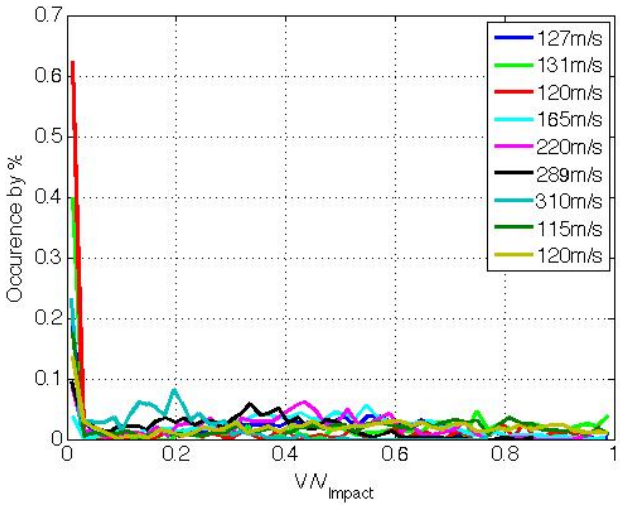

Figure 5.13 A comparison of all velocity distributions across the range of tested projectile velocity. Data compiled using all velocities attained within the defined (box) domain over the entire event time. Both velocity and occurrences have been normalized for better comparison.

With the domain now well defined, recording interrogation window velocities (normalized with shot velocity) while the box remains in the field of view results in a sample of velocity states occurring in front of the dart nose, allowing a statistical characterization of momentum phenomena. The result is shown in Figure 5.13, where occurrences versus velocity (both normalized) from the set of all velocities found in the domain throughout the entire penetration event.

The first thought that occurs when considering Figure 5.13 is what a mess it is. Just the visual shows no apparent trend, correlation, or really any information to go off at all. This, of course, is entirely misleading. Between the busyness resulting from plotting the all experimental trials together and the various influences of discretization and slight differences in resolution, the comparison is made to confuse.

To combat this, smaller subsets of the experimental data were compared separately from the rest, and in doing so a trend did begin to appear. An example of this closer work can be seen in Figure 5.14.

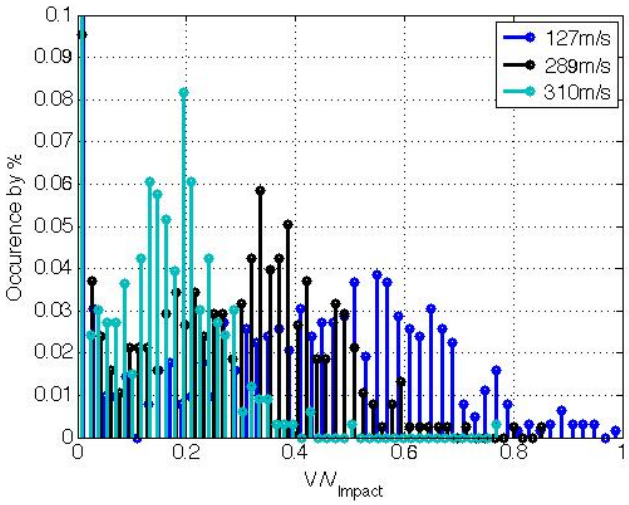

Figure 5.14 A closer look of a selected few distributions revealing a trend. Both occurrence and velocity are again normalized with total occurrences and penetration speed respectively, velocity (as a magnitude) possesses only positive values.

Before diving into a discussion, note only three shots are presented. This is entirely for visual as, given previous demonstration, the histogram can get quickly convoluted. That being said, a few distinct characteristics and even trend becomes quickly apparent with a little more focus in tow.

Beginning with the lower end of tested projectile velocities, a very gradual Gaussian-like distribution of velocities occur with a mean near to the projectile velocity (~50%). As the projectile velocity is increased, the distributions steepen, while simultaneously, the average velocity at this "state" decreases closer and closer to zero.

Before considering the physics at play, statistical measurements are taken to further confirm the behavior hinted to. Figure 5.15 plots both the average velocity of the observed distribution and the change in standard deviation, with respect to shot velocity.

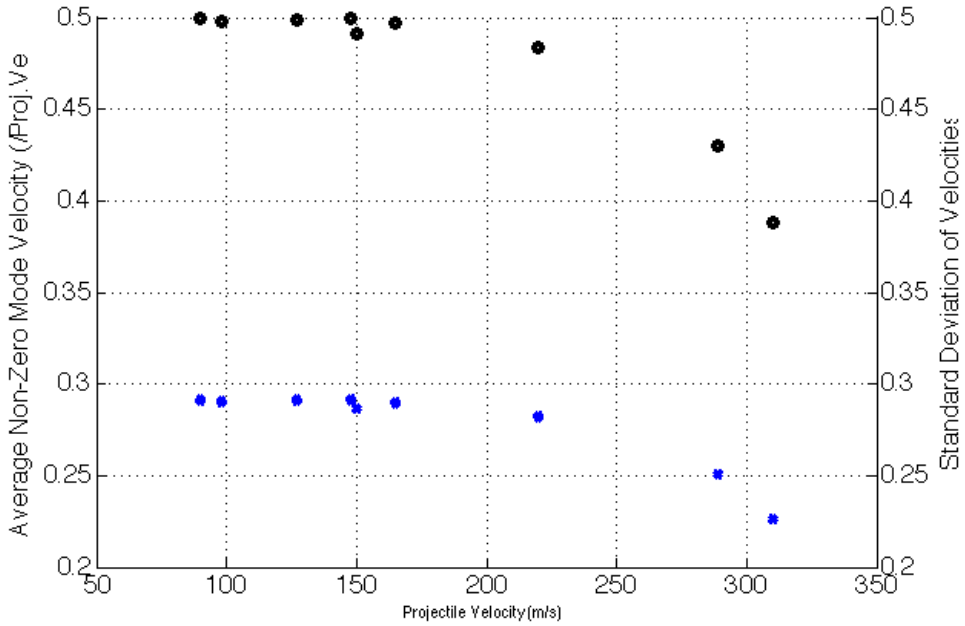

Figure 5.15 Statistical characteristics of the velocity distribution seen throughout a penetration event, compared across the range of projectile velocities. Black represents the mean while the blue is the standard deviation.

Now, what does this physically mean? Reviewing the various interactions at play in the system, we have the dart penetrating the granular media and in doing so imparting its momentum onto grains near the nose forcing them out of the way. The grains impacted initially distribute this momentum to the surrounding grains through force chains which, through processes such as friction and compaction, dissipate.

With that in mind, what some would expect is that as more projectile momentum initially penetrates the system correspondingly more overall grains would be effected, by force chains and the like, with higher momentum (velocities) experienced by near nose grains.

Based on the evidence in Figures 5.14 and 5.15, however, it would appear that a contradictory (and seemingly opposite) phenomena is occurring. Keeping in mind the velocities have been normalized, it would seem that on the lower end momentum is simply imparted to the system and the same momentum near that of the projectile velocity propagates through the near nose contacts, distributing and effecting most localized areas to a varying degree. This results in a fairly even distribution across the entire velocity spectrum with slight Gaussian behavior averaged at around half of the projectile velocity.

Now though, we increase projectile velocity, and this is where things get interesting. As the sand target is loaded with greater momentum, instead of a nice quasi-uniform distribution over the whole range of velocities, a much more distinct Gaussian distribution forms. The mean of this is a lesser percentage of the new (higher) dart velocity, but much more grains are reaching the second velocity mode.

This infers that while not all grains do not attain the same percentage of momentum related to that of the dart, more momentum is being distributed and more grains effected.

As mentioned previously this trend continues more and more, almost exponential based on Figure 5.15, with each step up in projectile velocity resulting in more grains involved, but with proportionally less instead of more average momentum when compared to lower regime counterparts. Working to clarify the issue, consider now Figure 5.16.

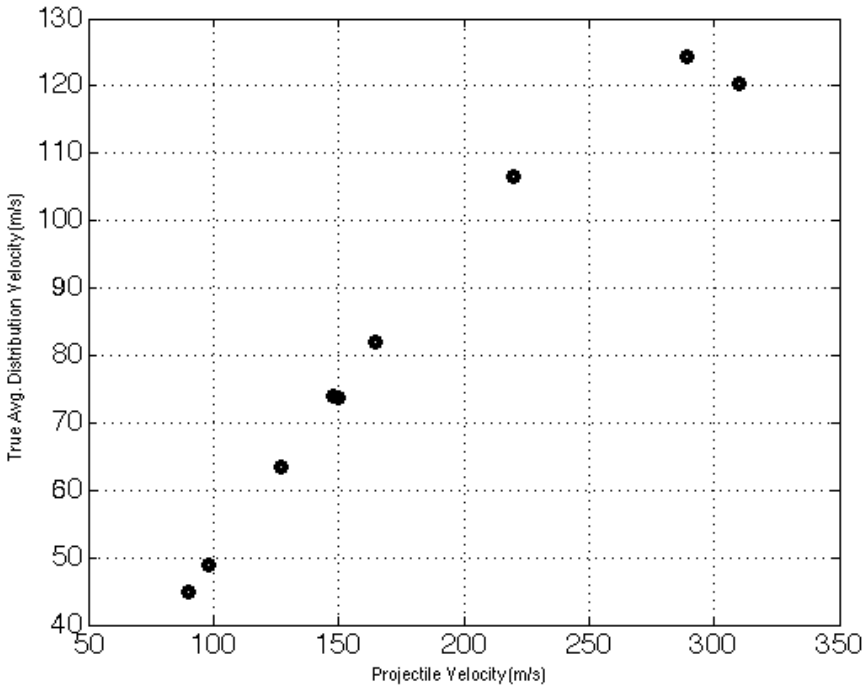

Figure 5.16 The non-normalized "true" velocity state attained by the analyzed distribution plotted against dart impact speed.

In Figure 5.16, we simply multiply the normalized velocity averages by their corresponding dart speeds results in the true velocities being seen on average near the nose. This result reveals a positive trend that rectifies the expected results with the observed normalized behavior. Specifically, this may be interpreted as indeed more and more grains attaining a higher velocity due to greater penetration energy well also being distributed to more grains.

However, due behavioral trends seen in the normalized results, it is suggested that a lesser and lesser percentage of momentum is actually being directly imparted (consistent with a high level of irreversible effects). To better convince us, on the higher end of the velocity in Figure 5.16, the linear trend could be tapering off, which would validate such an assumption. Unfortunately, this last bit cannot be said with certainty at no data has been collected at higher regimes.

Lastly, and probably easiest to spot, all of these distributions are not simply Gaussian in nature, but in reality have a bimodal structure. Interestingly, all shots share the same alternative, and some may even say primary node, at (or around) zero velocity. This is not completely surprising as potentially a large percentage of grains could be untouched by force chains and thus momentum transfer. Additionally, as these distributions consider grain (interrogation window) velocities at all points throughout an event, there are many cases where velocity hasn't yet propagated through.

5.1.6 Wave Propagation Analysis

As PIV inherently captures velocity field behavior, related to the propagation of momentum and stress, it may be used to extract one more interesting system characteristic: elastic wave speed. Through just observation, this may be visually seen quite well by subtracting the undisturbed sand background image from the penetration event. The result is highly contrasted around the compacted areas through which the elastic (compaction) wave has propagated revealing a clear view of the wave boundary (Figure 5.17). Having this raw footage, wave speed could be approximated manually, but an even better measurement can be made algorithmically.

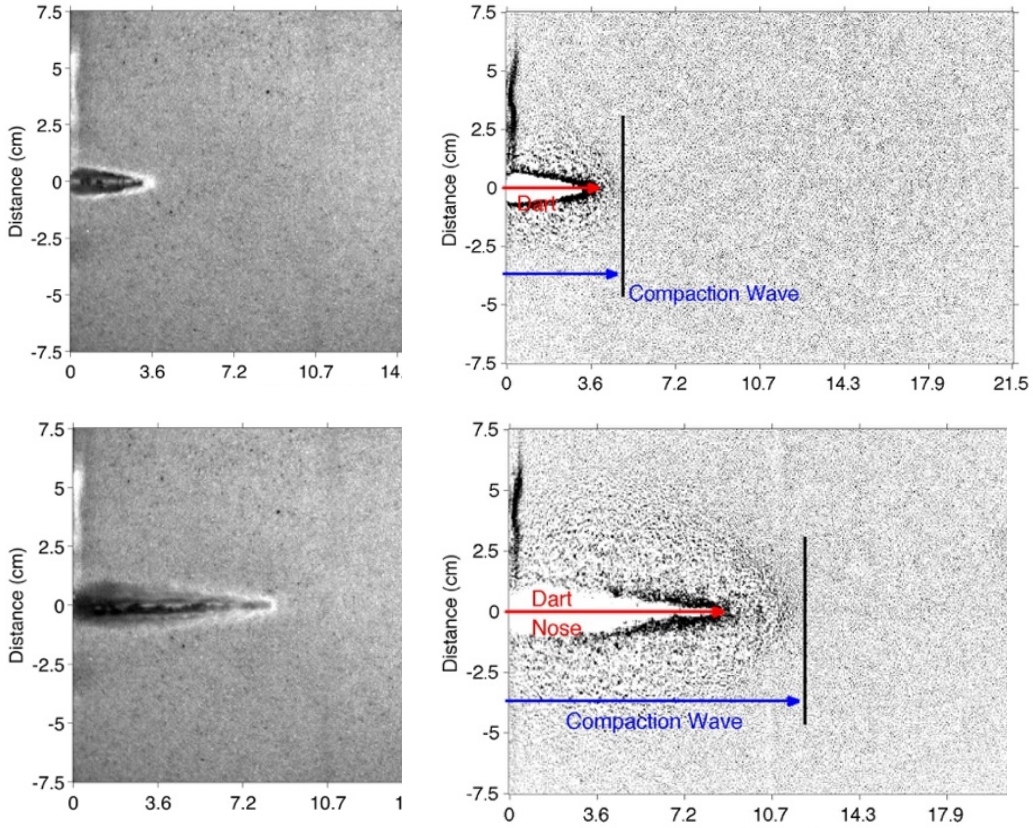

Figure 5.17 Subtracting a calibration image of the sand target from raw high speed footage results in a crisp view of the compaction (elastic) wave.

To do this, we again can utilize PIV results. Implicitly, velocimetry yields the spatial velocity over time and naturally picks up the wave propagation has is proven by contour plots. However, in this case only the boundary itself is of concern. Once the boundary location is calculated at two different times a wave speed may be found.

A MATLAB script is therefore written to incrementally search for the wave boundary. Specifically, a threshold velocity value (one meter per second) is searched for incrementally along the shot line beginning from the right side of the domain. Recording the location at that frame, wave position over time is calculated.

The slope of this, equivalent to dividing the change in distance by time, yields a temporal velocity over time. This can additionally be done for several horizontal slices along the domain provide a complete data set from which to average.

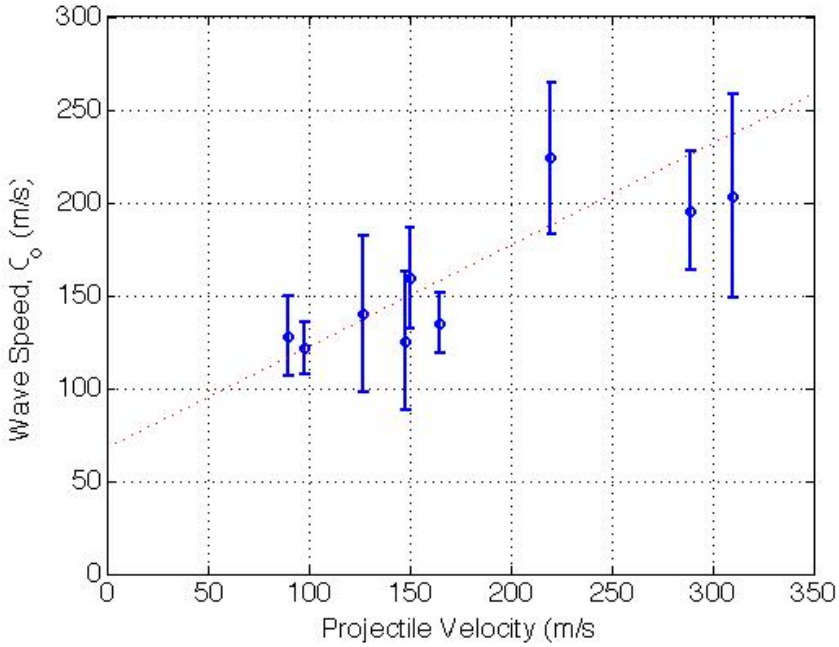

Figure 5.18 There resulting elastic wave speed calculated by algorithmically evaluating PIV data. The produced experimental scatter plot is compared to a linear trend fit with a slope and intercept of 0.5462 and 67.838 respectively and a determination coefficient of 0.79.

As shown, the wave speed has a positive (quasi-) linear correlation with increasing projectile velocity. However, just as has been present in all other analysis, there is scatter which does cause data to deviate from the linear fit in a statistically significant way. This continues to suggest the fundamental influence of heterogeneous effects.

Before physically interpreting this, as a sanity check, these results were compared to published literature which report the bulk sound speed through sand to be anywhere between 100 and 300 meters per second [57, 58], using relations such as equation (5.8).

$$c = \sqrt{\left(\frac{\partial P}{\partial \rho}\right)_s} \qquad (5.8)$$

These regime compares excellently with observed experimental results in the realm of 100 to 250 meters per second. The trend likewise makes some basic sense, as pressure would increase with penetration velocity and thus increase the sound speed. A slight discrepancy, however, is while the observed trend is at least quasi-linear, current theory would expect a half power trend. The results, though, definitely does not invalidate this theory if the whole picture is kept in mind.

First and foremost, note that because the given system is granular, elastic wave propagation may, and in this case does, result in compaction which is why the labels have been used interchangeable, and by definition infers an increase in density. This idea alone means that though pressure is definitely increasing with projectile velocity, so too can density, and so the sound speed trend could appear linear when in fact this is only the case because these two variable are changing together.

Additionally, the observed behavior may not be purely elastic and therefore is not precisely modeled by this relation. For simplicity, lets assume the tested velocity regime, whether elastic, plastic, or a (more likely) a combination of both is well explained by single relationship similar to what is present in eq. (5.8). During these penetration events, as the dart passes into the sand it imparts pressure (via momentum) which propagates through the system as elastic and plastic waves as discussed previously (see Chapter 2). Both elastic compaction and plastic deformations (via grain failure and void collapse), cause densification which would dampen wave propagation.

However, change in density is limited as plastic deformation is present only near nose and therefore factors such as maximum packing factor and granular locking come into

play [32]. Conversely, all wave types contribute to pressure increase aided and abetted by the same granular phenomena preventing densification and further propagated by force chains. In other words, it would be expected for the increase in pressure associated with higher projectile velocities would eventually dominate over change in density.

All that being equal, our observation here is limited in the grand scheme of things for the simple reason that any present nonlinearities could not be evident over the relatively small region tested. Additionally, as has been hinted at by in various interpretations of data from multiple approaches, heterogeneity inherent in the sand could throw any known rule book out the window.

Lastly, and also very likely, error is quite widespread as is evident in Figure 5.18, perhaps too much so to accurately perceive more intricate correlations. Limitations, in this case, are due to a combination of discretizing space, and the related fundamental spatial averaging nature of interrogation windows themselves. These factors can distort measured wave locations potentially doing so to the results themselves.

Overall, suffice it to say that while the precise relationship between projectile velocity and compaction wave speed is not finely resolved using digital image correlation, it may be approximated and validated against other published results. More so, while other methods measure wave interactions with boundaries (such as acoustic testing), this measure wave propagation within the target leading to quantification methods discussed in depth in Sections 5.1.2 and 5.1.3. With refinement, this could be a viable alternative for measuring wave speed in the context of visually accessible experiments.

5.2 CHARACTERIZATION OF THE IN-SITU STRESS RESPONSE

5.2.1 Observations, Structure, and Signatures of Heterogeneity

While the novelty of this work lies primarily within obtaining useful insights and results from the new experimental technique observing in-situ velocity, a complete characterization would be incomplete without also considering the sand target's stress response. Fortunately, this is a much simpler process as stress may be measured directly via the embedded piezo electric gauge.

Without further a du, in Figure 5.19 we plot an exemplary set of quartz gauge data with respect to time comparing the tested range of projectile velocities. Before considering in trends or structure please first note the difference in tested velocity range. When investigating the lower length (grain) scale at the NSWC facility at Indian Head, the operational limits of the gun were tested and a hire velocity of 350 m/s was achieved. This was recorded via the Cordin high speed camera, with a much more focuses frame of view, and as such could not be included in the previous continuum scale velocity discussion. In terms of velocimetry, this will be addressed further in Section 5.3, but can readily be compared other experiments in terms of stress.

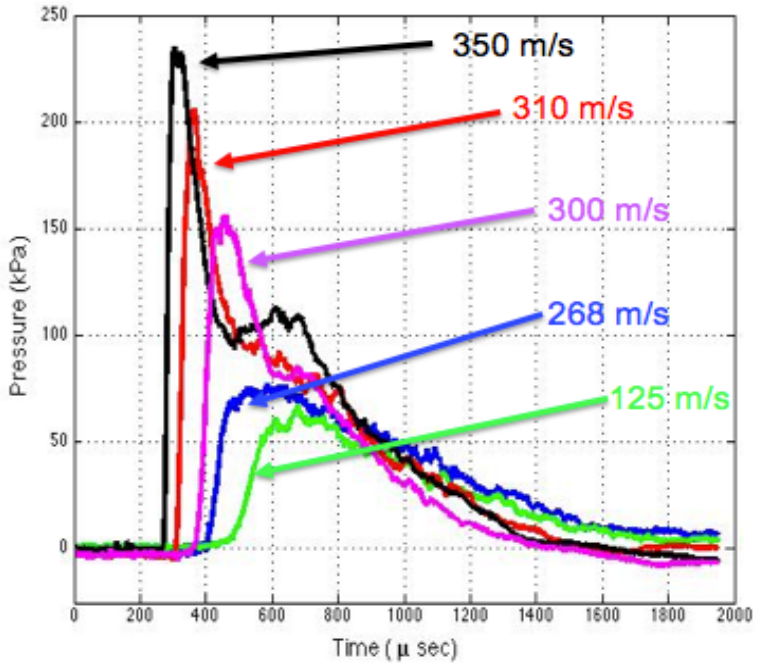

Figure 5.19 A representative series of stress gauge data during a penetration event demonstrating two unique types of behavior indicative of unique elastic and plastic responses.

Coming back to Figure 5.19, two distinct behaviors can be immediately identified. At penetration speeds less than approximately 300 m/s the response wave appears similar to that of acoustic (elastic) waves with a more gradual increase and corresponding decay in stress. In contrast, above some transition zone at or around 300 m/s, this front drastically increases in slope becoming more and more plastic, and even reminiscent of a shock wave.

Looking more in depth at the more plastic wave structures, the observed drastic spike is correspondingly followed by an almost immediate release in stress, a dwell, and then another, gradual, final release. Going through these systematically, as a check, let us first consider arrival time. The stress gauge is located 1.75 inches (4.445 cm) below the shot line. At this distance, approximating the average wave speed to be about 150 meters per second, as per *Section 5.2.6*, the expected arrival time is about 300 microseconds aligning well with the measured results. Assured the correct response is being measured

we can continue on, keeping in mind that the physical hypothesis presented here is just that and cannot be said with absolute certainty.

From what it known with regards to wave attenuation and slope, results in Figure 29 make intuitive sense. At lower velocities, there is both associated lower strain rates and a lower overall regime of imparted stress. As such, waves are more likely to either attenuate down from any plastic strength they initially possessed, and a lower strain-rates (loading) are expected to have lesser slopes in their dynamic response [79].

Complimentary to this, at higher velocities, plastic and even shock like behavior can very well be expected given both higher loading and lesser attenuation. The contradiction to this, however, would be that during plastic deformation, processes like grain fracture and void collapse would eat up more energy and potentially speed up attenuation. The truth though, seems to be some middle ground with plastic behavior manifesting in conjunction with additional structure conjectured here, and detailed below, to be due to heterogeneity.

While in homogeneous materials the steep rise would be accompanied by some plateau stress associated with the material's thermodynamic equilibrium requirements. As is obvious here, that is not the case for the sand target. Instead an immediate drop in pressure is observed. Within the context of homogeneous materials experiencing shock, this drop is often times associated with the stress wave reaching a free surface and thus reflected wave interactions reduce the pressure back down to zero. Also similar to observations of materials undergoing shock, granular (and heterogeneous) materials in general tend to distort in rise or fall in pressure due to elastic/plastic compressibility. The observed initial release during the course of penetration exhibits both of these traits.

Turning these connections into hypothesis, this could infer that the high stress wave being propagated through the target, after initially spiking and resulting in grain destruction, meets enough void space to induce a large drop in pressure. However, instead of dropping to zero (gauge pressure) is would happen in the case of meeting a free surface, compaction of the grains instead catches up, and the resultant densification causes the dwell seen consistently around 500 microseconds. After which, the penetration event ends allowing the system to finally relax back to hydrostatic pressure.

Unfortunately, these observations are not directly comparable to our observed velocity results, as the stress gauge is placed on the on the very fringe (and in some cases entirely out of) the field of view. However, this only limits us from comparing traces side by side, not overall observed behavior. To that extent, stress and velocity results do appear to corroborate one other. In comparing the PIV results to the stress wave structure, a spike in momentum is also seen after initial penetration, just as velocity is show to drop, to zero or diverge, (like stress) in the presence of grain failure and void collapse.

As stress and momentum are implicitly linked, it could be questioned as to why motion (momentum transfer) many times does not reach the beyond the FOV to the gauge, yet large stress are still seen. To answer this, a simple reference to statics can be made as load can still be felt without the presence of motion given proper constraints and the realistic prevalence of body deformation.

5.2.2 Conditional Similitude

Just as with velocity field characterization, especially considering the presence of the aforementioned heterogeneous phenomena, it is of specific interest to determine any

behavioral correlation with changing projectile velocity, and to especially determine, as was with PIV results, if any self-similar behaviors exist. Towards that end, a non-dimensional approach was again taken this time with respect to both stress and time using projectile velocity, in the form of a pseudo-Bernoulli dynamic stress, and a characteristic distance **D,** in this case the distance between the gauge and shot line, as seen here

$$\sigma = \frac{P}{\frac{1}{2}\rho {v_{shot}}^2} \tag{5.9}$$

$$\tau = \frac{t}{D/v_{shot}} \tag{5.10}$$

where ρ is still the density of the target sand. τ then serves as the non-dimensionalized time and likewise σ as the normalized stress. A factor of one thousand is added to the non-dimensionalized stress to make the numbers a bit neater.

These results are further implement on the gauge measurements shown in Figure 5.19, along with the rest of the data set. The result, shown in Figure 5.20, identify two apparent and very distinct cases. Experiments conducted higher penetration velocity, and therefore characterized by more plastic behaviors, display a high degree of similitude overlaying quite well on one another.

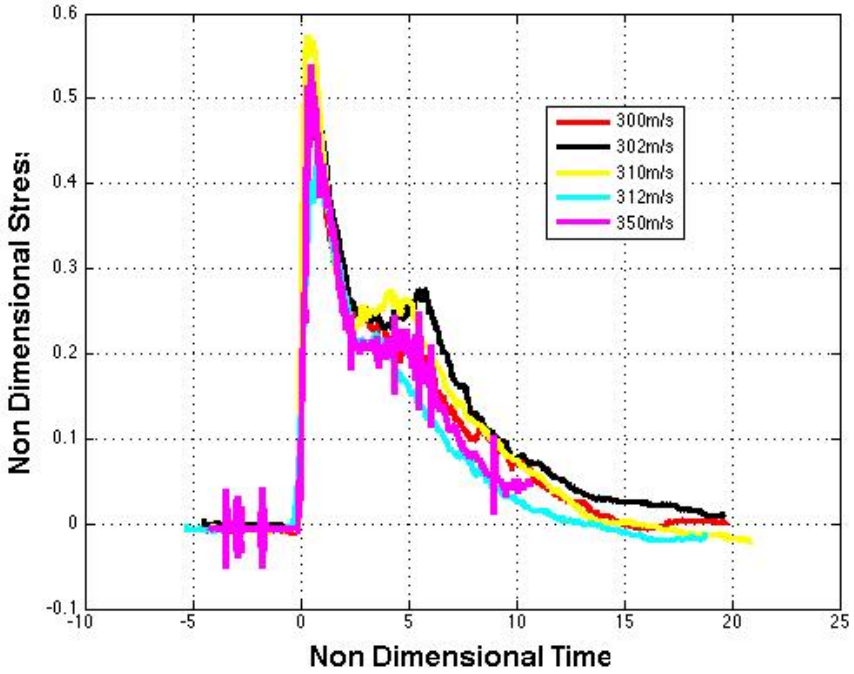

(a)

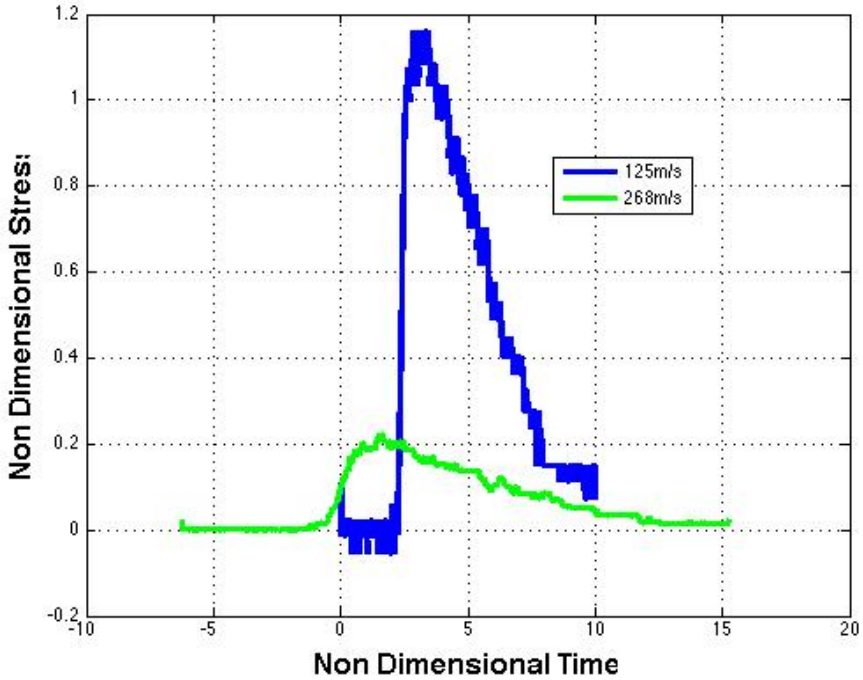

(b)

Figure 5.20 (a) Non-dimensional stress responses of events with shot velocities greater than 300 m/s, showing self similar behavior with slight variations. (b) More attenuated response behaviors seen at projectile penetrations less than 300 m/s, in contrast, are not self similar potentially dominated by heterogeneity.

In contrast, lower velocity shots show absolutely no semblance to their positively correlating self similar counter parts. While only two lower velocity shots are shown for efficient visual presentation, all conducted shots done below approximately 300 m/s are all over the place with not patterns apparent in the scatter. So, the sixty-four-thousand-dollar question becomes: how is this so?

One hypothesis, and a common thread of this work, is to of course blame the grains. Physically though, this is fairly easy to swallow. At lower loading, less grains are involved in a said dynamic event as the force granularly (and probabilistically) propagates through, as is suggested by statistical analysis of the velocity distribution and by current theories regarding force chains. This would mean any given, in this case, penetration event could vary just as much as which force chains occur could, and depending on how these combine and distribute, and at what stress level, results could vary greatly regardless of similarities seen in momentum diffusion (as the former is not entirely representative of the later).

On the other end of the spectrum, higher loading at greater impact velocities are not as subject to these effects. The greater strain rate, once again complimented by PIV observations, induces much more grain involvement in the distribution of load, in a way forcing the granular system to act more in bulk. As such, the higher the load, the more likely any underlying self similarity possessed by the continuum material is to manifest.

Coming full circle, a more complete characterization of the Ottawa sand target can begin to form. While developed fully in Chapter 6, velocity results suggest underlying self similar phenomena in the form of strengthening momentum transform with respect to projectile velocity which may be quantified in multiple potential ways, and gives way to even more derivable values. However, this trend is subject to sometimes significant scatter

seemingly due to granular and heterogeneous phenomena influenced by granular arrangement, plastic deformation, and compressibility. Going a long way towards describing the kinetics at play, the picture is completed by stress measurements which tell a similar story. Through both data sets, stress and velocity can be identified either spatially throughout the target, with regard to time at a given location, or both.

Most importantly, these insights are made using in-situ results which may both be used in comparison with both other empirical studies and, if corroborated, used to validate computational simulations which may then be used to complete the fundamental puzzle. However, these discussions have been limited solely to a bulk, continuum, way of thinking. With granular interactions only being explored in such a way as being averaged within an interrogation window. That being said, for an even more thorough characterize of the Ottawa sand target, the granular scale should be considered.

5.3 INVESTIGATING THE GRAIN SCALE

To take the dive and investigate penetration phenomena at the grain scale, the experimental setup is altered slightly, as detailed in Chapter 3. Most importantly, this required the implementation of the Cordin 550 rotating mirror camera instead of the Photron. To do so, the NSWC at Indian was kind enough to allow us into their facility.

Though limited in number of frames, the fps was set to approximately 400,000 for each shot (~2.5 microseconds) and a resolution of 1000 x 1000 pixels over a, much smaller, 15 x 15 mm field of view (with approximately 40 pixels per sand grain). Recall the average temporal discretization for the Photron was on the order of 0.1 milliseconds, in other words the Cordin is almost 100 times as finely resolved. This is essential to capture any

acceptable number of frames over such a small FOV. Two example images can be seen in Figure 5.21.

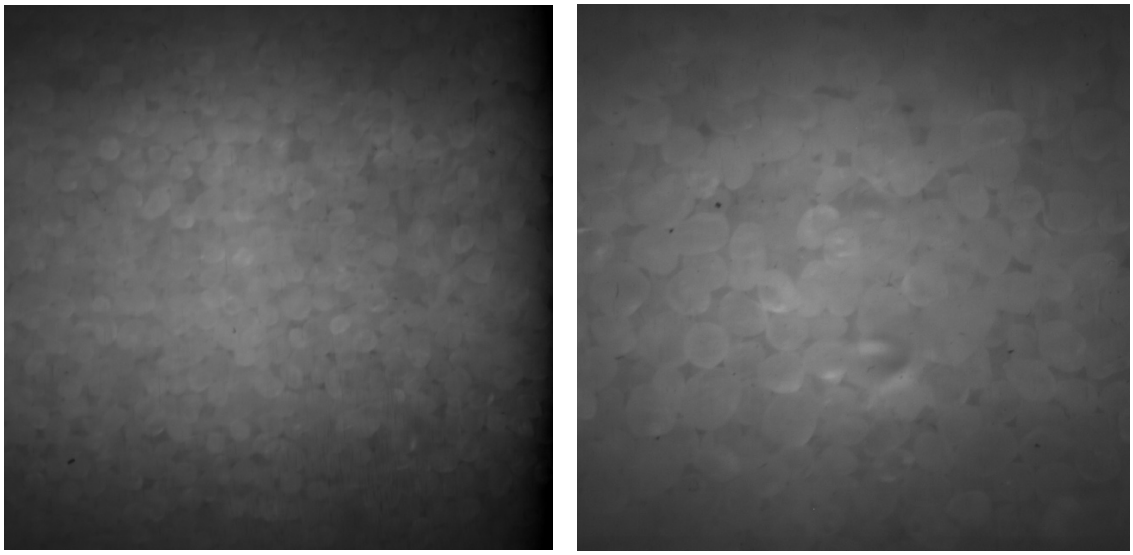

(a) (b)

Figure 5.21. High speed frames of the Ottawa sand target taken with the Cordin 550 camera. (a) A field of view of 15 by 15 mm. (b) FOV of about 7 by 7 mm.

Given the speed at which the images were taken, lighting becomes even more critical than in the case of the Photron. While timing a halogen flash light to trigger during the experiment provided the necessary intensity needed, because exposure time was so reduced a vignetting effect, the dark circular outline, occurs.

The last and major problem, is jitter. Think of the Cordin as miniature, turbo boosted, washing machine. Any slight mass eccentricity results in a dynamic instability that can physically vibrate the camera. Of course, the frequency and intensity of this vibration varies depending on the eccentricity, however at small fields of view (such as the ones used here), any slight misalignment is magnified many times over. Though difficult to see when looking at static images, consider Figure 5.12.

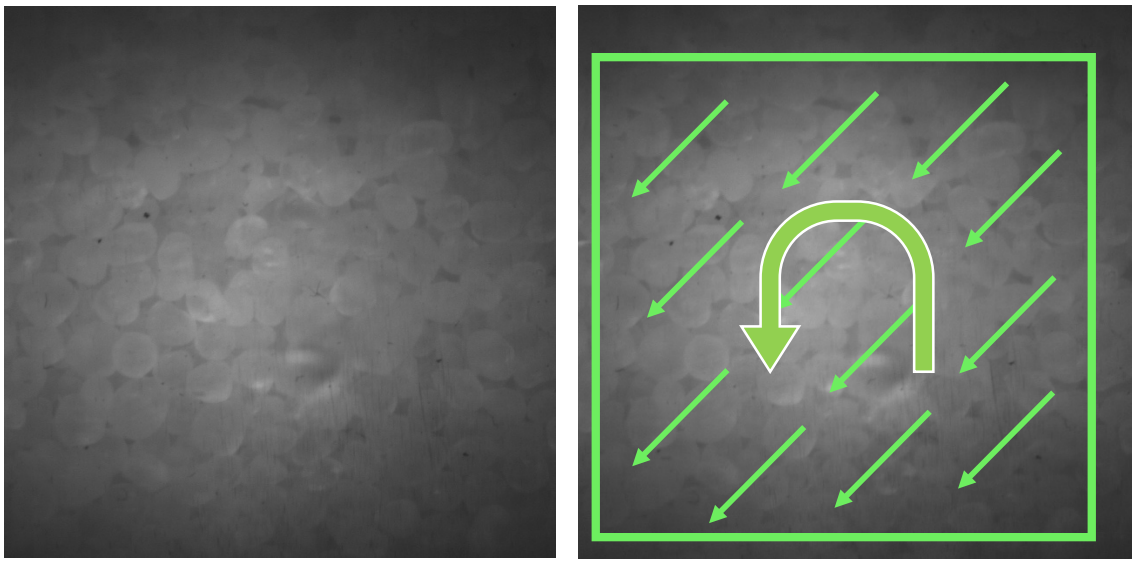

Figure 5.22 Shown are two sequential images taken from Cordin 550 record. Even though the target itself is not moving, the frame itself is slightly shifted and rotated, behavior which is schematically emphasized here for visual aid.

These inherent sources of error, one can already assume, making image analysis difficult, especially as the PIV method relies of finding physical change in an image to calculate a correlation. While lighting can, and is, cropped out to help analysis, jitter itself distorts detecting true velocity due to penetration with bulk translation and rotations. While PIV still may be performed, the same methods for quantitative characterization no longer apply as not all calculated velocities within the field may be physical.

While not completely eliminating the problem, some additional post-processing can go a long way. Previously mentioned, there are many clever people out there who have run into similar problems and created methods by which to rectify it. Used in this study, the function (MATLAB) *imwarp* takes two images that are suppose to be equivalent, but known to be distorted (warped), and use like point comparison (similar to DIC's own correlation procedure) to rotate and translate the second image until it better matches the first. In effect, identifying the distortion occurring, as visualized in Figure 5.22, and

applying the opposite on the image to bring it back to “normal”. The function itself results in a single rotation matrix to facilitate correction.

Both from observation of the raw footage, and the knowledge that vibration due to eccentricity tends to be cyclic, it can be reasonably assumed that the same distortion is consistently occurring throughout each camera run. That being said, a calibration data set is taken of the target prior to each experiment. This footage of unchanging sand is then subjected to the imwarp function, retrieving rotation matrices meant to correct 63 images back to the orientation of the first. Conducting the actual experiment, this same set of rotations can then be applied to the dynamic event, with a slight catch of having to manually determine the “beginning” of the cycle, or where of the experimental set to implement the first rotation. While sounding risky, this is actually fairly manageable as jitter is fairly consistent and a particularly huge leap is easy to identify.

While it won’t be attempted to show the improvement statically, the process goes a long way to minimizing jitter. This is especially so with regard to the human eye, unfortunately though, PIV is not so easily satisfied due to pixel by pixel comparison, and as such we resign ourselves to limiting discussion to overall trends.

Keeping this in mind, (image corrected) PIV analysis from a single shot is first presented sequentially in Figure 5.23. This particular experiment was conducted with a 310 meters per second projectile velocity, done at the NSWC facility, with an exact FOV of about 18 by 17 mm. PIV parameters were set for a spatial discretization of 32 by 32 interrogation windows each being just over half a millimeter. Every other frame was taken (5 microseconds apart) starting right before initial penetration.

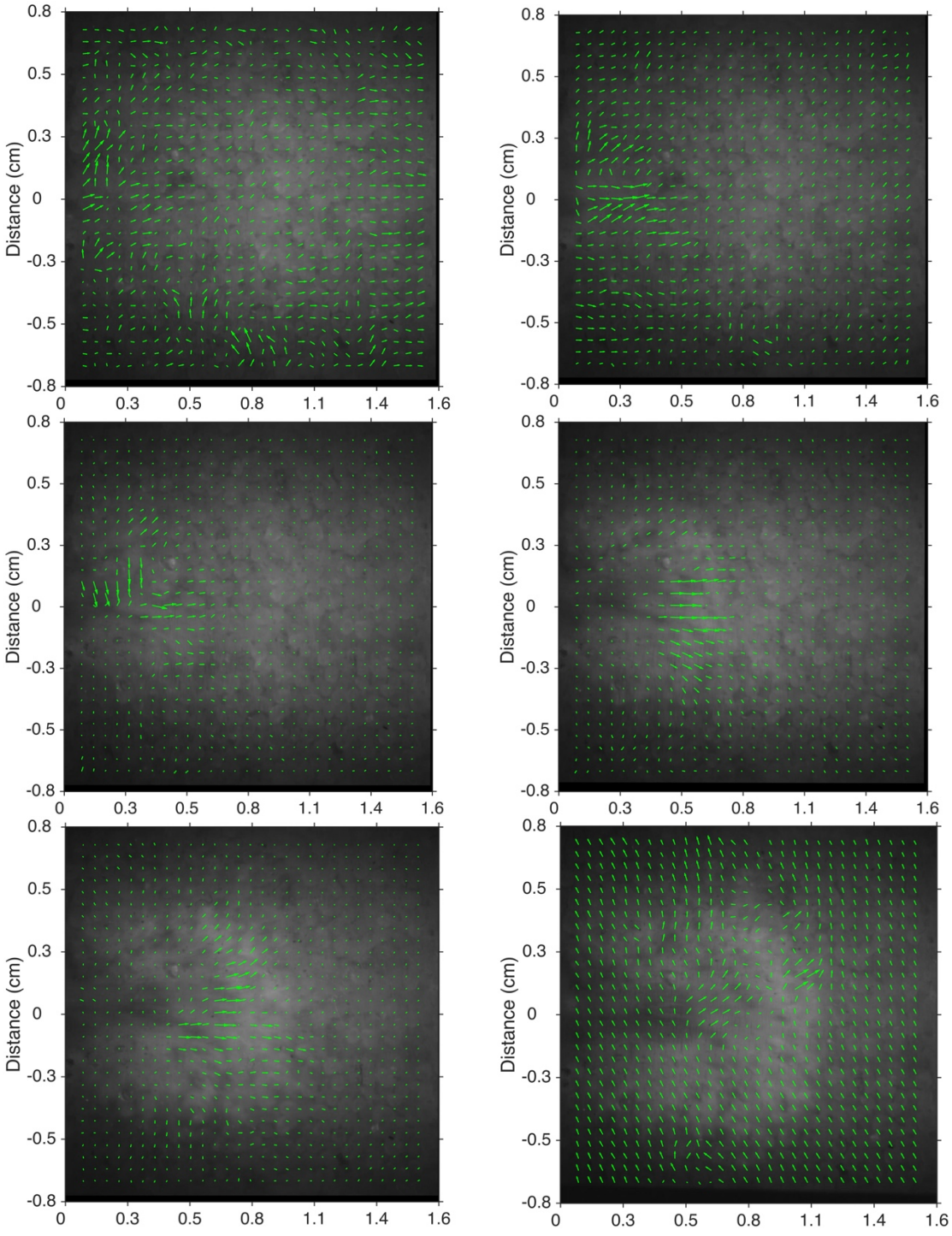
Distance (cm)
0.8
0.5
0.3
0
-0.3
-0.5
-0.8
0
0.3
0.5
0.8
1.1
1.4
1.6

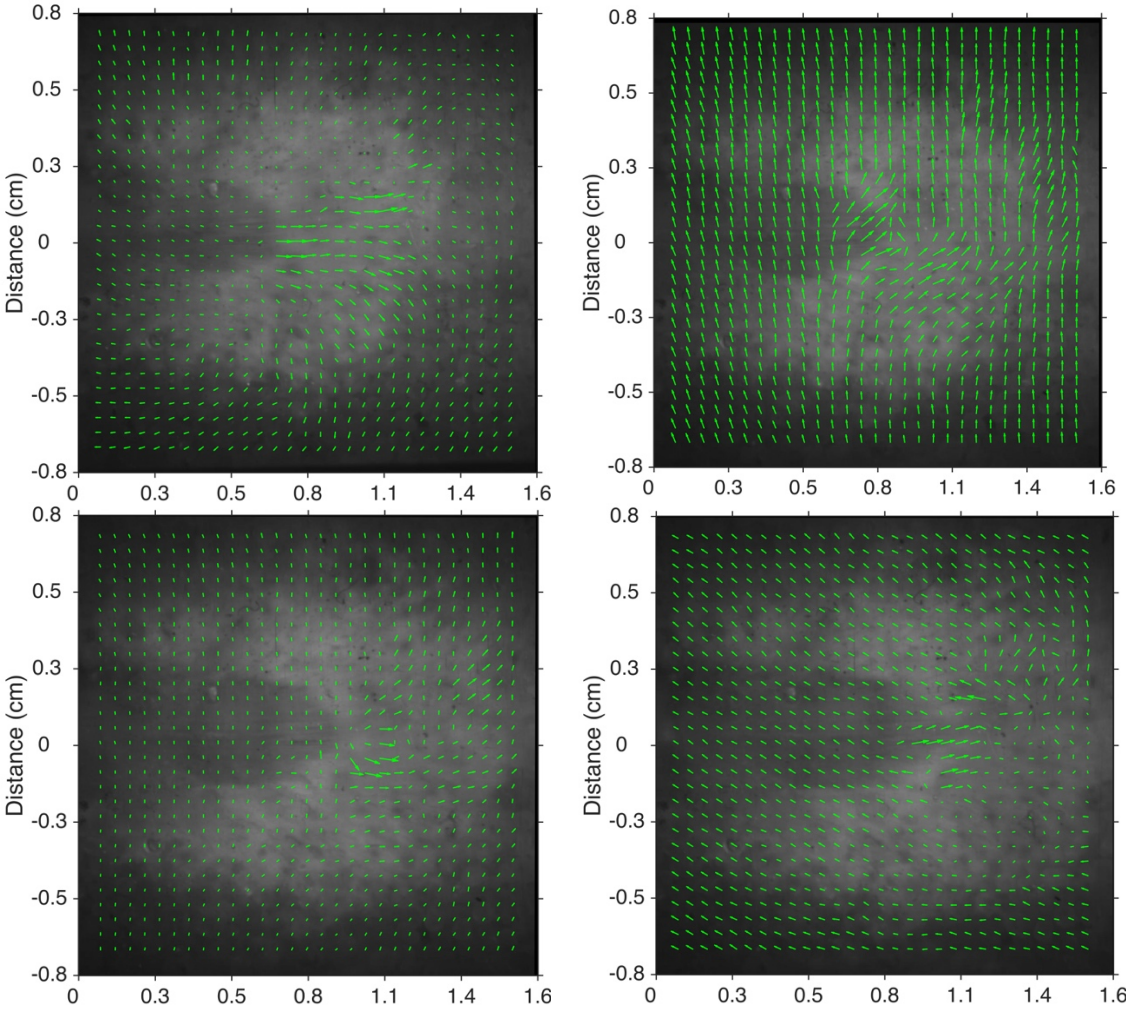

Figure 5.23. A temporal sequence of PIV calculated velocity fields extracted from grain scale FOV high speed imagery. Images are 5 microseconds apart starting at time zero just before the dart enters the domain.

Fortunately, the large frame rate allows us to have a plethora of images from which to view the event, despite the significantly focused field of view. This is especially good when observing the set shows how drastically the "jitter problem" distorts the results, and as such we need all the help we can get to pick out any potential trends.

Overall, weeding out huge translations and rotations caused by jitter, this scale seems to corroborate with continuum scale results with some increased complexity. At this scale convergence, when achieved, would appear to be more indicative of single grain

motion instead of the average seen in previous results, mainly because interrogation windows now generally cover one or two grains instead of having to average several. This, however, is sort of a double edged sword in that resolving this behavior is reliant on correlating the same grain which, given the fairly homogenous surface, is sometimes difficult.

This issue is seen throughout Figure 5.23, as even when the presence of jitter seems minimal, only a partially logical velocity field is resolved with the rest being zero (i.e. incorrectly converged). Therefore, it would seem that applying PIV at this scale would be more successful at lower spatial resolution, this however is contradictory to attempting to resolve grain interactions in the first place.

While this method is then overall inadequate in consistently resolving grain scale interactions, instances of heterogeneous mechanisms like grain fracture and visible stress bridges (force chains), and even the physical plastic wave boundary may not only be seen, but in some cases resolved by PIV (though to what degree of realism is unknown).

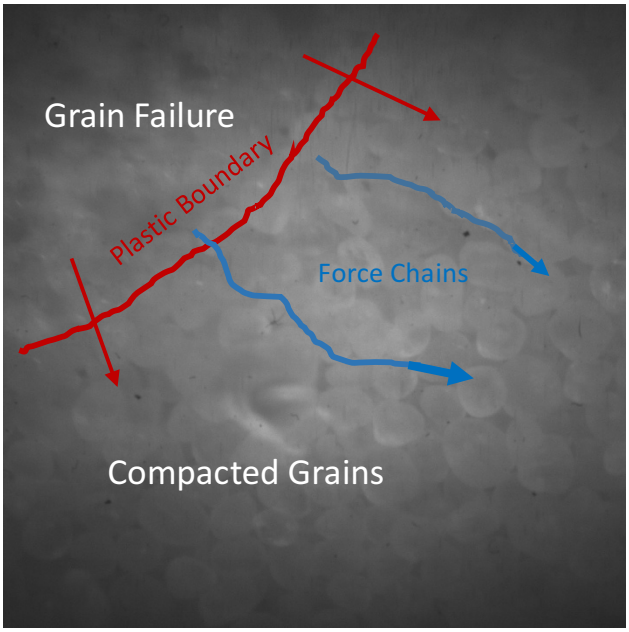

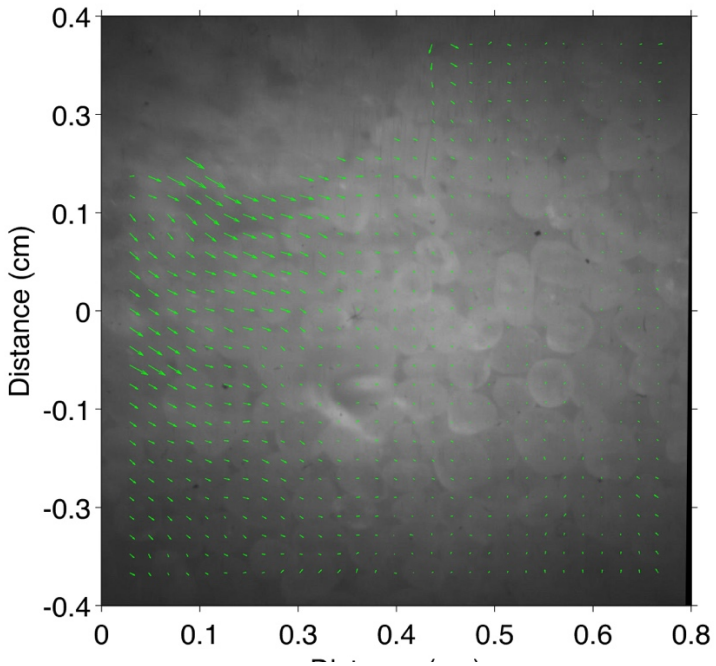

Figure 5.24. Grain scale high speed footage (Cordin 550). Conducted with a attained projectile velocity of 350 m/s

The results shown in Figure 5.24, do an excellent job visually demonstrating both the limitations and the usefulness of the overall investigation into grain scale behavior during dynamic penetration. This particular shot was done at 350 m/s, with an 8 by 8 mm field of view with the space divided into 32 interrogation windows in both directions for PIV. This, shot was particularly unique in that it was the highest velocity attained (really driving grain failure and associated phenomena) and was centered not on the dart, but rather directly *below* with the top boundary being the shot line.

Reviewing this footage, representative of the other shots done at this scale, we may easily observe initial elastic compression resulting in bulk densification via grain compaction and formation of force chains. This is quickly followed by the plastic wave seen causing catastrophic grain failures to the point where the boundary is readily

identified. In other words, this is an excellent qualitative source of data, and demonstrates the dominating presence of granular effects, as well as the conjectured order of events.

From just this qualitative approach, while the intricate kinetics cannot necessarily be described, approximations of grain interactions can be made. Doing so, it is seen that at lower velocities approximately 75% of grains will be involved in a force chains, receiving some measure of the darts momentum, with the average length being 1-10 grains. This somewhat corresponds with the distributions quantified on a bulk scale showing a more even distribution of window (grain) velocities up to the that of the dart. Increasing loading, and the corresponding imparted momentum, this is increased to almost 90% with lengthened chains of 8-15 grains additional densification (see Figure 34), lending again to continuum observations.

When seeking a quantitative description however, our experimental method seems to fall short. At best, as seen in Figures 33 and 34, PIV may only partially resolve in-situ velocity behavior at this scale. While issues such as jitter alone create quite a non-ideal scenario in which to utilize digital processing techniques, even in a perfect (non-moving) setup issues would still be had. This is due to the fundamentals of PIV itself.

By definition, PIV detects average motion within a window area. At a continuum scale this expected and it is ideal to detect average velocity as the bulk behavior is considered to be just the average of any granular interactions. Decreasing the length scale of interest, and seeking greater resolution, average velocities become both inadequate and unattainable as the characteristics of interest become the grains themselves. At this level, applying PIV, when it converges, then breaks down to an average motion of several spatial

points within a grain instead of the grain itself, and it is here in which the method is revealed to be inappropriate in application. It is at this point that other options must be considered.

From this point, though not done in the course of this study, *Particle Tracking Velocimetry* (PTV) shows great potentially, in taking the next step for quantification. Instead of identifying motion via correlation of sequential images, PTV identifies unique grains and an associated location with each from. This is excellent for understand grain interactions and is currently being used in many studies concerning fundamental granular mechanics [80, 81]. Of course, if this was easy it would have been done already. The key step in this algorithmic process is the identification of *individual* grains within an image require methods such as edge finding. When dealing with non-synthetic, more "realistic" materials such at the Ottawa sand target in this work, grain identification becomes quite non-trivial and is a current topic of interest. Even so, while the success continuum quantifications made here can go towards a better fundamental understanding of dynamic penetration in granular target and may be used to validate continuum and hydrodynamic computations, PTV technique would could take things a step further and confirm particle based (peridynamic, MPM) simulations and cement mesoscale understanding.

Wrapping up, the methods used to quantify in situ velocity behavior within a sand target, developed in tandem with the novel experimental technique, fail to consistently resolve velocity behavior on a sub-continuum scale. However, the experimental technique itself, in enabling the event to be visually accessible, provides an unprecedented ability to observe grain interactions, up to and including catastrophic failure, in-situ. These new qualitative observations, combined with in-situ empirical relations found on the bulk scale, aid in more thoroughly characterizing a sand target undergoing ballistic dart penetration.

6. CONCLUDING REMARKS

Through the course of this investigation, a series of ballistic dart penetration experiments were conducted by launching a flat nosed right circular cylinder dart into a target composed of dry, loose, Ottawa sand. This was done over a range of projectile velocities, and being visually accessible, was recorded using high speed photography. The in-situ images were then processed using Particle Image Velocimetry, from which two dimensional, temporally resolved, velocity fields were extracted.

This resultant data was then used to characterize in situ velocity behavior in an effort to gain insight into the fundamental kinetics at place. To fully explore the potential of this experimental technique, several different approaches were taken to specifically quantify behavioral trends. In observing and measuring various behaviors, empirical descriptions regarding momentum diffusion, dilatant shear stress, irreversibilities, statistical velocity distribution, and directly measuring wave propagation were discussed and proposed.

In first seeking to investigate the propagation of momentum from the dart projectile to the system, a diffusion radius was defined from contour plots of the experimental velocity fields. Leveraging non-dimensional techniques, calculating this radius across the range of tested projectile velocities revealed a positive linear correlation as determined by the presence of self similarity when normalized. Additionally, diffusion was seen to decay following an inverse power law which was empirically approximated.

Using an alternative perspective, treating the sand target as a shear-thickening (dilatant) continuum fluid, the PIV generated velocity fields and more specifically one dimensional velocity profiles perpendicular to penetration were extracted for use in

determining an approximate shear. Using the Ostwald-de Waele Power Law, the corresponding velocity gradient is proportional (by some exponential factor, the fluid behavior index) to stress, and thus implementing the known velocity information an analytical model for shear was found. While a one dimensional, steady, equation was presented, a three dimensional unsteady approximation could be feasible achieve with the addition of more extensive experimental stress measurements to fully define necessary material constants characteristic of dilatant fluids. In the course of deriving this results, this provides an alternative avenue from which stress during a penetration event may be defined in-situ, via velocity measurements.

Given the heterogeneous nature of our sand target, the role irreversible mechanisms have to play specifically through granular phenomena such as grain orientation, fracture, and compressibility are of particular interest. While on the continuum scale, granular interactions can not be properly resolved, the calculated velocity fields do provide a metric of system energy. Using an energy balance applied to a control volume (FOV), an energy measure of the lumped effected of irreversibility may be found in terms of dart and sand kinetic energy. While technically valid only prior to when grains have left the FOV, as then not all motion may be accounted for, this term can serve as a metric of irreversibility during initial stages of penetration. Crunching the numbers, the results suggest that as little as 15% of projectile (kinetic) energy is transferred to the target as motion and even in the best cases 64%. This infers the rest is utilized by mechanisms such as friction, grain failure, compression, and even heat generation.

As PIV results are a just a slightly complicated-to-get-to set of velocity vectors, the the resultant distribution of the set may be statistically investigated. Implemented more

simply than it sounds, the velocity states seen throughout each separate penetration event were binned and distributions calculated. Each distribution was bimodal in nature, within one state at zero velocity and another at a unique velocity state. Disregarding the nonzero state as expected given grains not involved in momentum transfer, this second velocity state was shown to be linearly increasing with projectile velocity. This linearity however is questionable, as viewing the data normalized with dart speed shows the mode to be a lesser and lesser percentage of the experimented velocity, suggesting a gradual plateau to a steady velocity "state". This could be related to associated stress propagation with a plateau in and around yield, however this remains unproven without backing from experimental stress measurements. This done suggest though that with increasing velocity, more and more momentum is being transferred to an increasing percent of grains which makes intuitive sense.

A last derivable characteristic from high speed imagery and associated velocity fields is a direct measurement of elastic wave speed in-situ of the penetration event. This is achieved by algorithmically evaluating velocity values to identify a single wave boundary. Knowing this location over time, and doing so over mean spatial slices, reveals a pseudo-linear correlation of elastic wave speed with projectile velocity. Agreeing with published results, this provides an alternative to more intensive additional experimental techniques usually used for similar measurements.

All of these approaches serve as ingredients, adding to our soup of characterizing our target of interest given its subject to dart penetration. Unfortunately, the full recipe still alludes us as the subtleties of heterogeneity are yet to be complete resolved. Though not "seen" per say, in a sense well enough to analytically (or empirically) predict behavior,

mechanisms attributed to the granular nature of the material are definitely “heard” as they manifest in the form of drastic scatter in all calculated results. Aside from varying projectile velocity, the only potentially critical change between experiments is the emptying and refilling of the sand tank. While seemingly innocent, just this simple act allows grains to arrange differently, and thus probabilistically varying grain interactions such as force chain formation and sand compaction. Naturally, this creates underlying discrepancies which were observed across the board.

Our journey however is not quite complete, and complimentary to the new methods used for determining velocity behaviors, the stress response of the sand target was also measured. Elastic waves present at lower velocity penetrations appear to be dominated by heterogeneous mechanisms displaying gradual rise times and plateauing as a function of maximum densification whereas high speed shots induce more shock like behavior characterized by a much steeper rise, an initial release due to fracture and plastic deformation, a dwell due to densification, and a final release. As a result, elastic responses share no seeable self similarity whereas high stress responses are driven to a more bulk response showing not only similitude but observable behaviors characteristic to heterogeneous mechanisms.

In an effort to further investigate and quantify these obviously critical granular interactions, the bulk lens through which results had been view was stripped away (literally) and a smaller field a view, on the order of 20 or so total grains in dimension, was investigated using the same techniques. Unfortunately, due to averaging assumptions implicit in PIV correlation, the comparative velocity fields at such a scale could not be consistently resolved. Qualitatively however this was a phenomenological gold mine.

Elastic compaction, stress bridge, grain failure, and even the plastic wave boundary could all be observed, from which the presence of mechanisms conjectured to contribute significantly to behavior was confirmed.

Overall, these results go towards increasing the fundamental understanding of the behavior of sand undergoing ballistic penetration, and particularly adds new insights into the dominating effects cause by granular heterogeneity. The in-situ experimental method shown demonstrates the ability to resolve granular flow and has been used to successfully characterize both velocity field and stress response characteristics including identifying various behaviors as heterogeneous in origin. While many developed experimental models have been based on pre and post experimental metrics, this setup enabled the creation of in-situ empirical models and has potential for quantifying heterogeneous energy consumption.

While potentially informational, the methods shown here have limitations in accuracy due to discretization in both time and space as well as convergence. With some refinement, potentially much more accurate and resolved measurements could be made of grain scale interactions as well as wave propagation. In application, the defined radius of momentum diffusion, if validated by other methods as accurate, could be used to predict effectiveness of a penetrator at various depths throughout an event. Computationally, many metrics discussed here such as kinetic energy during initial penetration, radius of momentum diffusion given a threshold, and the statistical mode velocity could be used to ensure the physical accurate of penetration simulations which in turn can more feasibly test a large range of parameters in a cost effective way.

6.1 FUTURE WORK

As the saying goes, this is only the beginning. The work done here is only a small tip of a potentially very large ice berg. Maintaining the same experimental setup, with faster and higher resolution cameras (now available), even more frames could be seen throughout a penetration event, and spatial discretization could be reduced, allowing for a crisper view of results already seen. If the field of view was expanded, the entire event could be tracked allowing the decay of momentum to be seen and the in target trajectory to be evaluated. While several quantitative techniques were discussed, treating the sand as a dilatant fluid was the least developed and therefore could be the most improved upon. With the implementation of more stress gauges, the indices of behavior could be defined and an empirical fit for stress could be determined in space and time.

The biggest expansion would be to increase the tested velocity range. This study was specifically conducted at a sub-ordinate regime of impact speed, so exploring into ordinate and hypervelocity regimes would be particularly interesting (and applicable) as new phenomena would begin to take hold and dominate. There have been extensive studies showing the drastic ramifications of changing dart geometry which could to be studied and quantified using this technique. Especially given the implications of heterogeneity seen throughout, geometry should further be studies with respect to target grain geometry and distribution. If bulk behavior was still retained, this would be expected to greatly influence the observed scatter.

7. BIBLIOGRAPHY

[1] Yankelevsky, DZ. "Local response of concrete slabs to low velocity missile impact." *Int. J. Impact Eng*., **19**, 4, 331–343 (1997).

[2] Watanabe, K., Tanaka, K., Iwane, K., Fukuma, S., Takayama, K., and Kobayashi, H. Sand Behavior Induced by High-Speed Penetration of Projectile. AFOSR Report, AOARD-094011, Tokoyo, Japan, Feb (2011)

[3] Allen, WA, Mayfield, EB and Morrison HL. "Dynamics of a projectile penetrating sand," *J. Appl. Physics* 28(3,11), 370-376, 1331-1335 (1957).

[4] Taylor, T., Fragaszy, R.J. and Carlton, L.H., Members, ASCE., Projectile Penetration In Granular Soils. *J. Geotech Eng-ASCE.*, **117**, 4, (1991).

[5] Bernard RS and Creighton DC. "Projectile penetration in Soil and Rock: Analysis for Non-Normal Impact," US Army Engineer Waterways Experiment Station, Technical Report SL-79-15, 1979.

[6] LaJeunesse, J.W., 2015. Implications of heterogeneity in the shock wave propagation of dynamically shocked materials.

[7] Zhuang, S., Ravichandran, G. and Grady, D.E., 2003. An experimental investigation of shock wave propagation in periodically layered composites. *Journal of the Mechanics and Physics of Solids*, *51*(2), pp.245-265.

[8] Euler, L. "Neue Grundsatze der Artillerie." Reprinted as "Euler's Opera Omnia."Berlin (1922).

[9] Gran, JK and Frew DJ. "In-target radial stress measurements from penetration experiments into concrete by ogive-nose steel projectiles", *Int. J. Impact Eng.* **19**(8) 715-726, (1997).

[10] Forrestal, M.J., Longcope, D.B., and Lee, L.M., Analytical and Experimental Studies on Penetration into Geological Targets, from the proceeding of The Interaction of Non-Nuclear Munitions with Structures, US Air Force Academy, Colorado, Report AD-A132-115, pg 23-26, May, (1983).

[11] Forrestal, M.J., Altman, B.S., Cargile, J.D. and Hanchak, S.J., 1994. An empirical equation for penetration depth of ogive-nose projectiles into concrete targets. *International Journal of Impact Engineering*, *15*(4), pp.395-405.

[12] Silling, S.A., Epton, M., Weckner, O., Xu, J. and Askari, E., 2007. Peridynamic states and constitutive modeling. *Journal of Elasticity*, *88*(2), pp.151-184.

[13] Borg J.P., Vogler T. J. "Mesoscale Simulations of a Dart Penetrating Sand" International Journal of Impact Engineering 35 (2008) pg. 1435-1440

[14] Collins, J.A. and Sierakowski, R.L., Studies on the Penetration of Eglin Sand. AFRL Report AFATL-TR-76-122 (1976).

[15] Borg, J. and Sable, P., 2015, June. In situ Characterization of Projectile Penetration into Sand Targets. In *APS Shock Compression of Condensed Matter Meeting Abstracts* (Vol. 1, p. 6004).

[16] Borg, J.P. and Vogler, T.J., 2013. Rapid compaction of granular material: characterizing two-and three-dimensional mesoscale simulations. *Shock Waves*, *23*(2), pp.153-176.

[17] Van Vooren, A., Borg, J.P., et. al "Sand Penetration: A Near Nose Investigation of a Sand Penetration Event" (2013).

[18] Borg J.P., Morrissey, M.P. Perich, C.A. Vogler, T.J. and Chhabildas, L.C. "In situ velocity and stress characterization of a projectile penetrating a sand target: Experimental measurements and continuum simulations." International Journal of Impact Engineering 51 (2013) pg. 23-35

[19] Meyers, Marc A. *Dynamic behavior of materials*. John wiley & sons, 1994.

[20] Lohse, D. and van der Meer, D. "Structures in sand streams". *Nature*. **459**(25) June (2009)

[21] Piekutowski, A., Formation of bowl-shaped craters. *Proc. Lunar Planet. Sci. Conf. 11th*, 2129-2144 (1980).

[22] Houa, M., Penga, Z. Liua, R. Wua,Y Tiana, Y., Lua, K and Chanb, C.K., Projectile impact and penetration in loose granular bed. Science and Technology of Advanced Materials **6** 855–859 (2005)

[23] Corwin, E.I., Jaeger, H.M. and Nagel, S.R., Structural Signature of Jamming in Granular Media, *Nature*. **435**, 1075 (2005).

[24] Poncelet, J.V. "Cours de Mecanique Industrielle" Bruxelles (1829).

[25] Robins, B. "New Principles of Gunnery." London (1742).

[26] Forrestal MJ, Altman, BS, Cargille JD, and Hanchack SJ. "An empirical equation for penetration depth of ogive-nose projectiles into concrete targets." *Int. J. Impact Eng.* **15**(4) 395-405 (1994).

[27] Boguslavskii, Y., Drabkin, S. and Salman, A., Analysis of vertical projectile

penetration in granular soils. *J. Phys. D: Appl. Phys.* **29** 905–916 (1996).

[28] Stone, G.W., Projectile Penetration into Representative Targets Sandia Report 1490 UC-704 October(1994)

[29] Bless, S.J., D., Berry, T., Pedersen, B. and Lawhorn, W., Sand Penetration By High-Speed Projectiles. Shock Proceedings from the Shock Compression of Condensed Matter-2009, Nashville, TN (2009).

[30] Corbett, GG, Reid, SR and Johnson, W. "Impact loading of plates and shells by free-flying projectiles: A review." *Int. J. Impact Eng.,* **18**, 141–230 (1996).

[31] Backman, M.E. and Goldsmith, W., 1978. The mechanics of penetration of projectiles into targets. *International Journal of Engineering Science*, *16*(1), pp.1-99.

[32] Forrestal, MJ, and Luk VK. "Penetration into soil targets," *Int. J. Impact Eng.,* 12, 427-444, 1992.

[33] Guzman, I.L., Iskander, M., Bless, S. and Qi, C., 2014. Terminal depth of penetration of spherical projectiles in transparent granular media. *Granular Matter*, *16*(6), pp.829-842.

[34] Bless, S., Omidvar, M. and Iskander, M., 2015. High-Speed Penetration of Granular Geomaterials. *Rapid Penetration into Granular Media: Visualizing the Fundamental Physics of Rapid Earth Penetration*, p.93.

[35] Holsapple, Keith A., and Kevin R. Housen. "Momentum transfer in asteroid impacts. I. Theory and scaling." Icarus 221.2 (2012): 875-887.

[36] Holsapple, K. A. "The scaling of impact processes in planetary sciences." Annual Review of Earth and Planetary Sciences 21 (1993): 333-373.

[37] Housen, K.R. and Holsapple, K.A., 1999. Scale effects in strength-dominated collisions of rocky asteroids. *Icarus*, *142*(1), pp.21-33.

[38] Fall, A., Lemaitre, A., Bertrand, F., Bonn, D. and Ovarlez, G., 2010. Shear thickening and migration in granular suspensions. *Physical review letters*,*105*(26), p.268303.

[39] Barnes, H.A., 1989. Shear-thickening ("Dilatancy") in suspensions of nonaggregating solid particles dispersed in Newtonian liquids. *Journal of Rheology (1978-present)*, *33*(2), pp.329-366.

[40] Chen, Cheng-lung, and Chi-Hai Ling. "Granular-flow rheology: role of shear-rate number in transition regime." *Journal of engineering mechanics* 122.5 (1996): 469-480.

[41] Bender, Jonathan, and Norman J. Wagner. "Reversible shear thickening in monodisperse and bidisperse colloidal dispersions." *Journal of Rheology (1978-present)* 40.5 (1996): 899-916.

[42] Bi, Dapeng, et al. "Jamming by shear." Nature 480.7377 (2011): 355-358.

[43] Ciamarra, Massimo Pica, et al. "Jamming phase diagram for frictional particles." Physical Review E 84.4 (2011): 041308.

[44] Waitukaitis, Scott R., and Heinrich M. Jaeger. "Impact-activated solidification of dense suspensions via dynamic jamming fronts." Nature 487.7406 (2012): 205-209.

[45] Royer, John R., et al. "High-speed tracking of rupture and clustering in freely falling granular streams." *Nature* 459.7250 (2009): 1110-1113.

[46] Albert, I., et al. "Granular drag on a discrete object: Shape effects on jamming." Physical review E 64.6 (2001): 061303.

[47] Wagner, Norman J., and John F. Brady. "Shear thickening in colloidal dispersions." Physics Today 62.10 (2009): 27-32.

[48] Brown, Eric, et al. "Shear thickening and jamming in densely packed suspensions of different particle shapes." Physical Review E 84.3 (2011): 031408.

[49] Murdoch, N., et al. "Granular convection in microgravity." Physical review letters 110.1 (2013): 018307.

[50] Yamada, T.M. and Katsuragi, H., 2014. Scaling of convective velocity in a vertically vibrated granular bed. *Planetary and Space Science*, *100*, pp.79-86.

[51] Nesterenko, Vitali. *Dynamics of heterogeneous materials*. Springer Science & Business Media, 2013.

[52] Cambou, Bernard, Michel Jean, and Fahrang Radjai, eds. *Micromechanics of granular materials*. John Wiley & Sons, 2013.

[53] Peters, Ivo R., and Heinrich M. Jaeger. "Quasi-2D dynamic jamming in cornstarch suspensions: visualization and force measurements." Soft matter 10.34 (2014): 6564-6570.

[54] Stone, M. B., et al. "Local jamming via penetration of a granular medium." Physical Review E 70.4 (2004): 041301.

[55] Lade, Poul V., Jerry A. Yamamuro, and Paul A. Bopp. "Significance of particle crushing in granular materials." Journal of Geotechnical Engineering 122.4 (1996): 309-316.

[56] Jerry, A. Yamamuro, and V. Lade Poul. "Effects of strain rate on instability of granular soils." (1993): 304-313.

[57] Oelze, Michael L., William D. O'Brien, and Robert G. Darmody. "Measurement of attenuation and speed of sound in soils." Soil Science Society of America Journal 66.3 (2002): 788-796.

[58] Baltodano-Goulding, Rafael. Tensile strength, shear strength, and effective stress for unsaturated sand. Diss. University of Missouri--Columbia, 2006.

[59] Hostler, Stephen R. Wave propagation in granular materials. Diss. California Institute of Technology, 2004.

[60] Hostler, S.R. and Brennen, C.E., 2005. Pressure wave propagation in a shaken granular bed. *Physical Review E*, *72*(3), p.031304.

[61] Littlewood, D.J., 2010, January. Simulation of dynamic fracture using peridynamics, finite element modeling, and contact. In *ASME 2010 International Mechanical Engineering Congress and Exposition* (pp. 209-217). American Society of Mechanical Engineers.

[62] Borg, J.P. and Vogler, T.J., 2009. The effect of water content on the shock compaction of sand. In *DYMAT-International Conference on the Mechanical and Physical Behaviour of Materials under Dynamic Loading* (Vol. 2, pp. 1545-1551). EDP Sciences.

[63] Borg, J.P. and Vogler, T.J., 2013. Rapid compaction of granular material: characterizing two-and three-dimensional mesoscale simulations. *Shock Waves*, *23*(2), pp.153-176.

[64] Borg, J.P. and Chhabildas, L.C., 2011. *Three-Dimensional Dynamic Loading of Sand*. MARQUETTE UNIV MILWAUKEE WI DEPT OF MECHANICAL ENGINEERING.

[65] Parab, Niranjan D., et al. "Experimental assessment of fracture of individual sand particles at different loading rates." International Journal of Impact Engineering 68 (2014): 8-14.

[66] Omidvar, Mehdi, Magued Iskander, and Stephan Bless. "Soil-projectile interactions during low velocity penetration." International Journal of Impact Engineering (2016).

[67] Magued, Iskander, et al. "Visualizing kinematics of dynamic penetration in granular media using transparent soils." (2014): 1-17.

[68] Iskander, Magued. Modelling with transparent soils: Visualizing soil structure interaction and multi phase flow, non-intrusively. Springer Science & Business Media, 2010.

[69] Carlucci, D., and Jacobson, S., "Ballistics: Theory and Design of Guns and Ammunition", CRC Press. 2nd Edition (2014)

[70] Rochester Institute of Technology, n.d. Web. <https://people.rit.edu/~andpph/text-figures/highspeed/image032.gif>

[71] Mori N, Chang KA (2003) Introduction to mpiv. MATLAB routine available: http://www.oceanwave.jp/softwares/mpiv Accessed 2012 May 20

[72] Liu, J. and Iskander, M., 2004, "Adaptive Cross Correlation for Imaging Displacements in Soils," J. Comput. Civil Eng., Vol. 18, No. 1, pp. 46–57.

[73] Hild, F. and Roux, S., 2006, "Digital Image Correlation: From Displacement Measurement to Identification of Elastic Properties—A Review," Strain, Vol. 42, No. 2, pp. 69–80.

[74] Westerweel, J., 1997. Fundamentals of digital particle image velocimetry. *Measurement science and technology*, *8*(12), p.1379.

[75] Newton, Isaac. Principia. Maclehose, 1871.

[76] "Non-Newtonian Models." Non-Newtonian Models - SimScale Platform Documentation. SimScale GmbH, 2015. Web. 4 Mar. 2016. <https://docs.simscale.com/docs/content/simulation/model/materials/OF_Non-Newtonain-Models.html>.

[77] G. W. Scott Blair et al., J. Phys. Chem., (1939) 43 (7) 853–864

[78] Kolloid Zeitschrift (1929) 47 (2) 176-187

[79] Swegle J. and Grady D. "Shock Viscosity and Prediction of Shock Wave Rise Times" Journal of Applied Physics 58 (1985)

[80] Houa, M., Penga, Z., Liua, R., Wua, Y., Tiana, Y. Lua, K. and Chan, C.K. Projectile impact and penetration in loose granular bed. Science and Technology of

Advanced Materials 6, 855–859 (2005)

[81] Cooper, William L., and Bradley A. Breaux. “Grain Fracture in Rapid Particulate Media Deformation and a Particulate Media Research Roadmap from the PMEE Workshops.” International Journal of Fracture 162, no. 1–2 (March 26, 2010): 137–150. doi:10.1007/s10704-010-9467-8

[82] Chinella, J.F., Pothier, B. and Wells, M.G., 1998. *Processing, Mechanical Properties, and Ballistic Impact Effects of Austempered Ductile Iron* (No. ARL-TR-1741). Army research lab aberdeen proving ground md.

[83] Stovall, T., De Larrard, F. and Buil, M., 1986. Linear packing density model of grain mixtures. *Powder Technology*, *48*(1), pp.1-12.

8. APPENDICES

8.1 MECHANICAL PROPERTIES OF QUARTZ

Tabular Equation of State Parameters[a]	Value	Pressure Dependent Geological Yield Parameters[a]	Value
Bulk Density, ρ_{00} [*g/cc*]	1.56	Max. Strength, *Y'* [MPa]	300
Grain Density, ρ [*g/cc*]	2.56	Yield Surface Slope, *dY/dP*	2
Pore compaction pressure, P_s [MPa]	232	Yield strength at zero pressure, Y_0 [MPa]	0.3
Zero stress shock speed, c_0 [*km/s*]	5.99	Poisson ratio, ν	0.32
Hugoniot slope, s	2.345	Tensile strength, σ_s [GPa]	0.0001

8.2 PARTICLE IMAGE VELOCIMETRY MATLAB SCRIPT

```
clc;
clear all;

%% Digital Image Correlation - PIV %%

%Digital Image Correlation (DIC) in this case used for
particle image
%velocimetry (PIV). This code applies an Eulerian mesh
grid, coined
%interrogation windows, to two successive images and
statistically compares
%each interrogation window. Maximum correlation corresponds
to the shift of
%the window between the two frames (dx and dy) and with dt
known via frames
%per second this yields velocity.

%% Credits %%

%Original Code - Nobuhito Mori, Kyoto University (MATLAB
Central Exchange), 20 Sep 2002 (Updated 13 Jul 2009)
%Customized Code - John Borg, Marquette University, 2009
%Refined Code - Peter Sable, Marquette University, 2015

%% Initial Parameters %%

%Interrogation window size in 2D, should be larger than 20
is typically 32
```

```
%or 64 corresponding with bit resolution, plays a major
role in
%convergence. Ideally the window should be large enough to
encompass not
%only the item moving, but be large enough to capture it
once its moved
%over the course of one frame. %Generally is square.
nx_window =30; %units in pixels
ny_window =30;

%Interrogation window size corresponds directly with vector
field
%resolution, so to increase this grid spaces may overlap.
Typically, if
%this is not zero it is at most 0.5 (over which you may as
well just
%decrease your window size). This allows a game to be
played with window
%size, and overlap to help with resolution and convergence.
overlap_x=0.5; %ratio
overlap_y=0.5;

%DIC literally overlays two interrogation windows and
shifts them over each
%other to statistically compare each pixel. That being
said, this can get
%very computationally intensive and in many cases as the
particles may not
%move that much. iu and iv max allow this to be capped to
where the windows
%only have to do say (for an example) half the work.
iu_max=30; %64; %units in pixels
iv_max=30; %64;

%The frames per second setting used by the high speed
camera gives the time
%separation betwen images 1 and 2 (in seconds).
dt=1/12000;

%Shot velocity in meters per second.
shotvel=289;

%The field of view of the images should be defined prior to
the shot via a
%series of calibration images, specifically placing some
known distance
```

```
%measurement in the view. Try to ensure planarity. With
distance known,
%conver this to pixels (visual software like GIMP help).
pscale=10/70; %mm/px


%% MPIV FUNCTION INPUT %%

%The brunt of the work done by this program is via the
"mpiv" function.
%This is quite robust and has many required inputs to
specify types of
%filters, whether it interpolates, its recursive nature and
what not, below
%are these inputs:

%piv_type='mqd' %This is locked in as the preferred type.

i_recur=2; %number of recursions and checks:
%0 - PIV without double check
%1 - PIV with double check
%>1 - PIV with double check and recursions

i_plot=0; %1 - plot during PIV process, other - do nothing

i_filter=1; %filter to get rid of outlier results
%1 - standard deviation filter
%2 - median filter
%0 - do nothing

vec_std=3; %threshold value to eliminate stray vectors
(usually 1.5 to 3)

i_interp=3; %interpolation method to fill in extraneous no
converged windows
%1 - linear interpolation
%2 - cubic spline
%3 - kriging interpolation
%0 - do nothing

%% Notes From Original Author - Nobuhito Mori %%

%To smooth out unrealistic changes in vectors:
%(strongly recommended if you use 50% overlap ratio)
%[iu_s, iv_s]=mpiv_smooth(iu_i, iv_i, 1);

%For vorticity:
```

```
%[vor]=mpiv_vor(iu_s, iv_s, 1);

%% Image Processing Loop %%

%Make a directory of all images to be processed in order
%variable = directoryfunction('file names and location');
a=dir('../Photron/shot*.jpg');
iptsetpref('ImshowAxesVisible','on'); %ensures axis
settings are activated for imshow function
%For Loop processing each set of successive images
h=waitbar(0,'Digital Image Correlation in progress...');
for ii=2:length(a)-1;
    waitbar(ii/(length(a)-1));
    cd
~/Desktop/DartPenetration_Data/Shot78_21815_289mps/PIV
%specify working directory if necessary depending on file
placement

    ['processing images: ' a(ii).name ' ' a(ii+1).name]
%print which files currently being processed

    im1=imread(['../Photron/' a(ii).name]); %load first
image into matlab
    %im1=rgb2gray(im1); %to grayscale
    im1=flipdim(im1,2); %flip image if necessary so it
reads from left to right (if preferred)

    im2=imread(['../Photron/' a(ii+1).name]); %load second
image into matlab
    %im2=rgb2gray(im2); %to grayscale
    im2=flipdim(im2,2); %flip image if necessary so it
reads from left to right (if preferred)

    %%% Background Subtraction %%%
%     imBk1=imopen(im1,strel('disk',20)); %identify image
background
%     imBk2=imopen(im2,strel('disk',20));
%     im1=imadjust(imsubtract(im1,imBk1)); %subtract
background and adjust for contrast
%     im2=imadjust(imsubtract(im2,imBk2));
%     im1=wiener2(im1,[3 3]); %Filter noise
%     im2=wiener2(im2,[3 3]);
%
%     im1=imsubtract(im1,50);
%     im2=imsubtract(im2,50);
    %%%  END Background Subtraction %%%
```

```
    %mpiv function, takes input parameters and using a tool
box outputs interrogation window displacement and velocity
matrices

[xi,yi,iu,iv]=mpiv(im1,im2,nx_window,ny_window,overlap_x,ov
erlap_y,iu_max,iv_max,pscale,dt,'mqd',i_recur,i_plot);

    %Assign filter conditions
    iu0=iu;
    iv0=iv;

    %mpiv filter, filters extraneous results specifically
outliers beyond a certain standard deviation (or median)
and replace with specific interpolations
    [iu0_ft, iv0_ft, iu0_ip,
iv0_ip]=mpiv_filter(iu0,iv0,i_filter,vec_std, i_interp, 1);

    Au_ip(ii,:,:)=iu0_ip; %saves velocity information in a
larger arcing matrix
    Av_ip(ii,:,:)=iv0_ip;

    figure; imshow(im1); %shows first images

    xticklabels= 0: size(im1,2)/6 : size(im1,2); %sets
label tick spacing array
    xticklabels= round(xticklabels*pscale)/10; %converts to
units from pixels and ensures integers
    xticks= linspace(1, size(im1,2), numel(xticklabels));
%sets actual ticks (not labels)

    %the same is done in the y-direction
    yticklabels = size(im1, 1)/2 : -size(im1,1)/6 : -
size(im1, 1)/2;
    yticklabels = round(yticklabels*pscale)/10;
    yticks = linspace(1, size(im1, 1), numel(yticklabels));

    %implement ticks and labels in coordinate space
    set(gca, 'XTick', xticks, 'XTickLabel', xticklabels)
    set(gca, 'YTick', yticks, 'YTickLabel', yticklabels)
    set(findobj('type','axes'),'fontsize',18)

    hold %keep this space as to add vector field (quiver
function)
    quiver(xi,yi,squeeze(Au_ip(ii,:,:))',
squeeze(Av_ip(ii,:,:))', 'g') %,
'LineWidth',1.5);set(gca,'YDir','reverse')
    xlabel('Distance (cm)')
```

```
    ylabel('Distance (cm)')

    cd ../ %change working directory to where you would
like images placed if necessary
    eval(['print -djpeg DIC_' num2str(ii) '.jpg -r600'])
    str2=['frame_' num2str(ii) '.jpg'];


    cd PIV/
    %contourplot_log
    close all
end

close all

save vars_recov7.mat
```